Radiation Belt Radial Diffusion at Earth and Beyond

Solène Lejosne[1] and Peter Kollmann[2]

1. Space Sciences Laboratory, University of California, Berkeley, CA, USA
2. Johns Hopkins University, Applied Physics Laboratory, 11100 Johns Hopkins Road, Laurel, MD 20723-6099, USA.

Corresponding author: solene@berkeley.edu

ORCID LEJOSNE: 0000-0003-4238-8579
ORCID KOLLMANN: 0000-0002-4274-9760

ABSTRACT

The year 2019 marks the 60th anniversary of the concept of radial diffusion in magnetospheric research. This makes it one of the oldest research topics in radiation belt science. While first introduced to account for the existence of the Earth's outer belt, radial diffusion is now applied to the radiation belts of all strongly magnetized planets.

But for all its study and application, radial diffusion remains an elusive process. As the theoretical picture evolved over time, so, too, did the definitions of various related concepts, such as the notion of radial transport. Whether data is scarce or not, doubts in the efficacy of the process remain due to the use of various unchecked assumptions. As a result, quantifying radial diffusion still represents a major challenge to tackle in order to advance our understanding of and ability to model radiation belt dynamics.

The core objective of this review is to address the confusion that emerges from the coexistence of various definitions of radial diffusion, and to highlight the complexity and subtleties of the problem. To contextualize, we provide a historical perspective on radial diffusion research: why and how the concept of radial diffusion was introduced at Earth, how it evolved, and how it was transposed to the radiation belts of the giant planets. Then, we discuss the necessary theoretical tools to unify the evolving image of radial diffusion, describe radiation belt drift dynamics, and carry out contemporary radial diffusion research.

KEYWORDS

Radiation Belts – Radial Diffusion – Drift – Particle Acceleration – Adiabatic Invariants – Earth – Jupiter – Saturn

ACKNOWLEDGMENTS

Contributions

The authors acknowledge the contributions of S. N. Bentley, B. Mauk, A. Osmane and E. Roussos. Sarah N. Bentley helped improve the overall quality of a preliminary manuscript on radial diffusion at Earth. She provided careful proofreading, together with detailed comments and insightful suggestions. Adnane Osmane proofread and commented on a preliminary manuscript on radial diffusion at Earth. He also authored the paragraph entitled, "A brief discussion on the general concept of diffusion in planetary radiation belts," **Section 5.3.2**. Elias

Roussos helped proofread the sections on planetary magnetospheres. Barry Mauk helped improve the overall quality of the manuscript.
S.L. thanks T.P. O'Brien for providing feedback on the paragraphs devoted to space weather. Both authors thank the anonymous reviewer for their help improving the quality of the manuscript.

General acknowledgments
S.L. thanks the scientists who, over the years, invited her to give seminars and to discuss radial diffusion within the radiation belt community, in particular J.F. Ripoll and A.Y. Ukhorskiy. She is also particularly grateful to R.B. Horne and the British Antarctic Survey for the visits and the many fruitful discussions. The sum of all these interactions ultimately lead to this ambitious project. S.L. would also like to thank the community of scientists who provided advice regarding the publication of a scientific review, namely N. Ganushkina, M. Liemohn, M. Oka, C.T. Russell, Y. Shprits, and M. Thomsen. She is grateful to F.S. Mozer and J.G. Roederer for their continuous support and encouragement.

Funding
The work of S.L. was performed under JHU/APL Contract No. 922613 (RBSP-EFW) and NASA Grant Award 80NSSC18K1223. P.K. was partially supported by the NASA Office of Space Science under task order 003 of contract NAS5-97271 between NASA/GSFC and JHU.

63 **TABLE OF CONTENTS**
64

FREQUENTLY USED SYMBOLS

α	local pitch angle
α_{eq}	pitch angle at the magnetic equator
$\boldsymbol{A}$	magnetic vector potential
A	proportionality coefficient for the asymmetry of the disturbance magnetic field $\boldsymbol{b}$
$\boldsymbol{b}$	disturbance magnetic field
$\mathscr{b}$	geocentric stand-off distance to the subsolar point on the magnetopause
$\boldsymbol{B}$	magnetic field
ΔB	asymmetric perturbation of the dipole field, in the model of Fei et al. (2006)
B_E , B_P	magnetic equatorial field at the surface of the Earth (E) or the planet (P)
B_d	amplitude of the dipole field
B_m	magnetic field at the mirror point
c	speed of light in vacuum
D_1, D_2, D_{ij}	Fokker-Planck coefficients
D_{LL}	radial diffusion coefficient
$D_{LL,m}$	D_{LL} due to magnetic fluctuations, including the effect of the induced electric fields
$D_{LL,b}$	D_{LL} due to magnetic fluctuations, in the absence of any kind of electric field
$D_{LL,e}$	D_{LL} due to electric potential fluctuations
$D_{LL,\epsilon}$	D_{LL} due to electric field fluctuations, regardless of their nature
ds	infinitesimal displacement along a field line
dl	infinitesimal displacement along a guiding drift contour (Γ)
ε	total energy of the guiding center (kinetic and potential)
E_o	rest mass energy (511 keV for an electron, 938 MeV for a proton)
$\boldsymbol{E}$	electric field
$\boldsymbol{E_{ind}}$	induced rotational electric field
η	flux tube content per magnetic flux
f, f_o, F	drift-averaged distribution functions; different notations correspond to different sets of variables: $f(J_1, J_2, J_3, t)$; $f_o(M, J, L, t)$; $F(M, J, \Phi, t)$
φ	magnetic local time
Φ	magnetic flux through a particle drift shell; proportional to J_3
γ	Lorentz factor
Γ	guiding drift contour
$\Gamma(\alpha_{eq})$	pitch angle factor for $D_{LL,m}$ ($\Gamma(\alpha_{eq}) = D_{LL,m}/D_{LL,m,eq}$)
H	Hamiltonian function
I	geometric integral ($= J/2p$)
J	second adiabatic invariant
J_3	third adiabatic invariant
(J_i, φ_i)	action-angle variables associated with the ith quasi-periodic motion (1st: gyration; 2nd: bounce; 3rd: drift)
K	adiabatic constant ($=I\sqrt{B_m}$)

166	Kp	3-hour geomagnetic activity index
167	Λ	quantity approx. conserved in case of strong pitch angle scattering (=$p^3 \oint ds/B$)
168	L	normalized equatorial radial distance
169	L^*	Roederer's parameter (proportional to $1/\Phi$)
170	M	first adiabatic invariant
171	m_o	particle rest mass
172	N, $d\mathcal{N}$	number of particles
173	n	particle number density
174	r	radial distance
175	r_0	unperturbed equatorial radius of a drift contour
176	ν	drift frequency *(*$= \Omega/2\pi$)
177	Ω	angular drift velocity
178	$\boldsymbol{p}$	particle momentum
179	$\boldsymbol{p}_\perp, p_\parallel$	$\boldsymbol{p}$ components perpendicular ($\perp$) and parallel ($\parallel$) to the magnetic field direction
180	P	transition probability – for example from J_3 to $J_3 + \Delta J_3$
181	P_X	power spectrum of the signal X
182	Π	probability
183	q	electric charge of a particle
184	R_E, R_P	Earth/planetary equatorial radius
185	S	proportionality coefficient for the symmetry of the disturbance magnetic field $\boldsymbol{b}$
186	Σ	height-integrated Pedersen conductivity
187	θ	magnetic colatitude
188	t, Δt	time, time interval
189	τ_C	characteristic time for the variation of the fields
190	τ_G	gyration period
191	τ_B	bounce period
192	τ_D	drift period
193	T, E, W	kinetic energy of the guiding center
194	U	electrostatic potential
195	$\boldsymbol{V_D}$	bounce-averaged drift velocity
196	V_L	dL^*/dt: bounce-averaged Lagrangian velocity of the guiding center in L^*
197	[ ]	square brackets = expected value (average value) of the bracketed quantity
198	⟨ ⟩	angle brackets = average change per unit time of the bracketed quantity
199	~	symbol for "approximately equal"
200	∝	symbol for "directly proportional"
201		

1. MOTIVATION

1.1. What is radial diffusion, and why this review?

Radial diffusion in a nutshell

If trapped radiation belt particles were experiencing constant magnetic and electric fields, they would stay at a constant average equatorial distance from the planet. In reality, radiation belt particles are constantly moving radially, towards or away from the planet, due to electric and magnetic field fluctuations. The individual path of a particle is similar to that of a random walk, and the net movement of the radiation belt population can be described by a diffusion equation. Thus, radial diffusion itself is not an actual physical mechanism. It is instead a mathematical formalism that describes the average outcome of various physical processes during which time-varying fields transfer energy to and from charged particles. Radial diffusion therefore plays not only a role in explaining the observed spatial distribution of radiation belt particles in space but also in explaining their acceleration to high energies.

The concept of radial diffusion was introduced during the year following the discovery of the Earth's radiation belts (Van Allen and Frank 1959) in order to explain their existence. It was then transposed to the radiation belts of other magnetized planets, partly even before in-situ measurements became available (Mead and Hess 1973; Van Allen et al. 1980a).

Why a review on radial diffusion?

Once viewed as the most important acceleration mechanism for the Earth's radiation belts, radial diffusion remains an elusive process despite many years of research. Doubts upon the efficacy of the radial diffusion process remain. Various definitions exist. There is a variety of analytic expressions to quantify radial diffusion present in the literature. The role played by the different possible drivers of radial diffusion remains uncertain. For all these reasons, advancing radial diffusion research constitutes a major scientific challenge to tackle in order to guarantee further progress in our abilities to understand and to model radiation belt dynamics.

In this review, we present the motives underlying the developments of different radial diffusion models. We describe the methods developed over the years to quantify radial diffusion. We also provide the necessary theoretical tools to better navigate radial diffusion research; the interested reader may want to refer to this special section (**Section 5**) when necessary.

Outline of the review

1. **Section 1** is the "MOTIVATION" Section. In the remainder of this section, the importance of radial diffusion research is detailed.
2. **Section 2** is the "FOUNDATION" Section. It deals with early works on radial diffusion. After a brief introduction of adiabatic invariant theory, the section presents the variety of observations that led to the introduction of the concept of radial diffusion. The early theoretical picture of the radial diffusion process at Earth is discussed, together with the

seminal work of Fälthammar (1965). This includes a derivation of the radial diffusion equation (equation 2-30). Pioneering methods for quantifying radial diffusion coefficients are also presented.

3. **Section 3** is the "EXPANSION" Section. It deals with radial diffusion at the outer planets. While some of the concrete diffusion drivers may be different than at the Earth, the general physics is the same and can be studied well because the different configuration of outer planet radiation belts allows the formation and observation of diffusion signatures that are not obvious at Earth.
4. **Section 4** is the "EVOLUTION" Section. It deals with the latest developments in radial diffusion research at Earth. In particular, the new sets of formulas proposed by Fei et al. (2006) to describe similar drivers as in **Section 2.3** are introduced and discussed.
5. **Section 5** is the "NAVIGATION" Section. It provides the necessary theoretical toolkit to address radial diffusion research. It introduces the third adiabatic invariant and discusses mechanisms leading to its violation (that is, physical processes at the heart of radial diffusion). This section also discusses when radial diffusion can be viewed as a pragmatic approximation and when it offers an acceptable description of planetary environments.
6. **Section 6** is the "CONCLUSION" Section. A summary of the key points of this review is provided, together with a discussion of some of the challenges associated with modern radial diffusion research.

Scope of the review

This review deals with the statistical description of cross drift shell motion for trapped radiation belt populations that conserve the first two adiabatic invariants (definitions of the concepts of adiabatic invariants and drift shell are provided in **Section 2.1** and **Section 5.1**). While there exist some "anomalous" and "neoclassical" radial diffusion processes, they require violation of one or two of the first two adiabatic invariants, because they are driven by a combination of pitch angle scattering and shell splitting (e.g., Roederer and Schulz 1969; O'Brien 2014; Cunningham et al. 2018). These processes are out of the scope of this review.

1.2. Why radial diffusion research?

1.2.1. Scientific challenge

Radiation belt dynamics is governed by a variety of concurrent source and loss processes whose individual contributions are difficult to evaluate (e.g., Walt 1996). Radial diffusion acts both as a source and a loss mechanism as it redistributes trapped particles throughout a magnetosphere, depending on the overall radial distribution (see also **Section 2.3.2**). Thus, uncertainty in the amplitude of radial diffusion leads to uncertainty in the relative contribution of other processes to the observed particle distribution.

Take, for example, the formation of the third narrow Earth radiation belt at ultra-relativistic energies in 2012, which led to scientific controversy. The creation of this third radiation belt was

first explained in terms of losses to the magnetopause by radial diffusion, combined with scattering into the Earth's atmosphere by electromagnetic ion cyclotron waves (Shprits et al. 2013). A competing explanation later claimed that losses to the magnetopause by radial diffusion were the only necessary mechanism to create the third radiation belt (Mann et al. 2016), and led to a series of rebuttals (Shprits et al. 2018; Mann et al. 2018).

More importantly, radial diffusion toward the Earth from an external source was originally thought to be the dominant acceleration mechanism for the radiation belts. Subsequent observations of local peaks in the radial profiles of electron phase space density brought about a paradigm shift (see also **Section 2.3.2**). As a result, the most recent works now consider that internal local acceleration prevails in the Earth's radiation belts (e.g., Thorne 2010). It was also suggested that local acceleration be applied to the giant planets (Woodfield et al. 2014, 2018). Yet, observational evidence demonstrated the importance of radial diffusion for accelerating particles at Jupiter and Saturn (Kollmann et al. 2018). Also at Earth, the debate continues (e.g., Su et al. 2015). Radial diffusion and local acceleration are in a "battle royale" (Jaynes et al. 2018a) for the title of dominant acceleration mechanism.

In order to reach a careful understanding about the physics of a magnetosphere, evaluation of all the different mechanisms at play is required, and this includes radial diffusion. Without considering all processes, it is impossible to resolve the different controversies surrounding radiation belt dynamics.

1.2.2. Space weather challenge

Radial diffusion plays a central role in a complex set of physical processes that determines the structure, intensity and variability of the radiation environment through which satellites must operate. Inability to accurately specify and forecast energetic radiation belt particles hampers our ability to use technological systems in space.

Indeed, the Earth's radiation belts with their "killer" electrons at relativistic energies pose serious threats to spacecraft, such as internal charging hazards (e.g., Horne et al. 2013). Energetic ions cause displacement damage in semiconductor devices. All radiation poses total dose hazards over the lifetime of a spacecraft. Yet, as our society relies more and more on space systems (for crucial purposes such as communication, navigation, Earth observation, defense, timing signals, etc.), the number of satellites flying within or through the Earth's radiation belts is constantly increasing. In addition, the increased use of electric propulsion means that spacecraft spend more time in the heart of the belts – they need a few months after launch to reach geostationary orbit, compared to a few days in the traditional case of chemical propulsion (e.g., Horne and Pitchford 2015).

Reliable and cost-effective spacecraft design requires good knowledge of the radiation environment (e.g., Xapsos et al. 2013). Radiation drives the requirements for spacecraft and scientific instruments orbiting Earth as well as the outer planets. In particular, the spacecraft

design community needs a specification of the mean and worst-case radiation environments in which the satellites will operate (O'Brien et al. 2013). These requirements can be determined by empirical models based on a compilation of data from prior missions (e.g., Sawyer and Vette 1976; Vette 1991; O'Brien et al. 2018) and physics-based numerical simulations (e.g., Maget et al. 2007; Maget et al. 2008; Glauert et al. 2018; Horne et al. 2018). However, empirical models rely on samples with limited accuracy and limited coverage (in space, time, energy, etc.). A common way to alleviate this difficulty is to combine data analysis with physical models. One of the benefits of theoretical modeling is that it can reconstruct a complete picture of the space environment based on sparse experimental information. In addition, physics-based models can reproduce realistic dynamics for the radiation belts, including the effects of geomagnetic storms. This feature is particularly helpful for post-event analysis, when spacecraft that are not necessarily equipped with sensors to monitor their local environment report anomalies during the course of a mission (e.g., Green et al. 2017).

Diffusion-driven models as a solution

In order to minimize the computational resources required and the execution time of the codes, many physics-based models rely on the adiabatic theory of magnetically trapped particles (introduced **Section 2.1**) in order to reduce the number of variables to handle. Rather than focusing on the dynamics of individual particles, they solve a diffusion equation to describe the average variations of distribution functions – quantities that relate directly to particle flux measurements (e.g., Beutier and Boscher 1995; Subbotin and Shprits 2009; Su et al. 2010; Tu et al. 2013; Glauert et al. 2014). The same models, appropriately modified, have also been used to study the radiation belts of Jupiter (e.g., Santos-Costa and Bourdarie 2001; Woodfield et al. 2014; Nénon et al. 2017, 2018) and Saturn (Santos-Costa et al. 2003; Lorenzato et al. 2012; Clark et al. 2014; Woodfield et al. 2018). Models that are simpler but still diffusion-driven have also been applied to Uranus and Neptune (Selesnick and Stone 1991, 1994; Richardson 1993).

One of the objectives of radial diffusion research is to generate the radial diffusion coefficients that appear in the corresponding diffusion equation. These coefficients are core inputs required by the physics-based models to develop realistic radiation belt dynamics. Therefore, an accurate evaluation of these coefficients is paramount.

The most commonly used radial diffusion coefficients for the Earth's radiation belts are the ones proposed by Brautigam and Albert (2000) and by Ozeke et al. (2014). Because both formulations are simple functions of location and magnetic activity, their use is straightforward. (See also **Sections 2.4.2** and **4.3** for information about the formulas by Brautigam and Albert (2000) and by Ozeke et al. (2014), respectively). For the giant planets, the diffusion coefficient is commonly parameterized as a power law in distance with exponents based either on the theory by Brice and McDonough (1973) or on fits to observations (**Section 3.2**). In all cases, doubts remain as to the validity of these parameterizations.

In effect, different works have yielded different values for the radial diffusion coefficients, and still today, the scattering among all possible values spans several orders of magnitude (e.g., Walt

1971a, Fig. 6; Tomassian et al. 1972, Fig. 7; Mogro-Campero 1976; Van Allen 1984, Tab. III; Roussos et al. 2007, Fig. 9; Huang 2010, Fig. 6). While physical arguments can help explain part of this radial diffusion coefficient variability (**Section 2.4.2**), determining the most suitable coefficients to use in diffusion-driven models remains a challenge.

2. FOUNDATION: What are the origins of radial diffusion research?

Before presenting experimental evidence of radiation belt radial diffusion at Earth and at the giant planets, we briefly introduce the adiabatic theory of magnetically trapped particles in the first part of this section. Additional information is provided in **Section 5.1.1**.

2.1. Brief introduction to the adiabatic theory of magnetically trapped particles

Planetary radiation belts are formed of energetic charged particles with energies on the order of MeV. These particles are trapped in the planetary magnetic field, where they undergo three forms of quasi-periodic motion on three very distinct timescales: (1) a fast gyration about a field line, (2) a slower bounce motion along the field line, and (3) a slow drift motion around the planet (e.g., Schulz and Lanzerotti 1974; Walt 1994; Roederer and Zhang 2014; see also the illustration in **Fig. 11a, Section 5.1**). The magnitude of each of these three periodicities is characterized by an adiabatic coordinate (e.g. Northrop 1963; Roederer 1967). The fundamental temporal condition for conservation of an adiabatic coordinate is that the time variations of the fields are negligible on the timescale of the corresponding quasi-periodic motion.

The first adiabatic coordinate *M* is associated with gyro-motion. It is equal to

$$M = \frac{p_\perp^2}{2m_o B} \tag{2-1}$$

where m_o is the particle rest mass, B is the local magnetic field, $p = \sqrt{T^2 + 2Tm_o c^2}/c$ is the relativistic momentum, T is the kinetic energy, $p_\perp = p\,sin\,\alpha$ and $p_\parallel = p\,cos\,\alpha$ are the components of the momentum $\boldsymbol{p}$ perpendicular and parallel to the magnetic field vector, respectively, and α is the local pitch angle between the particle velocity and the local magnetic field. The first adiabatic coordinate *M* is sometimes called the magnetic moment, but it is only equal to the magnetic moment resulting from the gyro-motion in the non-relativistic case.

The second adiabatic coordinate *J* is associated with bounce motion. It is equal to

$$J = \oint p_\parallel ds \tag{2-2}$$

The integral goes over the full bounce motion along the magnetic field line, and ds is an element of arc of the field line.

Because all particles bounce through the equatorial plane while only particles with small pitch angles between their velocity and the magnetic field reach high latitudes of the planet, radiation belt intensities are highest in roughly toroidal regions around a planet, otherwise known as the radiation belts.

When the relativistic momentum p is conserved, it is easier to calculate numerically other quantities that are equivalent to the adiabatic invariants *M* and *J*. These adiabatic constants are the magnetic field at the mirror point $B_m = p^2/(2m_oM)$, the geometric integral $I = J/(2p)$ and/or the quantity $K = I\sqrt{B_m}$ (e.g., Roederer 1970, p.50).

In the case of strong pitch angle scattering, under which neither M nor J are conserved, it can be useful to consider that the quantity $\Lambda = p^3 \oint ds/B$ is approximately conserved (Schulz 1998). Strong pitch angle scattering is common for electrons in high intensity regions at most magnetized planets (Mauk 2014).

The third adiabatic coordinate is associated with drift motion. The drift velocity $\boldsymbol{V_D}$ of a radiation belt particle (q, M, J) is a function of both electric and magnetic fields. For instance, in the case of equatorial particles $(\alpha_{eq} = 90°)$, the drift velocity of the guiding center $(q, M, J = 0)$ is equal to

$$\boldsymbol{V_D} = \frac{-M\boldsymbol{\nabla}B \times \boldsymbol{B}}{\gamma q B^2} + \frac{\boldsymbol{E} \times \boldsymbol{B}}{B^2} \tag{2-3}$$

In the Earth's radiation belts, the electric drift velocity is typically very small in comparison with the magnetic drift velocity

$$\left|\frac{\boldsymbol{E} \times \boldsymbol{B}}{B^2}\right| \ll \left|\frac{M\boldsymbol{\nabla}B \times \boldsymbol{B}}{\gamma q B^2}\right| \tag{2-4}$$

Thus, the total guiding-center drift velocity is often approximated by the value of the magnetic drift velocity. This zeroth-order approximation is no longer valid in the radiation belts of the giant planets, because the corotation electric drift is larger at the giant planets (see also **Section 3.1.3**).

The third adiabatic invariant J_3 is inversely proportional to the parameter L^*, as will be discussed in **Section 5.1.1**. L^* is often approximated by the coordinate L, which corresponds to the normalized radial distance of a dipole magnetic field line at the magnetic equator. The pitfalls of such approximation will be highlighted in **Section 2.3** and **Section 5.1**.

If the magnetic and electric field around a planet were stationary, the particles would follow a deterministic motion. The guiding centers would maintain the same average radial distance to the planet, and they would evolve along unchanging closed surfaces called *drift shells* with constant energy (see also the illustration in **Fig. 11 Section 5.1**). Random fluctuations in the field on the timescale of the radiation belt particle drift period around the planet add a random velocity component, and their average effects can be described through radial diffusion.

Adiabatic vs non-adiabatic

In this review, we call "adiabatic" the conditions that conserve all three adiabatic invariants, while "non-adiabatic" refers to conditions that violate at least one of the three adiabatic invariants. Because the third adiabatic invariant is associated with the slowest of the three forms of quasi-periodic motion (the drift motion), it is most likely to be violated (much faster variations are required to violate the first or the second invariants).

It is useful to notice that in order to conserve M, $p_\perp$ will have to change when the local magnetic field experienced by the particle is changed. It is important to understand that changes in B are not equivalent to changes in L^* or the third invariant. The magnetic field (at any point on the field line) can change along a drift shell and the drift shell can change shape over time, even while all invariants are conserved (see discussion in **Section 5.1.2)**.

For scientific analysis, it is often useful to study whether measurements are consistent with the conservation of invariants, which requires conversion between the native coordinates of the measurement, energy T and pitch angle α, to the more physically meaningful adiabatic coordinates (e.g. Roederer and Lejosne 2018). The calculation of invariants from T, α, and spacecraft location requires an assumed global electromagnetic field model but is otherwise straightforward through the explicit equations provided above and in **Section 5.1.2**. More difficult is the other direction, where we select adiabatic coordinates to calculate the equivalent T, α, and location. There is usually no explicit analytic expression for this, but the solution can be done numerically or through a lookup table. What is usually found is that particles with pitch angles mirroring close to the magnetic equator change their energy faster for the same B-change at the magnetic equator than particles bouncing to high latitudes, assuming that they conserve at least the first two invariants. The energy change is weaker for relativistic particles. There is also a change in pitch angle for non-equatorial particles when B is changing. α becomes more equatorial in higher B, but this effect is minor in comparison to near equatorially mirroring particles. Thus, it is primarily the difference in the energy change that will modify an initial pitch angle distribution at constant energy (as is the native measurement) when the magnetic field is changing.

2.2. First experimental evidence of radiation belt radial diffusion

2.2.1. Existence of the Earth's outer belt

Radial diffusion was first introduced to account for the existence of the Earth's outer radiation belt, and characteristic signatures of a process slow enough to conserve the first two adiabatic invariants (equations (2-1) and (2-2)) were found in energetic particle measurements.

MeV neutrons resulting from the disintegration of atmospheric nuclei struck by GeV cosmic rays can decay in flight while still within the Earth's (or any other planet's) magnetic field, producing energetic electrons and protons. This mechanism, known as cosmic ray albedo neutron decay (CRAND), was first proposed to account for the existence of the Earth's radiation belts (Singer 1958; Vernov 1959; Kellogg 1959a). CRAND is still thought to be the major source of Saturn's proton belts (Kollmann et al. 2017; Roussos et al. 2018; Cooper and Sturner 2018). Yet, it was soon realized that CRAND could not sustain the high intensity of Earth's outer belt. Radial diffusion was introduced as another possible source process for the outer belt (Kellogg 1959b).

A few years later, Explorer 14 measurements reported systematic inward motion of the inner side of the peak of equatorial electron intensities ($E \geq 1.6$ MeV) for several weeks of geomagnetic quiet time following the magnetic storm of December 17-18, 1962 (**Fig. 1**). These data provided the first experimental evidence of radial diffusion in the Earth's outer belt (Frank et al. 1964; Frank 1965; Newkirk and Walt 1968a).

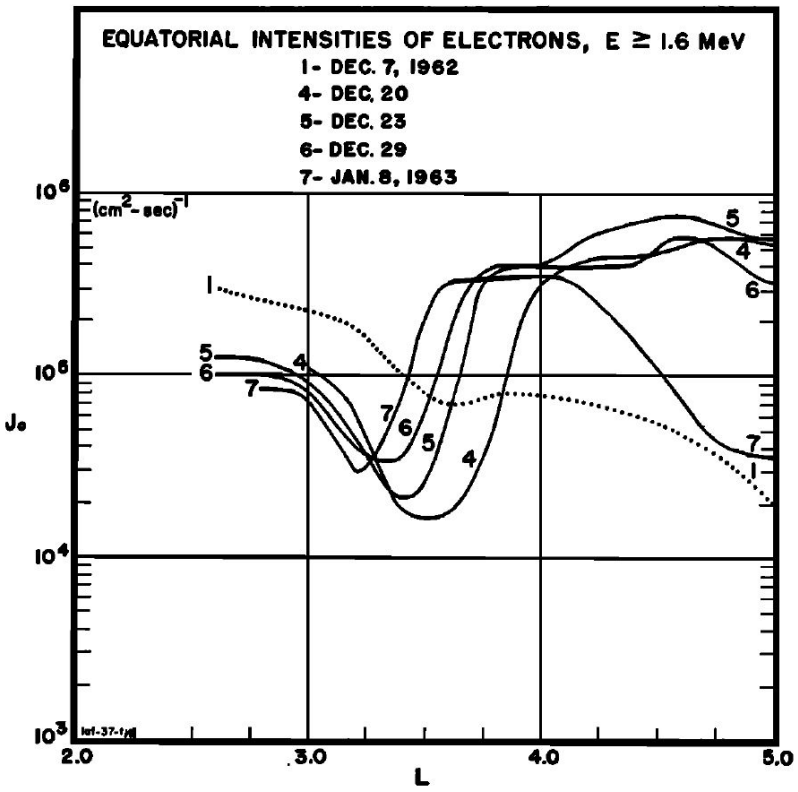

Fig. 1 The apparent inward motion of energetic electrons ($E \geq 1.6$ MeV) measured by Explorer 14 during a geomagnetically quiet time following the magnetic storm of December 17-18, 1962.

Newkirk and Walt (1968a) showed that this apparent radial motion was similar to that expected from diffusion by violation of the third adiabatic invariant (Frank et al. 1964).

A model-observation comparison for the average proton fluxes of the outer belt further supported the idea that radial diffusion is a primary source process for the Earth's outer belt (**Fig. 2;** Nakada et al. 1965; Nakada and Mead 1965).

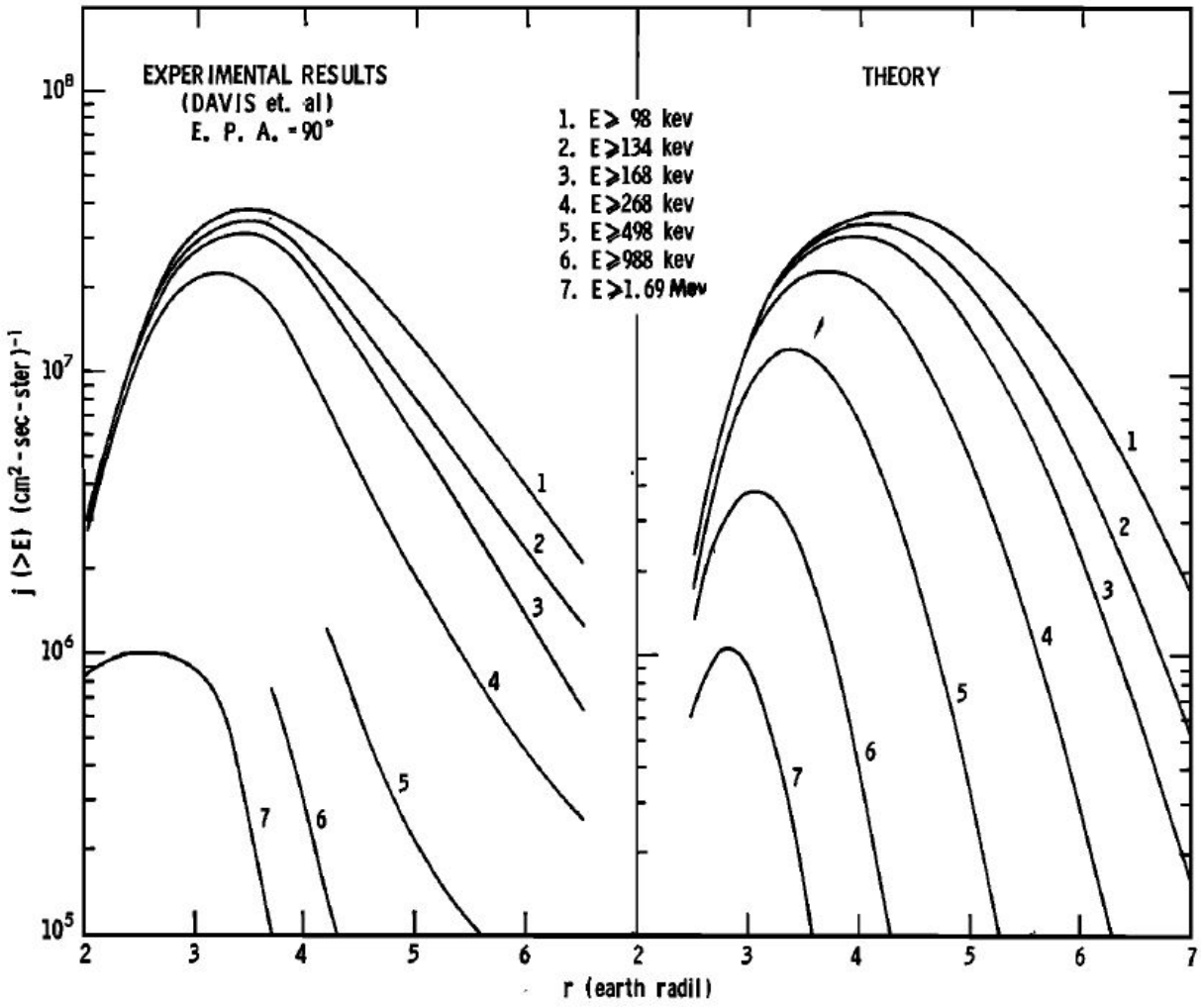

Fig. 2 Comparison of (left) the observed trapped proton integral fluxes with (right) the distribution expected for radial diffusion from an external proton source located at the outer boundary (Nakada and Mead 1965).

2.2.2. Artificial radiation belt dynamics

Studies of artificial belts produced by high altitude nuclear explosions during the Cold War yielded some of the earliest evaluations of the radial diffusion coefficients (Newkirk and Walt 1968b; Farley 1969a, 1969b).

High altitude nuclear explosions carried out by the United States and the Soviet Union (1958-1962) created artificial belts in the inner zone that persisted for years (e.g., Gombosi et al. 2017). Measurements of those energetic electron fluxes indicated that the initially localized peak progressively broadened in radial width (e.g., Brown 1966), providing evidence of radial diffusion in the inner belt (**Fig. 3**). The peak in electron intensity observed in **Fig. 3** at L=1.77 is an artificial radiation belt that resulted from a high-altitude nuclear explosion on November 1, 1962. The progressive radial broadening of the peak with time is a clear indication of radial diffusion in the Earth's inner belt.

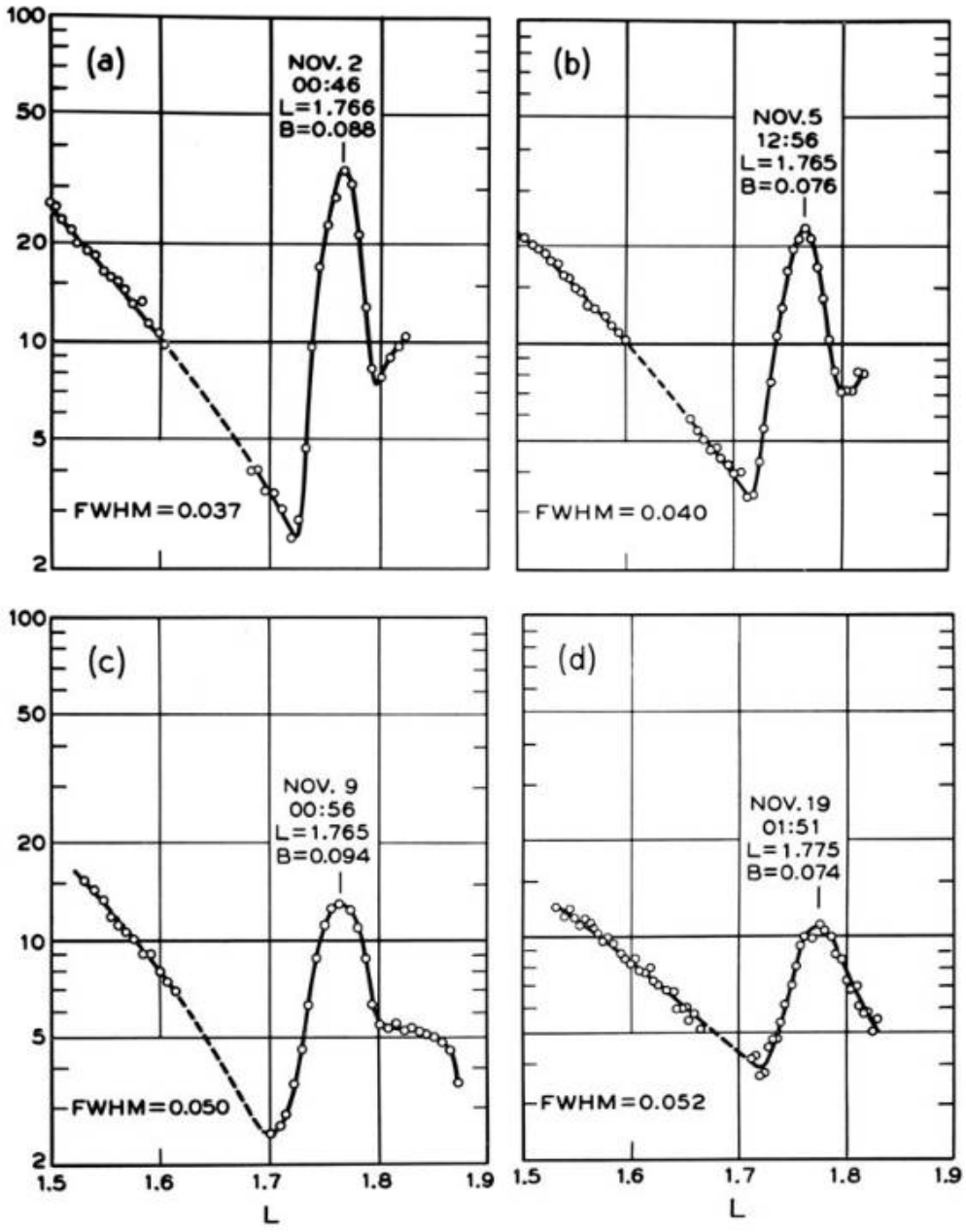

Fig. 3 Broadening of the narrow peak in the inner zone electron flux profile (> 1.9 MeV, omnidirectional flux) produced by the third U.S.S.R. nuclear test on November 1, 1962. The intensities displayed are relative. The date, time, and value of the magnetic field of each peak center are noted, together with the full width at half maximum (FWHM) of a Gaussian fitted to the peak. This figure was adapted to illustrate the cover of Schulz and Lanzerotti's (1974) book entitled "Particle Diffusion in the Radiation Belts." The data displays the simultaneous effects of radial diffusion and pitch-angle scattering (Brown 1966).

2.2.3. Diffusion signatures from giant planet moons

Microsignatures

The most direct observations of radial diffusion can be made after the introduction of a distinct disturbance into the radial intensity profile of a magnetosphere. In the case of Earth, such features usually arise from intensity enhancements following geomagnetic storms (e.g., **Fig. 1**). They can also be caused by high-altitude nuclear explosions (e.g., **Fig. 3**). At the Giant Planets, intensity depletions are common. Different from the Earth, the giant planets in our solar system have moons orbiting close enough to the planet that some of them are embedded in the radiation belts. The moons absorb particles that encounter them during their drift around the planet (Thomsen and Van Allen 1980; Hood 1983). The moons then cause a "drift shadow" where the intensities are depleted. Such features are referred to as "microsignatures" (Van Allen et al. 1980b; Roussos et al. 2007). With increasing azimuthal distance to the moon, the microsignature is observed to refill in the case of energetic electrons. This filling can be quantitatively described through radial diffusion (**Fig. 4**). Different to the evolution of intensity enhancements at Earth that evolve through at least a mix of radial, pitch angle and energy diffusion, at the giant planets there is little ambiguity in identifying the role played by radial diffusion in controlling the evolution of a microsignature: Local source or loss processes will affect both the microsignature and its environment. Pitch angle diffusion is thought to affect the microsignature and its environment the same way. (An exception might be when the pitch angle diffusion results from waves driven by the particle distribution that is modified in the microsignature. However, the role of pitch angle diffusion on the intensities in regions of microsignatures has not been extensively studied.) Convective transport processes acting coherently on the plasma (through interchange or large-scale non-radial electric fields) will displace the microsignature (Roussos et al. 2010), not refill it. Thus, any such process will not be included in a diffusion coefficient derived from microsignatures, even though, for example, interchange may be also describable through diffusion (**Section 3.1.2**), but on scales larger than the microsignature. This is why microsignature-derived coefficients are sometimes referred to as describing "microdiffusion." Overall, the analysis of microsignature refilling is a relatively robust, though purely phenomenological method to describe radial diffusion, at least on small scales.

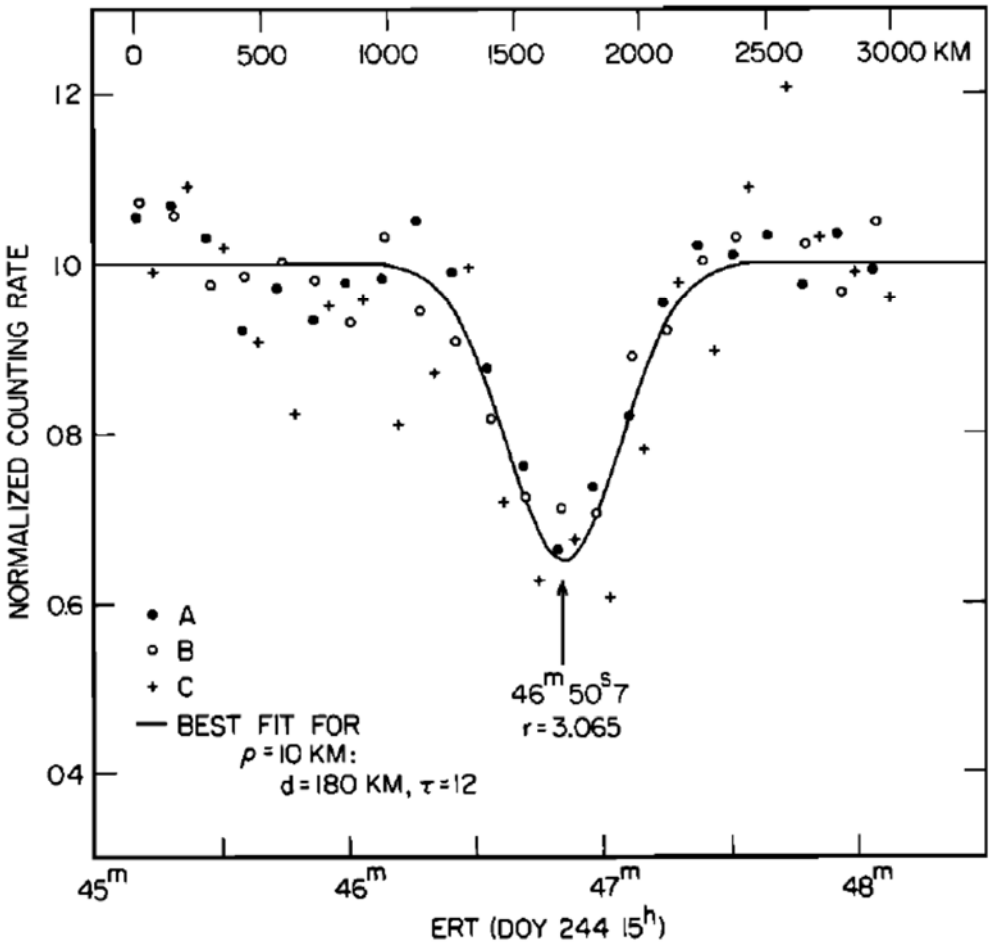

Fig. 4 The 2 MeV electrons downstream of Saturn's moon Mimas. Points: measurements. It can be seen that Mimas has depleted the electron intensities. Line: fit to the data assuming refilling by radial diffusion as a function of time and azimuthal distance to the moon (Van Allen 1980b).

Macrosignatures

If radial diffusion is slow and/or the moon absorption is very efficient, the microsignature does not refill after one particle drift around the planet. This will lead to a deeper microsignature over time, until a steady state is reached (Mogro-Campero 1976; Kollmann et al. 2013). Such a feature is called "macrosignature." Macrosignatures are mostly found for ions (**Fig. 5**) because their net drift around Jupiter and Saturn is faster than that of electrons of similar kinetic energy so that ions have less time to refill the drift shadow before the next moon encounter (see also Sec. 3.1 in Roussos et al. 2016). Electrons over a wide energy range at Jupiter and Saturn drift relatively slowly near the relevant moons because, unlike in the Earth's radiation belts, their magnetic drift is competing with the corotation drift that is directed in the opposite direction. Only at very high energies (>10MeV close to Saturn) do electrons drift fast enough to also show macrosignatures (Kollmann et al., 2011). Macrosignatures show clearly the presence of radial diffusion: The extent of depleted intensities is found to be much broader in L-shell than what can

be explained by the size and eccentricity of the moon, the gyroradius effect, and non-circular drift paths. The extended depletion arises from the fact that radial diffusion continuously acts to enhance the intensity in the macrosignature at the price of depleting the intensities outside of the macrosignature.

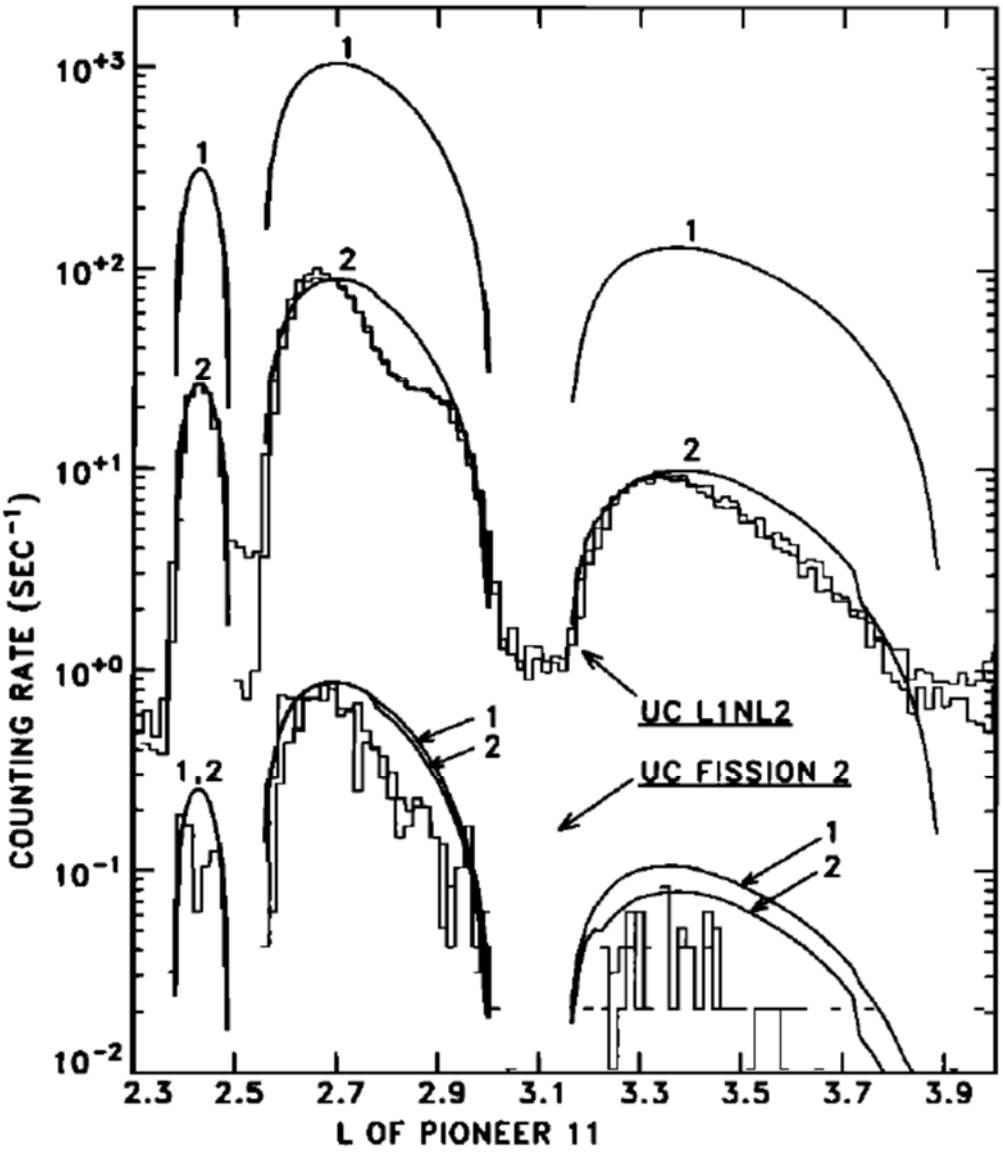

Fig. 5 Intensity of (1) 15 MeV and (2) 250 MeV protons at Saturn. The broad intensity minima around L=2.3, 2.5, 3.1, and 3.9 are macrosignatures caused by the absorption by various moons of Saturn as well as its main rings. Jagged lines: measurement. Smooth lines: Fit to the data assuming steady state radial diffusion (Cooper 1983).

2.3. Early theoretical work

2.3.1. Parker's core mechanism for radial diffusion in the Earth's outer belt

It was Parker (1960) who first described a physical mechanism by which particles on the same drift shell could be transported to neighboring shells in the Earth's outer belt, with a scenario as follows (**Fig. 6**).

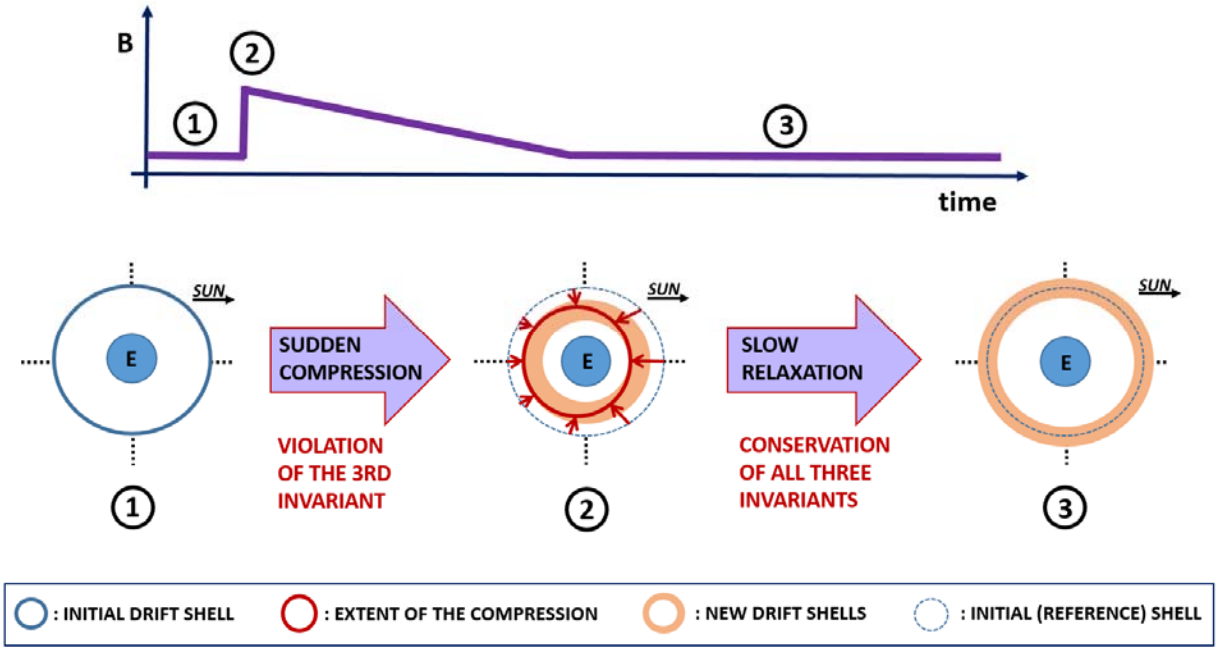

Fig. 6 (Top panel) Schematic drawing of a sudden compression of the magnetosphere, indicated by an increase of the magnetic field in the magnetosphere. (Bottom panel) Schematic drawing of the displacement and broadening of a ring of equatorial particles. The particles initially drift in a dipole field (blue circle at step 1), and their motions are suddenly modified by the induced electric fields during magnetic field compression (red arrows in step 2). The particles slowly return close to their initial location during the slow relaxation even though the ring of particles has ultimately broadened (light brown band in step 3). See text for details.

The initially dipole magnetic field (1) is suddenly compressed (2), and then slowly returns to its initial configuration (3).

(1) Guiding-centers of equatorially trapped energetic particles drift around the Earth, following paths of constant equatorial magnetic field intensity in stationary conditions (see also **Section 5.1**). Consider a ring of particles in a dipole field, all drifting along a circle of constant radius **Fig. 6-1**.
(2) When the field is suddenly compressed, the particles follow the field lines (Parker, 1960). Their motions depend on the longitude at the time of the compression. Because the compression is stronger on the dayside than on the nightside, particles are transported closer

to Earth on the dayside. Particle radial motions are represented by red arrows in **Fig. 6-2**. As a result, different portions of the initial ring of particles now populate different shells as the particles drift around the Earth – the different drift shells are represented in light red-brown area in **Fig. 6-2**. This mechanism is at the heart of the radial diffusion process: Particles are moved inward and outward in a way that is well defined when distinguishing local times (see for example equation (2-37) below). When considering a drift shell average and many such events, particle motion turns into a random, diffusive motion.

(3) Then, as the field returns slowly to its initial configuration, no additional motion across drift shells occurs. Yet, because of the sudden compression, the initially narrow ring of particles has broadened around its initial position – the blue ring in **Fig. 6-1** has become the light red-brown area in **Fig. 6-3**.

It is worth noting that cross drift shell motion is zero on average over all local times (see also **Section 5.2.2**), even though there is general inward radial motion during the compression (all the red arrows point inward, as seen in **Fig. 6-2**). Also, all invariants are conserved during the relaxation, even though the radial distance is changing. This apparent inconsistency comes from the fact that the parameter of interest for radial diffusion is the third adiabatic invariant, or the equivalent L^* coordinate, not radial distance (see also **Section 5.1**). Even though the red arrows indicate $dr/dt < 0$, as shown in **Fig. 6-2**, some correspond to $dL^*/dt > 0$, while others correspond to $dL^*/dt < 0$, depending on magnetic local time, and it results in the average displacement in L^* being zero.

Key points:

- *Timescale:* The timescales of this scenario are always longer than the population bounce period; hence the first two adiabatic invariants are conserved. Therefore, "suddenly" means "with a characteristic time that is extremely rapid compared to the population drift period." It indicates that the third invariant alone can be violated (e.g., Northrop and Teller 1960). "Slowly" means "with a characteristic time that is extremely slow compared to the population drift period," so that all three adiabatic invariants are conserved. (The typical timescales invoked in the Earth's radiation belts are of the order of a few minutes for the sudden magnetic compression, and a few hours for the relaxation.)
- *Particle motion and frozen-field condition:* During the violation of the third invariant, it is implicitly assumed that the plasma obeys the so-called "frozen-field condition," where particles can be visualized as if following the field lines. When the field is suddenly compressed, an induced rotational electric field $\boldsymbol{E_{ind}}$ is set up according to Faraday's law. Provided that there is no component of the electric field parallel to the magnetic field direction, and that the Earth's surface is a perfect conductor, the local magnetic field line velocity coincides with the electric drift $(\boldsymbol{E_{ind}} \times \boldsymbol{B})/B^2$ (Birmingham and Jones 1968; Fälthammar and Mozer 2007). That "the particles follow the field lines" means that the drift velocity is $(\boldsymbol{E_{ind}} \times \boldsymbol{B})/B^2$ during that time.
- *Asymmetry:* That particles populate different drift shells originates from the fact that the magnetic field compression depends on local time (it is stronger on the dayside than on the nightside). If the magnetic field compression were not dependent on local time, the

configuration would stay symmetric: all particles would be transported radially inward by the same amount, and they would stay on a common ring. Thus, no broadening of the ring of particles would occur. In other words, it is essential that the variations of the electromagnetic field depend on local time in order to drive radial diffusion.

In summary, sudden field variations that depend on local time cause motion across drift shells. A more comprehensive description for this mechanism is provided in **Section 5.2.1**.

Although an event such as the one described in this section only constitutes a small perturbation for the radiation belts, the cumulative effect of a large number of such events can be significant. In the presence of a continuum of events similar to the one presented in **Fig. 6**, the initially narrow ring of particles keeps broadening. A radial diffusion coefficient is a characterization of the average rate at which the broadening occurs. (See, for instance, Equation (2-44).)

In summary, radial diffusion was introduced to describe the average rate at which a trapped population changes drift shells in the presence of a large number of small uncorrelated perturbations. This formalism is germane to the Fokker-Planck equation, which describes the evolution of a distribution function as a result of small random changes in the variables (e.g., Davis and Chang 1962). In the following, we review step by step the derivation of the Fokker-Planck equation, together with its reformulation in terms of a diffusion equation.

2.3.2. From the Fokker-Planck equation to the diffusion equation

Radial diffusion equation in action variables

If the electromagnetic fields were completely specified all the time, Liouville's equation could be used to determine the exact effects of field perturbations on particle distributions by following particle trajectories through phase space (e.g., Dungey 1965). However, it is experimentally impossible to characterize the electromagnetic fields at every location and at every time. Instruments only provide local, instantaneous measurements that can be converted into global but only statistical information on the fields. Alternatively, one can use numerical models (such as magnetohydrodynamics – MHD – codes) to fully specify the electromagnetic fields and inject test particles to simulate the resulting radiation belt dynamics. Yet, test particle simulations are usually not the preferred approach (because, for instance, they are still computationally very expensive). Due to these limitations, the Fokker-Planck formalism, which aims to calculate the time evolution $\partial f/\partial t$ of a distribution function f, is usually the preferred method. This approach reduces the number of variables to specify by relating average properties of the electromagnetic fields to average characteristics of the radiation belt dynamics.

Let us consider $(J_i, \varphi_i)_{i=1,2,3}$, the set of action-angle variables associated with a radiation belt population. J_3 is the third adiabatic coordinate, and φ_3 is proportional to the drift period. The objective of this paragraph is to describe the evolution of the number of particles $d\mathcal{N}$ with a set of action variables comprised between J_1 and $J_1 + dJ_1$, J_2 and $J_2 + dJ_2$, and J_3 and $J_3 + dJ_3$, from

719 a time t to a time $t + \Delta t$ – where Δt is a time interval that is long in comparison with the
720 population drift period. To do so, we introduce the drift-averaged distribution f so that

$$d\mathcal{N}(t) = f(J_1, J_2, J_3, t) dJ_1 dJ_2 dJ_3 \tag{2-5}$$

721 In this description, we neglect all phase dependencies (φ_i) – assuming phase mixing (e.g.,
722 Schulz and Lanzerotti 1974), and we consider that the first two adiabatic invariants of the
723 radiation belt population remain constant.
724
725 The evolution of the distribution function is described in terms of a Markov process in J_3 (e.g.
726 Chandrasekhar 1943; Lichtenberg and Lieberman 1992; Walt 1994; Roederer and Zhang 2014):

$$f(J_1, J_2, J_3, t + \Delta t) = \int f(J_1, J_2, J_3 - \Delta J_3, t)\, P(J_1, J_2, J_3 - \Delta J_3; \Delta J_3, \Delta t) d(\Delta J_3) \tag{2-6}$$

727 where $P(J_1, J_2, J_3 - \Delta J_3; \Delta J_3, \Delta t) d(\Delta J_3)$ indicates the probability that an ensemble of phase points
728 that have a set of action variables equal to $(J_1, J_2, J_3 - \Delta J_3)$ experiences an increment equal to ΔJ_3
729 after a time interval Δt. Thus, the transition probability P represents the physical mechanisms
730 responsible for the violation of the third adiabatic invariant. By definition of the transition
731 probability:

$$\int P(J_1, J_2, J_3; \Delta J_3, \Delta t) d(\Delta J_3) = 1 \tag{2-7}$$

732 It is assumed that the increment ΔJ_3 after Δt is small *($\Delta J_3 / J_3 \ll 1$);* that is, it is assumed that the
733 transition probability P is large only for small ΔJ_3. A Taylor expansion for the integrand
734 equation (2-6) yields

$$\begin{aligned} &f(J_1, J_2, J_3 - \Delta J_3, t) P(J_1, J_2, J_3 - \Delta J_3) \\ &\qquad = f(J_1, J_2, J_3, t) P(J_3) - \Delta J_3 \frac{\partial}{\partial J_3}(fP) + \frac{{\Delta J_3}^2}{2} \frac{\partial^2}{\partial J_3^2}(fP) \end{aligned} \tag{2-8}$$

735 We want to find an expression for $\partial f / \partial t = (f(J_1, J_2, J_3, t + \Delta t) - f(J_1, J_2, J_3, t))/\Delta t$. Inserting
736 the Taylor expansion (2-8) into equation (2-6) leads to

$$\frac{\partial f}{\partial t} = -\frac{\partial}{\partial J_3}(D_1 f) + \frac{1}{2} \frac{\partial^2}{\partial J_3^2}(D_2 f) \tag{2-9}$$

737 where D_1 is the average change in J_3 per unit time:

$$D_1 = \frac{1}{\Delta t} \int \Delta J_3\, P(J_1, J_2, J_3; \Delta J_3, \Delta t) d(\Delta J_3) \tag{2-10}$$

738 And D_2 is the average square change in J_3 per unit time:

$$D_2 = \frac{1}{\Delta t}\int (\Delta J_3)^2\, P(J_1, J_2, J_3; \Delta J_3, \Delta t) d(\Delta J_3) \tag{2-11}$$

739 Rewriting (2-9) in the case of a uniform distribution function ($\partial f/\partial t = 0$ and $\partial f/\partial J_3 = 0$)
740 yields a relation between D_1 and D_2:

$$D_1 = \frac{1}{2}\frac{\partial D_2}{\partial J_3} \tag{2-12}$$

741 (e.g. Walt 1994; Roederer and Zhang 2014). The coefficients D_1 and D_2 were discussed in
742 several works, including Herlofson (1960), Davis and Chang (1962), Tverskoy (1964) and
743 Fälthammar (1966). A derivation of the equation (2-12) from Hamiltonian theory is detailed in
744 the following paragraph in order to emphasize the underlying assumptions. With $D_{J_3 J_3} = D_2/2$,
745 the diffusion coefficient associated with the third invariant, it results that the evolution of the
746 drift-averaged distribution function is described by:

$$\frac{\partial f}{\partial t} = \frac{\partial}{\partial J_3}\left(D_{J_3 J_3}\frac{\partial f}{\partial J_3}\right) \tag{2-13}$$

747 A change of variables provides the diffusion equation in terms of magnetic flux ($\propto J_3$), or
748 L^* ($\propto 1/J_3$) coordinates (see, for instance, Roederer and Zhang 2014, and equations (2-28) and
749 (2-30) below).
750
751 *Derivation of the relation between the advection (D_1) and the diffusion (D_2) coefficients*
752 To understand the result provided in equation (2-12), we follow the derivation presented by
753 Lichtenberg and Lieberman (1992). This derivation highlights the importance of phase mixing,
754 i.e., of assuming that the distribution is uniform in φ_3 (Roederer 1970; Schulz and Lanzerotti
755 1974). For a time interval Δt that is small in comparison with the characteristic time for the
756 variation in J_3:

$$\Delta J_3 = J_3(t + \Delta t) - J_3(t) = \frac{dJ_3}{dt}\Delta t + \frac{d^2 J_3}{dt^2}\frac{(\Delta t)^2}{2} \tag{2-14}$$

757 with φ_3 the angle variable associated to drift motion, and H the Hamiltonian:
758

$$\begin{cases} \dfrac{dJ_3}{dt} = -\dfrac{\partial H}{\partial \varphi_3} \\ \dfrac{d\varphi_3}{dt} = \dfrac{\partial H}{\partial J_3} \end{cases} \tag{2-15}$$

759
760 Combining equations (2-14), and (2-15), it results that:

761

$$\Delta J_3 = -\frac{\partial H}{\partial \varphi_3}\Delta t + \frac{(\Delta t)^2}{2}\left(\frac{\partial}{\partial J_3}\left(\frac{\partial H}{\partial \varphi_3}\right)^2 - \frac{\partial}{\partial \varphi_3}\left(\frac{\partial H}{\partial \varphi_3}\frac{\partial H}{\partial J_3} + \frac{\partial H}{\partial t}\right)\right) \quad (2\text{-}16)$$

762

763 The first term on the right side of equation (2-16) is zero on average over φ_3, provided that the
764 distribution is uniform in φ_3. Indeed:
765

$$\left[\frac{\partial H}{\partial \varphi_3}\right] = \frac{1}{\int \Pi(\varphi_3)d\varphi_3}\int \frac{\partial H}{\partial \varphi_3}(\varphi_3)\Pi(\varphi_3)d\varphi_3 \quad (2\text{-}17)$$

766

767 where $\Pi(\varphi_3)d\varphi_3$ is the probability that particles are between φ_3 and $\varphi_3 + d\varphi_3$ with
768 $\int \Pi(\varphi_3)d\varphi_3 = 1$. When the distribution is uniform in φ_3, $\Pi(\varphi_3) = cst.$, and we obtain that

$$\left[\frac{\partial H}{\partial \varphi_3}\right] = \frac{1}{2\pi}\int_0^{2\pi} \frac{\partial H}{\partial \varphi_3}(\varphi_3)d\varphi_3 \quad (2\text{-}18)$$

769 because H is periodic in φ_3, it follows that

$$\left[\frac{\partial H}{\partial \varphi_3}\right] = \frac{1}{2\pi}(H(2\pi) - H(0)) = 0 \quad (2\text{-}19)$$

770 For similar reasons, the third and fourth terms in equation (2-16) are also zero when averaging
771 over φ_3. Thus averaging (2-16) over φ_3 and inserting it into (2-10) yields:

$$D_1 = \langle \Delta J_3 \rangle = \frac{\Delta t}{2}\frac{\partial}{\partial J_3}\left[\left(\frac{\partial H}{\partial \varphi_3}\right)^2\right] \quad (2\text{-}20)$$

772 where [ ] denotes the average of the bracketed quantity and ⟨ ⟩ denotes the average change per
773 unit time Δt of the bracketed quantity.
774 To describe D_2 (2-11), we take the square of equation (2-16), and we only keep the terms up to
775 the second order in Δt:
776

$$(\Delta J_3)^2 = \left(\frac{\partial H}{\partial \varphi_3}\right)^2 (\Delta t)^2 \quad (2\text{-}21)$$

777 Thus,

$$D_2 = \langle (\Delta J_3)^2 \rangle = \Delta t \left[\left(\frac{\partial H}{\partial \varphi_3} \right)^2 \right] \quad (2\text{-}22)$$

As a result:

$$\langle \Delta J_3 \rangle = \frac{1}{2} \frac{\partial}{\partial J_3} \langle (\Delta J_3)^2 \rangle \quad (2\text{-}23)$$

and we obtain the equation (2-12).

General diffusion equation

It should be noted that the diffusion concept is very general, and in principle, not limited to the third invariant. A more general expression is

$$\frac{\partial f}{\partial t} = \sum_{i,j} \frac{\partial}{\partial J_i} \left(D_{i,j} \frac{\partial f}{\partial J_j} \right) + Sources - Losses \quad (2\text{-}24)$$

where $D_{i,j}$ are the diffusion coefficients and J_i are the action variables. The violation of the first and second adiabatic invariants can be rewritten in terms of diffusion in kinetic energy D_{EE} and equatorial pitch angle $D_{\alpha\alpha}$, as well as cross terms $D_{\alpha E}$, $D_{E\alpha}$ (e.g. Schulz and Lanzerotti, 1974). Diffusion in the first and second adiabatic invariants is mathematically equivalent, and is less intuitive, but it can allow for more stable or more accurate numeric solutions of equation (2-24) (Subbotin and Shprits 2012).

The "Sources" and "Losses" terms account for changes in $\partial f / \partial \mathrm{t}$ that are not due to diffusion. These processes can be sorted into three categories:

1) Processes that are independent of the distribution function f. An example is the CRAND source process that provides particles regardless of the already existing population (Selesnick et al. 2007).

2) Processes that scale with the distribution function f. An example is charge exchange that effectively converts ions into neutrals that are not magnetically trapped anymore and are therefore lost from the considered region. The loss rate for this process is proportional to the distribution function (Kollmann et al. 2011).

3) Processes that steadily change a variable of the distribution function f. An example is gradual energy loss due to synchrotron emission (Santos-Costa and Bourdarie 2001) or while passing through a plasma, planetary atmosphere, or ring (Nénon et al. 2018).

No doubt solutions of the full 3-D diffusion equation are more realistic than solutions of the 1-D radial diffusion equation with parameterized loss (Subbotin et al. 2011). Yet, it is interesting to note that radial diffusion alone typically provide rather reasonable dynamics for the belts in the Earth's magnetosphere (e.g. Li et al. 2001; Shprits et al. 2005). This result further highlights the key role played by radial diffusion in driving radiation belt dynamics (Shprits et al. 2008).

Radial diffusion equation

Historically, the derivation of the diffusion equation has been done in a dipole field, by tracking the number of particles whose adiabatic invariants are comprised between M and $M + dM$, J and $J + dJ$, and L and $L + dL$ at time t, introducing the distribution function $f_0(M, J, L, t)$ such that

$$d\mathcal{N}(t) = f_0(M, J, L, t) dM dJ dL \tag{2-25}$$

Let us point out that the definition of the L coordinate in equations (2-25) and seq. can be a source of ambiguity. Strictly speaking, the L coordinate of these equations refers to the third adiabatic invariant. Thus, it corresponds to the Roederer's L^* coordinate (1970). Yet, for radiation belt particles in a dipole field, L^* merges with the normalized equatorial radial distance (thus $L = L^*$ in this special case).

A reformulation of the equation (2-9) is

$$\frac{\partial f_0}{\partial t} = -\frac{\partial}{\partial L}(\langle \Delta L \rangle f_0) + \frac{1}{2}\frac{\partial^2}{\partial L^2}(\langle (\Delta L)^2 \rangle f_0) \tag{2-26}$$

where $\langle \Delta L \rangle$ and $\langle (\Delta L)^2 \rangle$ represent the average displacement in L per unit time, and the mean square displacement in L per unit time, respectively. These two coefficients are related in a dipole field (Dungey 1965; Fälthammar 1966):

$$\langle \Delta L \rangle = \frac{L^2}{2}\frac{\partial}{\partial L}\left(\frac{\langle (\Delta L)^2 \rangle}{L^2}\right) \tag{2-27}$$

This result is equivalent to the equation (2-12) – when assuming a dipole field, or appropriately substituting L by L^* in the most general case.

Consequently, the equation (2-26) reduces to

$$\frac{\partial f_0}{\partial t} = \frac{\partial}{\partial L}\left(\frac{D_{LL}}{L^2}\frac{\partial}{\partial L}(L^2 f_0)\right) \tag{2-28}$$

where

$$D_{LL} = \frac{\langle (\Delta L)^2 \rangle}{2} = \frac{[(\Delta L)^2]}{2\,\Delta t} \tag{2-29}$$

The operator [ ] indicates an average, and the bracket operator ⟨ ⟩ indicates an average per time interval Δt. It is important to recognize that generally, $\langle (\Delta L)^2 \rangle \neq \langle (\Delta L) \rangle^2$. Assuming otherwise leads to wrong derivations of diffusion coefficients. If the diffusion driver is known, it may be possible to express D_{LL} through the power spectrum of the underlying field fluctuations under certain assumptions (see, for example, equations (2-43) and (2-51) derived in this section).

When comparing diffusion coefficients, it is important to note that while D_{LL} has the unit of 1/time, its meaning is similar to a (normalized) distance^2 per time in a dipole field. This means that D_{LL} cannot be directly compared with pitch angle diffusion $D_{\alpha\alpha}$ or energy diffusion D_{EE}/E^2, which have the same units but the dimensions of angle^2 per time and normalized energy^2 per time. Diffusion coefficients represent the potential of the respective diffusion to act. In the absence of gradients, however, there will be no net diffusive transport, regardless of the diffusion coefficient. Another way of comparing the importance of different diffusion modes is therefore to compare the respective $\partial f_0/\,\partial \mathrm{t}$ terms.

Sometimes, the distribution function is associated with the third adiabatic invariant J_3, rather than with the actual L coordinate. The third invariant J_3 is proportional to the magnetic flux Φ encompassed by the population drift shell. In that case, with $F(M,J,\Phi,t)$, the new distribution function, given that $Fd\Phi = f_0 dL$ and $d\Phi \propto dL/L^2$ in a dipole field, we obtain that

$$\frac{\partial F}{\partial t} = L^2 \frac{\partial}{\partial L}\left(\frac{D_{LL}}{L^2}\frac{\partial F}{\partial L}\right) \tag{2-30}$$

The value and functional dependence of the radial diffusion coefficient characterize the overall influence of cross drift shell motion on radiation belt dynamics.

When using diffusion theory to analyze data, it is instructive to express equation (2-30) as

$$\frac{\partial F}{\partial t} = L^2 \frac{\partial (D_{LL}/L^2)}{\partial L}\frac{\partial F}{\partial L} + D_{LL}\frac{\partial^2 F}{\partial L^2} \tag{2-31}$$

It can be seen that the diffusion rate scales with the first two derivatives of F. Measured data can be noisy, in which case the data needs to be fit to a smooth curve before determining these derivatives. While it is straightforward to fit noisy data with a function that describes F and $\partial F/\partial L$ well, there is usually ambiguity in determining $\partial^2 F/\partial L^2$, making it sometimes difficult in practice to determine the precise value of $\partial F/\partial t$ from radial diffusion.

In summary, the radial diffusion equation provides a description for the evolution of the distribution function that is valid on average over the drift phase. Working with a time resolution that is greater than the drift period is advantageous when it comes to describing radiation belts dynamics over long time scales (for instance, over many years), as this minimizes the computational resources required (e.g., Glauert et al. 2018, see also **Section 1.2.2**). On the other hand, the radial diffusion equation assumes that fluctuations in action variables are small $(\Delta J_3/J_3 \ll 1)$. It also relies on the assumption that the transition probability, P, as well as the distribution function, f, only depend on J_3 and are independent of the phase φ_3.

When the radial diffusion equation (2-30) applies, the distribution function evolves so as to smooth its radial gradient ($\partial F/\partial L = 0 \implies \partial F/\partial t = 0$). The distribution function F at the peaks decreases, and F in the valleys increases. That is why the formation of a local peak in the radial

profile of a population phase space density is usually viewed as the result of local processes (for instance: a local acceleration breaking either one or two of the first two adiabatic invariants, or a local loss).

Solving the radial diffusion equation in a simple analytic case

The most basic approach to study energetic particle measurements is to compare it to the assumptions that (1) no other processes occur besides radial diffusion, (2) radial diffusion scales with $D_{LL} = D_0 L^n$, and (3) a steady state with $\partial \mathrm{F} / \partial \mathrm{t} = 0$ is reached. Then, equation (2-30) is solved by

$$\begin{aligned} F &= AL^{3-n} + B \qquad \text{For } n \neq 3 \\ F &= A \ln(L) + B \qquad \text{For } n = 3 \end{aligned} \tag{2-32}$$

Phase space density profiles usually fall toward a magnetized planet (e.g., Paonessa 1985; Cheng et al. 1987, 1992; Schulz 1991; Kollmann et al. 2011). While this feature is indicative of additional sources or losses, it is important to point out that equation (2-32) illustrates that a falling profile alone does not mean that there are increasingly strong losses distributed along a path toward the planet.

The solution (2-32) requires two boundary conditions to determine its parameters A and B. These boundary conditions are able to implicitly impose non-diffusive processes that act outside of the considered region. A boundary condition with a straightforward physical interpretation is one that forces *F* to zero at a location of strong losses, like the planetary atmosphere. This boundary condition alone is able to explain generally falling phase space density profiles without the presence of distributed losses (like from an extended atmosphere or planetary ring) across the considered region.

The second boundary condition is often chosen at the outer boundary of the considered range. It represents an external reservoir of particles that diffuse into the considered region, but there is no direct relation to a physically meaningful source rate.

A signature for the onset of losses within the considered region, or any other process not described well by radial diffusion, is if the slope of a phase space density profile changes abruptly, which interestingly, is also found at all magnetized planets with radiation belts.

More realistic numerical solutions to the diffusion equation

Equation (2-32) is a solution to the diffusion equation in its simplest form and usually does not represent actual conditions in space realistically. Non-radial diffusion, as well as various sources and losses, need to be included (2-24). After compiling such a generalized diffusion equation, there is usually no longer an analytic solution for it (except for still very simple cases like in Thomsen et al. 1977), and the equation needs to be solved numerically. One detail that makes such a numerical calculation challenging is that different processes are assumed to conserve different variables that are used to parameterize the distribution function *F*: radial diffusion is assumed to conserve *M* and *J*, and energy diffusion and gradual energy loss are assumed to conserve α_{eq} and *L* and are usually expressed as a function of *E*, not the associated invariants. Similarly, pitch angle diffusion is usually defined in a way to conserve *E* and *L*. In such cases, it

is common to use two different grids to describe F. One is regularly spaced in M, J, and L, and it is used to describe radial diffusion. The results are then interpolated on a regularly spaced grid in E, α_{eq}, and L to compute the other diffusion modes (Varotsou et al. 2008; Subbotin and Shprits 2009).

2.3.3. Fälthammar's analytic expressions for radial diffusion through magnetic and electric potential disturbances

The objective of the very first theoretical works on radial diffusion in the Earth's radiation belts was to study the cumulative effect of many sudden impulses ("si") or storm sudden commencements ("ssc") with a time evolution similar to the one presented **Section 2.3.1** (that is, a sudden variation with a very short rise time, followed by a slow return to the initial configuration) (e.g. Parker 1960, Davis and Chang 1962). Fälthammar (1965, 1968) made fewer assumptions on the time variations of the fields. He described radial diffusion analytically, in a more general – yet still simplified – way. Because these works have been central to radial diffusion research, they are the object of this section.

In Fälthammar's works, two different drivers for radial diffusion are discussed separately: (1) magnetic disturbances and (2) electric potential disturbances. In both cases, the assumption is that the background field is a magnetic dipole field. Idealized electric and magnetic field fluctuations are introduced to describe small drift motion perturbations. In the following, as well as in **Section 4.2.1**, we will calculate the diffusion coefficients resulting from magnetic and electric disturbances using two different approaches that we then compare in **Section 4.2.2**. It will be shown how the statistical properties of these field fluctuations determine the radial diffusion coefficient.

Radial diffusion through magnetic disturbances

Magnetic field distortions in the Earth's outer magnetosphere are due to currents flowing on the magnetopause, on the neutral sheet, and within the magnetosphere (Schulz and Lanzerotti 1974). The Mead magnetic field model accounts for the permanent compression of the magnetosphere by the solar wind (Mead, 1964). In Fälthammar's works, the magnetic field considered is a simplified Mead geomagnetic field model, with a disturbance field $\boldsymbol{b}$ superimposed to the background dipole field. This disturbance consists of a symmetric part (S) – which is independent of magnetic local time –, and an asymmetric part (A) – which depends on local time. In spherical coordinates (r, θ, φ), with r the geocentric distance, θ the colatitude measured from the pole, and φ the azimuthal angle measured from the midnight meridian and counted positive eastward, the field perturbation vector expressed in the spherical base $(\boldsymbol{e_r}, \boldsymbol{e_\theta}, \boldsymbol{e_\varphi})$ is:

$$\boldsymbol{b} = \begin{pmatrix} S(t)\cos\theta + A(t)\, r \sin 2\theta \cos\varphi \\ -S(t)\sin\theta + A(t)\, r \cos 2\theta \cos\varphi \\ -A(t)\, r \cos\theta \ \sin\varphi \end{pmatrix} \quad (2\text{-}33)$$

This vector describes magnetic field distortions. This field model is curl-free by design, which is a limit to its use (currents within the magnetosphere are omitted).
In the equatorial plane, it is:

$$\boldsymbol{b}\left(r, \theta = \frac{\pi}{2}, \varphi\right) = -(S(t) + A(t)\, r \cos\varphi)\, \boldsymbol{e_\theta} \tag{2-34}$$

(e.g., Fälthammar 1965, 1968). Assuming frozen-in flux conditions, the induced electric field $\boldsymbol{E_{ind}}$ associated with the magnetic disturbance $\boldsymbol{b}$ is

$$\boldsymbol{E_{ind}} = \begin{pmatrix} -\frac{r^2}{7}\frac{dA}{dt}(t)\sin\theta\sin\varphi \\ \frac{2r^2}{7}\frac{dA}{dt}(t)\cos\theta\sin\varphi \\ -\frac{r}{2}\frac{dS}{dt}(t)\sin\theta + \frac{2r^2}{21}\frac{dA}{dt}(t)(3 - 7\sin^2\theta)\cos\varphi \end{pmatrix} \tag{2-35}$$

With these expressions, it is straightforward to derive the radial component of the drift velocity of equatorial particles, to first-order approximation in $|\mathrm{b}/\mathrm{B_d}|$:

$$\frac{dr}{dt} = \frac{E_{ind,\varphi}}{B_d} - \frac{M}{q\gamma B_d r_o}\frac{\partial b}{\partial \varphi} \tag{2-36}$$

where r_o is the initial unperturbed value of the particle radial location, $B_d = B_E R_E^3/r_o^3$ is the amplitude of the magnetic dipole field at the equatorial radial distance r_o, M is the relativistic magnetic moment, and γ is the Lorentz factor. In this model, the electric and magnetic perturbations are small in the sense that their contribution to the drift motion is much smaller than the contribution of the magnetic gradient.
For an equatorial particle trapped in the Earth's dipole field, the angular drift velocity is the angular magnetic drift velocity, and it is equal to $\Omega = 3M/(\gamma q r_o^2)$. With the drift phase φ reformulated in terms of angular drift velocity ($\varphi(t) = -\Omega t + \varphi_0$), the radial displacement for an equatorial particle initially located at r_o with a phase φ_0 is:

$$\begin{aligned} r(t) - r_o = &-\frac{5}{7}\frac{r_o^2\Omega}{B_d}\int_0^t A(\xi)\sin(\Omega\xi - \varphi_0)\, d\xi - \frac{r_o}{2B_d}\big(S(t) - S(0)\big) \\ &-\frac{8}{21}\frac{r_o^2}{B_d}(A(t)\cos(\Omega t - \varphi_0) - A(0)\cos(\varphi_0)) \end{aligned} \tag{2-37}$$

where ξ is another parameter describing time.
This expression is only valid in its current form if there are no other contributions to the drift velocity, particularly no significant contribution from corotation drift, as it is important at the fast

rotating gas giant magnetospheres where it can cancel out the magnetic drifts (Roussos et al. 2018b).

With the exception of the integral term in (2-37) that we define here as

$$X(t) = -\frac{5}{7}\frac{r_o^2 \Omega}{B_d}\int_0^t A(\xi)\sin(\Omega\xi - \varphi_0)d\xi \quad (2\text{-}38)$$

all the other terms on the right-hand side of equation (2-37) are bounded, and these terms are of the order of $b/B_d \ll 1$. Thus, only $X(t)$ can potentially lead to large cumulative effects. Therefore, it is important to take a closer look at this integral.

- If the signal A has frequencies close to the angular drift velocity Ω, the amplitude of the integral X can increase with time, and the radial displacement can become significant.
- The integral $X(t)$ only depends on the signal A, i.e., it only depends on the asymmetric perturbations of the magnetic field. This result is understandable given that symmetric variations of the fields cannot broaden drift shells (see also **Sections 2.3.1** and **5.2.1**), thus they cannot contribute to radial diffusion.
- The integral $X(t)$ consists of the partial integration of two nearly equal contributions: (1) the induced electric field (first term in equation (2-36)) contributes 8/21 of the 5/7 factor in the radial displacement (i.e. about 55%), and (2) the magnetic disturbance (second term in equation (2-36)) contributes 1/3 of the 5/7 factor in the radial displacement (i.e. about 45%). Thus, one cannot arbitrarily omit the induced electric fields when evaluating radial diffusion caused by magnetic disturbances.

In theory, equation (2-37) can be used to determine $r(t)$ for each particle, which can then be used to construct the full particle distribution function without the need for involving a diffusion formalism and accepting its approximations. In practice, such an approach is not possible (outside of a numerical model that traces particles) because the real field perturbations are not well known. So Fälthammar assumed that $A(t)$ are realizations of a stationary stochastic process. In other words, A fluctuates randomly, and its statistical properties are time-independent. In particular, because the background field is the dipole field, the mean of A is zero.
In that context, after a time, t, that is much longer than the autocorrelation time of the signal, A, and much longer than the particle drift period, $2\pi/\Omega$, the expected value of the square displacement $(r(t) - r_o)^2$ grows linearly with time, t. Thus, over a long period of time, t, the expected value of the square displacement per unit time will be constant and will be identical for all initial drift phases, φ_0:

$$\langle (r(t) - r_o)^2 \rangle = \frac{d}{dt}[(r(t) - r_o)^2] = cst. \quad (2\text{-}39)$$

where the symbol [ ] denotes the expectation value and the symbol ⟨ ⟩ denotes the average change per unit time. It is this constant rate of change value that determines the radial diffusion coefficient D_{LL}.

$$D_{LL} = \frac{1}{2}\langle\left(\frac{r(t) - r_o}{R_E}\right)^2\rangle \tag{2-40}$$

This step is crucial as it turns individual particle motions, $r(t)$, that in principle are deterministic (but in reality not well known) into a stochastic parameter that drives the time evolution of the distribution of particles (a quantity that can be measured).
With the idealized models chosen, the radial diffusion coefficient for this case is:

$$D_{LL,m,eq} = \frac{1}{2}\left(\frac{5}{7}\right)^2\left(\frac{r_o^2\Omega}{R_E B_d}\right)^2\int_0^\infty [A(t)A(t+\xi)]\cos(\Omega\xi)d\xi \tag{2-41}$$

where the subscript, m, indicates that radial diffusion is driven by magnetic disturbances, and the subscript, eq, refers to equatorial particles. Because A is a stationary signal, $[A(t)A(t+\xi)]$ is independent of time, t. It only depends on the lag, ξ. For ξ greater than the autocorrelation time of A, $[A(t)A(t+\xi)]$ is zero, and the integration over ξ can be extended to infinity.

By introducing $P_A(\Omega)$, the power spectrum of the asymmetric field perturbation, A, evaluated at the angular drift velocity, Ω:

$$P_A(\Omega) = 4\int_0^\infty [A(t)A(t+\xi)]\cos(\Omega\xi)d\xi \tag{2-42}$$

we obtain that:

$$D_{LL,m,eq} = \frac{1}{8}\left(\frac{5}{7}\right)^2\frac{R_E^2 L^{10}}{B_E^2}\Omega^2 P_A(\Omega) \tag{2-43}$$

In terms of magnetic drift frequency ($\nu = \Omega/2\pi$), the diffusion coefficient is also

$$D_{LL,m,eq} = \frac{\pi^2}{2}\left(\frac{5}{7}\right)^2\frac{R_E^2 L^{10}}{B_E^2}\nu^2 P_A(\nu) \tag{2-44}$$

In the case of randomly occurring events with a very short rise time and a very long recovery time, the power spectrum of the signal, A, is proportional to ν^{-2}. In that case, the ν terms cancel so that the radial diffusion coefficient is proportional to L^{10} ($D_{LL,m,eq} \propto L^{10}$), and it is independent of energy.

More generally, if the power spectrum of the signal, A, is proportional to ν^{-n}, the variations of the radial diffusion coefficient with normalized equatorial radial distance, L, first adiabatic invariant, M, or kinetic energy, T, are the following:

$$D_{LL,m,eq} \propto L^{6+2n} M^{2-n} \propto L^{12-n} T^{2-n} \tag{2-45}$$

The expression to the right is only true for non-relativistic equatorial particles and the assumed dipole field. In other words, the so often assumed L^{10} variation of $D_{LL,m,eq}$ results from: (1) a specific model for the magnetic field disturbance, where the asymmetric perturbations of the field are proportional to L, and (2) a specific regime for the time variations of the fields, with a random succession of events with a very short rise time and a very long recovery time.

For a given kinetic energy, the radial diffusion coefficient $D_{LL,m}$ for off-equatorial particles is proportional to the diffusion coefficient in the equatorial case $D_{LL,m,eq}$ (Fälthammar 1968; Schulz and Lanzerotti 1974)

$$D_{LL,m} = \Gamma(\alpha_{eq}) D_{LL,m,eq} \tag{2-46}$$

where $\Gamma(\alpha_{eq})$ is a multiplying factor that depends strongly on the pitch angle at magnetic equator, α_{eq}. $\Gamma(\alpha_{eq})$ is obviously equal to 1 in the equatorial case ($\alpha_{eq} = 90°$), and it is close to 0.1 for the most field-aligned particles. A representation of this pitch-angle multiplying factor is provided **Fig. 7**.

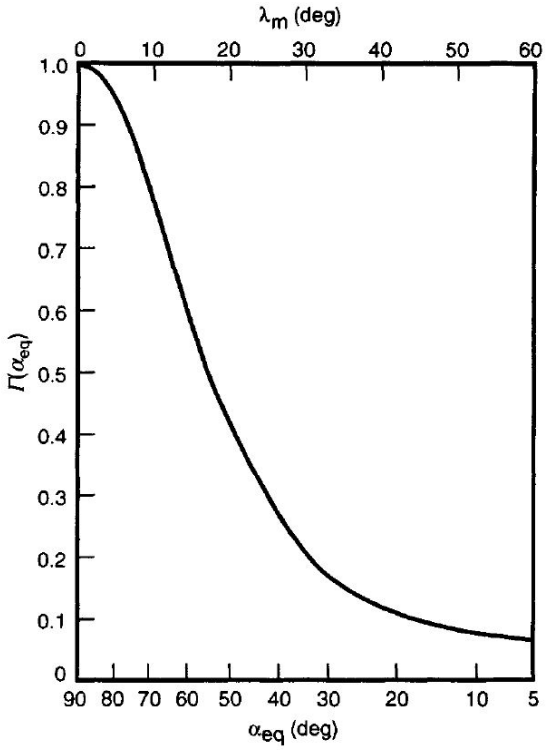

Fig. 7 Pitch-angle factor $\Gamma(\alpha_{eq})$ for the radial diffusion coefficient driven by magnetic fluctuations, as a function of the equatorial pitch angle α_{eq} and the mirror latitude λ_m. For a given energy, the diffusion coefficient decreases up to a factor of 10, as the equatorial pitch angle decreases (Walt 1994).

In comparison, the angular drift velocity does not vary much with equatorial pitch angle (less than a 50% difference between the angular drift velocities of equatorial and field-aligned particles for a given energy – e.g, Schulz 1991). Therefore, the pitch angle dependence of $D_{LL,m}$ is described by $\Gamma(\alpha_{eq})$. It shows that equatorial particles diffuse more efficiently than off-equatorial particles in the case of magnetic disturbances.

Radial diffusion through electric potential disturbances

Similar calculations can be applied to the case of electric potential disturbances ($\boldsymbol{\nabla} \times \boldsymbol{E} = \mathbf{0}$) in the absence of magnetic field perturbations. The background magnetic field is a dipole. We specify only the component of the electric field fluctuation that leads to radial motion: the azimuthal component. It is described by a partial Fourier sum around r_o:

$$E_\varphi(r_o, \varphi, t) = \sum_{n=1}^{N} E_{\varphi n}(t) \cos(n\varphi + \gamma_n) \tag{2-47}$$

where the phases γ_n do not vary with time t. Equation (2-47) can be used to represent a time-dependent dawn-to-dusk electric field, for example.

If there are no other electric fields besides E_φ, or if there is a purely radial corotational electric field (**Section 3**), the radial component of the drift velocity of equatorial particles is:

$$\frac{dr}{dt} = \frac{E_\varphi}{B_d} \tag{2-48}$$

The quantities $E_{\varphi n}(t)$ are assumed to be individually and jointly stationary and ergodic, so that $[E_{\varphi n}(t)] = [E_{\varphi n}(t+\tau)]$, $[E_{\varphi m}(t-\tau)E_{\varphi n}(t)] = [E_{\varphi m}(t)E_{\varphi n}(t+\tau)]$ and these quantities are independent of *t*, both when $m = n$ and $m \neq n$.

The fluctuating part of the electric field is:

$$\tilde{E}_{\varphi n}(t) = E_{\varphi n}(t) - [E_{\varphi n}] \tag{2-49}$$

From these fluctuations, the diffusion coefficient is:

$$D_{LL,e} = \frac{1}{2}\left(\frac{1}{R_E B_d}\right)^2 \sum_{n=1}^{N} \int_0^{\infty} \left[\tilde{E}_{\varphi n}(t)\tilde{E}_{\varphi n}(t+\xi)\right] \cos(n\Omega\xi)\, d\xi \quad (2\text{-}50)$$

where the subscript e in $D_{LL,e}$ stands for electric potential disturbances, and Ω stands for the angular drift velocity. The equation (2-50) accounts for radial diffusion driven by electric field fluctuations. With $P_E(n\nu)$, the power spectrum of the nth harmonic of the electric field fluctuations evaluated at the nth harmonic of the drift frequency ν, the diffusion coefficient is

$$D_{LL,e} = \frac{L^6}{8R_E^2 B_E^2} \sum_{n=1}^{N} P_E(n\nu) \quad (2\text{-}51)$$

This expression is valid for all equatorial pitch angles.

The radial diffusion coefficient driven by electric field fluctuations varies with L^6, provided that $\sum_{n=1}^{N} P_E(n\nu)$ is independent of L. The drift frequency ν does not vary much with equatorial pitch angle. Therefore, unless $P_E(n\nu)$ varies strongly with frequency, radial diffusion driven by electric field fluctuations is nearly independent of equatorial pitch angle for particles of a given kinetic energy.

Radial diffusion as an aggregate

In Fälthammar's work, electric potential disturbances and magnetic disturbances are discussed separately because they are thought to originate from different sources. In practice, when both diffusion mechanisms are concurrent, it is assumed that they are uncorrelated. Therefore, it is usually assumed that the total radial diffusion coefficient D_{LL} can be written as the sum of the two different diffusion coefficients:

$$D_{LL} = D_{LL,m} + D_{LL,e} \quad (2\text{-}52)$$

This representation requires an artificial division of the electric field perturbation into two parts: an induced component, which is accounted for in $D_{LL,m}$, and an electric potential component, whose statistical properties define $D_{LL,e}$. This can pose a limit to the implementation of these formulas. Indeed, an electric field measurement is always the sum of induced and electrostatic components, and their individual contributions can be difficult to evaluate.

2.4. Methods to quantify radial diffusion

2.4.1. Solving the Fokker-Planck equation to quantify radial diffusion

Early works relied on particle flux measurements to solve the Fokker-Planck equation, assuming that radial distribution of the radiation belts was determined exclusively by radial diffusion and

loss processes. The radial diffusion coefficient was adjusted so that the modelled distribution would fit observations.

Assuming a time-stationary distribution, the objective was to fit the average radial distribution of the trapped particles. This technique was first applied by Nakada and Mead (1965) in the case of trapped protons in the outer belt (**Fig. 2**). In the presence of time-varying radial structures in the belts, the objective was to reproduce the observed time evolution of the radial distribution. This was done to investigate the inward motion of electrons with $E \geq 1.6$ MeV during a geomagnetically quiet time interval of ten days following the magnetic storm of December 17-18, 1962 (Newkirk and Walt 1968a, **Fig. 1**). This technique was also applied in the years following the Starfish injection in the inner belt to account for the fact that the observed decay rate was 20 times smaller than the decay rate deduced from atmospheric scattering theory (Newkirk and Walt 1968b; Farley 1969a, 1969b). In all cases, the resulting radial diffusion coefficients were no more than tentative estimates. Early determinations of the radial diffusion coefficient would generally discuss the ambiguity of the approach.

Indeed, the soundness of the method relies on the validity of a multitude of criteria and assumptions. In practice, the validity of these criteria and assumptions remains uncertain. Below are a few examples of the intrinsic difficulties in determining radial diffusion coefficients directly from particle flux measurements.

- Conditions must be such that the Fokker-Planck equation is likely to apply. In particular, the assumption that field disturbances cause small drift motion perturbations must be valid (**Section 2.3.2**). Therefore, large injection events must be excluded from the analysis.
- There must be strong radial gradients in the particle population distribution so that the radial diffusion coefficient can be determined.
- It is usually necessary to assume that the radial diffusion coefficient is time-independent during the time interval considered.
- The radial diffusion coefficient must be the only unknown. Uncertainty in the importance of other processes leads to uncertainty in the value of the radial diffusion coefficient.
- Solving the Fokker-Planck equation requires setting boundary conditions or arbitrary constants of integration (see, for instance, equation (2-32)).
- The drift-averaged distribution function, f, must be determined accurately. This can be a major difficulty when particle measurements are scarce, or when the magnetic field geometry is uncertain, such as in the outer belt (e.g. Green and Kivelson 2004).

Even though methods were designed to circumvent some of these difficulties (Lanzerotti et al. 1970), limitations remained (Walt and Newkirk 1971; Lanzerotti et al. 1971).

Additional information on early methods for determining radial diffusion coefficients from particle data is provided in Walt's review of radial diffusion (1971b). Technical details are discussed thoroughly in Schulz and Lanzerotti's book, in particular Chapter 5 (1974).

2.4.2. Analyzing magnetic and electric field disturbances to quantify radial diffusion in the Earth's radiation belts

Magnetic field disturbances

Early quantifications of radial diffusion driven by magnetic field fluctuations were based on a restrictive version of the simplified Mead geomagnetic field introduced in **Section 2.3.3** (equation (2-33)). In this model, $S(t)$ and $A(t)$ are not independent parameters. Instead, they are both constrained to be directly related to the geocentric stand-off distance to the subsolar point on the magnetopause $\mathscr{b}(t)$:

$$S = B_1 \frac{R_E^3}{\mathscr{b}^3} \tag{2-53}$$

with $B_1 = 0.25\ G$, and

$$A = -B_2 \frac{R_E^3}{\mathscr{b}^4} \tag{2-54}$$

with $B_2 = 0.21\ G$. For typical solar wind conditions, $\mathscr{b} \sim 10\ \mathrm{R_E}$ (e.g., Mead 1964; Nakada and Mead 1965; Schulz and Eviatar 1969). The asymmetric part of the fluctuation is proportional to the symmetric part of the fluctuation ($\Delta A = -4B_2 \Delta S/(3B_1 \mathscr{b})$), and so are the power spectra:

$$P_A = \frac{16}{9}\left(\frac{B_2}{B_1}\right)^2 \frac{1}{\mathscr{b}^2} P_S \tag{2-55}$$

where P_A is the power spectrum of the asymmetric field perturbation and P_S is the power spectrum of the symmetric part of the fluctuation. In that context, the radial diffusion coefficient equation (2-43) is also

$$D_{LL,m,eq} = 2\Omega^2 \left(\frac{5B_2}{21 B_E B_1}\right)^2 L^{10} \left(\frac{R_E}{\mathscr{b}}\right)^2 P_S(\Omega) \tag{2-56}$$

(e.g. Lanzerotti and Morgan 1973). It is worth noticing that $4B_2/3B_1\mathscr{b} \sim 0.1 R_E^{-1}$. In other words, a fluctuation of the stand-off distance of the magnetopause $\Delta\mathscr{b}$ is more noticeable in the symmetric fluctuation of the magnetic field ΔS than in the asymmetric fluctuation of the magnetic field ΔA. This indicates that the symmetric part of the fluctuation is more readily measured. Consequently, the equation (2-56) is preferred to equation (2-43) when it comes to quantifying radial diffusion driven by magnetic disturbances.

The power spectrum of the symmetric part of the fluctuation P_S can be estimated using satellite measurements. This was done, for instance, by Lanzerotti et al. (1978), who analyzed magnetic field variations measured by the ATS 6 satellite at geostationary orbit during the month of

August 1974. Noticing a dependence of magnetic power with the *Kp* index, they provided radial diffusion coefficients at $L = 6.6$ as a function of geomagnetic activity.

At orbits other than the geostationary orbit, spacecraft cross different L shells in a short time. This complicates the power spectrum analysis. Thus, efforts have been made to derive the symmetric fluctuation power spectrum, P_S, from ground observations. For instance, Nakada and Mead (1965), and later Lanzerotti and Morgan (1973), considered that the disturbance in the horizontal (H) component of the magnetic field measured on the ground is about 50% larger than the symmetric fluctuation at the magnetic equator. Therefore, they assumed that the symmetric fluctuation power spectrum P_S is proportional to the power spectrum of the horizontal component of the magnetic field fluctuations measured on the ground. Nakada and Mead (1965) analyzed ground-based measurements of the frequency and amplitude of both sudden impulses and sudden commencements to quantify radial diffusion. Lanzerotti and Morgan (1973) analyzed power spectra of geomagnetic field fluctuations measured by conjugate stations near L=4, for approximately 6 days in December 1971, and 12 days in January 1972. Once again, their analysis revealed a strong dependence of magnetic power with geomagnetic activity.

Brautigam and Albert's formulation of radial diffusion driven by magnetic disturbances

From the discrete values determined at $L = 4$ by Lanzerotti and Morgan (1973), and at $L = 6.6$ by Lanzerotti et al. (1978), Brautigam and Albert (2000) determined a parameterization of the radial diffusion coefficient as a function of L and Kp index – an index chosen to quantify geomagnetic activity. A L^{10} dependence of the radial diffusion coefficient was assumed, even though the experimental data points at $L=4$ and $L = 6.6$ did not display such dependence. A least squares fitting technique was implemented to determine $D_0^M(Kp) = D_{LL,m,eq}L^{-10}$. It resulted that

$$D_{LL,m,eq}^{B\&A}(L, Kp) = 10^{(0.506Kp-9.325)}L^{10} \ \ (day^{-1}) \qquad (2\text{-}57)$$

where "*B&A*" stands for Brautigam and Albert's empirical law for radial diffusion. Discrepancies between the modelled values and the experimental values are within a factor of 6. Despite this apparent lack of representativeness, modern radiation belt simulations that use Brautigam and Albert's empirical law for radial diffusion equation (2-57) yield plausible results when solving the Fokker-Planck equation (e.g. Kim et al. 2011). That is why this empirical law became a well-accepted reference quantification for radial diffusion in the Earth's radiation belts.

Electric potential disturbances

Estimates of radial diffusion driven by electric potential disturbances (equation (2-51) **Section 2.3.3**) suffered from a lack of in-situ measurements. Early works by Cornwall (1968) and Birmingham (1969) quantified radial diffusion driven by electric potential disturbances by postulating functional forms for the autocorrelation function. They considered that the most important mode for electric field fluctuations was the fundamental mode of a uniform dawn-to-dusk electric field (n=1 equation (2-47) **Section 2.3.3**), and they provided estimates for the

average amplitude of the fluctuations (a few tenths of $\mathrm{mV/m}$) and for the correlation time (an hour).
Hours of DC electric field fluctuations measured by an array of balloons, located near $L = 6$ at approximately 30 km altitude, were analyzed and mapped to the magnetic equator to provide an estimate of the radial diffusion coefficient at that location (Holzworth and Mozer 1979). Electric field measurements obtained by balloons indicated that the magnetospheric electric field power spectrum depends on geomagnetic activity (Kp index), but not L nor local time (Mozer 1971). Direct evaluation of electric field power spectral densities was first provided by the Combined Release and Radiation Effects Satellite (Brautigam et al. 2005). Yet, unrealistic outputs were obtained when the coefficient for radial diffusion driven by electric potential disturbances was included in modern radiation belt simulations (e.g. Kim et al. 2011). Therefore, it became common practice to omit this process and to consider that radial diffusion is mainly driven by magnetic disturbances, as described by Brautigam and Albert (2000). In other words, it is now common practice to assume that $D_{LL} = D_{LL,m}^{B\&A}$, when modeling the Earth's radiation belt dynamics.

There are many published compilations of the radial diffusion coefficients determined during that era (see, for instance, Fig. 20 in the article by West et al., 1981). They show a clear scattering among all possible values at any given L shell. Consistency among the various theoretical and experimental radial diffusion coefficient estimates suggests that the underlying theory is valid.

3. EXPANSION: Radial diffusion beyond Earth

3.1. Radial diffusion drivers most relevant for the giant planets

The mathematical formalism of radial diffusion (equation (2-30)) is a universal concept that can arise at any magnetized planet, not just Earth. Because planets and their magnetospheres differ, the drivers of radial diffusion can be different, and we discuss several mechanisms below (namely, the ionospheric winds, the interchange process, and the corotation cancellation). Our focus will be on Jupiter and Saturn, because these are the best studied giant magnetized planets.

3.1.1. Ionospheric fields and thermospheric winds

A difference between Earth and the giant planets is that corotation plays a much larger role because the giant planets have larger magnetospheres coupled to ionospheres rotating with the planets at faster speeds. Jupiter is the most extreme case: It enforces azimuthal plasma speeds of at least half the rigid corotation up to distances as great as 50 planetary radii (which is outside its intense radiation belts) and yields speeds up to 500 km/s (Waldrop et al. 2015) (therefore comparable to nominal solar wind speeds). Different to Earth, a theoretical plasmapause of

Jupiter and Saturn would be beyond the dayside magnetopause, meaning that the entire magnetosphere is rotation-dominated (Mauk et al. 2009). The magnetospheric plasma approximately corotates with the ionospheric plasma because it is roughly frozen-in (Hill 1979). The ionosphere is forced to corotation due to friction with the dense atmosphere and therefore the planet itself. Thus, ionospheric plasmas roughly corotate with Jupiter and Saturn (Cowley et al., 2003, 2004), which is very different from the two cell convection pattern of the Earth's high latitude ionosphere (Cowley 1982).

Corotation yields a radial electric field that results in electric drifts ($\boldsymbol{E} \times \boldsymbol{B}/B^2$) of charged particles. Corotation, as well as any other electric field, does not yield diffusion as long as the fields are constant (see, for instance, equation (2-50), **Section 2.3.3**). However, if the ionospheric electric field changes for whatever reason over time, this affects the particle drifts in a way that can be described with radial diffusion. Mechanisms to explain how the ionospheric electric field can change are time variable winds or turbulence directly in the ionosphere (Brice and McDonough 1973), or reconnection affecting the polar caps (Coroniti 1974).

Theory

Several authors have studied the effect of varying ionospheric fields in a magnetic dipole field under different assumptions (Jacques and Davis 1972; Brice and McDonough 1973; Coroniti 1974). All of them yield radial diffusion coefficients with a *L*-shell dependence that ranges from $L^2(L-1)$ to L^5, which is weak compared to what was discussed in **Section 2.3**.
Here we follow Jacques and Davis (1972) to present an illustration of the concept in a time-stationary dipole field.

Let us assume that the footpoint of a dipole field line in the ionosphere is shifted over *N* steps due to an arbitrary process. Each step takes the time, t_1, and changes the location by $\Delta\theta$ in co-latitude. In a dipole field, with θ, the magnetic colatitude of the field line footpoint, we have

$$L = 1/sin^2\theta \tag{3-1}$$

This is because the ionosphere is at radial distance, $r = 1R_P$, with the planetary radius, R_P, and because *L* is normalized to the planet radius, R_P, and therefore dimensionless. Differentiating equation (3-1), it follows that

$$\Delta L/\Delta\theta = -2L(L-1)^{1/2} \tag{3-2}$$

As $\Delta\theta$ describes a stochastic process that can move θ in any direction, we can then calculate the radial diffusion coefficient according to equation (2-29).

$$D_{LL} = \frac{2L^2(L-1)[\Delta\theta^2]}{Nt_1} \tag{3-3}$$

It can be seen that radial diffusion under these assumptions scales with $L^2(L-1)$ and the properties of the fluctuation $[\Delta\theta^2]$ that are not known and therefore usually pragmatically assumed to be independent of L.

Coroniti (1974) calculates radial diffusion in a different way, by considering fluctuating dawn-dusk electric fields following dayside reconnection. The result is $D_{LL} \propto L^3$, and scales therefore similarly as in equation (3-3). The absolute value of D_{LL} can, in principle, be calculated from the reconnection period and duration, but these values are difficult to measure.

Brice and McDonough (1973) calculate a radial diffusion coefficient from electric potential fluctuations that arise from turbulence in the ionosphere. They find $D_{LL} \propto L^3$ for corotating particles with small magnetic drifts, $D_{LL} \propto L^{3.5}$ for non-relativistic particles with large magnetic drifts, and $D_{LL} \propto L^5$ for relativistic particles with large magnetic drifts. Again, there are no absolute values available from theory as the electric potential changes cannot be directly measured.

Experimental evidence

The mechanism suggested by Brice and McDonough (1973) is time-dependent winds in the ionosphere. Wind patterns can be affected by changes in solar extreme ultraviolet (EUV) heating. Signatures of changes in the radial diffusion coefficient have been observed following enhanced (Tsuchiya et al. 2011) or variable (Kollmann et al. 2017) EUV irradiance at Jupiter and Saturn. These observations indicate that radial diffusion may indeed be somehow related to ionospheric winds. Note that this does not mean that all intensity changes need to result from changes in the intensity of radial diffusion and/or EUV, as there are other reasons for that (de Pater et al., 1995; Roussos et al., 2018b).

A more literal test of the theory above is to calculate radial diffusion coefficients and compare their L-dependence with theory. Small exponents, between 2 and 4, are able to reproduce measurements of MeV electrons and protons at Jupiter (Birmingham et al. 1974; Mogro-Campero 1976; de Pater et al. 1994; Nénon et al. 2017; 2018) and MeV electrons at Saturn (Lorenzato et al. 2012), consistent with radial diffusion resulting from ionospheric winds, as discussed above. keV electrons (Roussos et al. 2007) and MeV protons (Kollmann et al. 2017) at Saturn do behave differently and show exponents in the range of 6 to 10, which is more consistent with the mechanisms discussed in **Section 2** that had been initially developed for Earth but should be applicable to some degree at all magnetized planets. The differences in exponents suggest that the diffusion coefficient may have additional dependencies on energy, L-shell, particle mass, or time, and that the ionospheric wind mechanism described above is only dominating in a limited range of these parameters. Han et al. (2018), for example, found evidence that diffusion from ionospheric winds needs to be combined with diffusion from dawn-dusk magnetospheric electric field perturbations driven by the solar wind (equation (2-51)) in order to explain the long-term dependence of Jupiter's electron belts.

There is no consistent picture on the actual parameter range yet. When considering model-data comparisons, it is important to keep in mind that several other processes besides radial diffusion (diffusion in other modes, interaction with neutral material, etc.) have to be incorporated in the models. Not all parameters are well known, and only a few studies made an effort to test how sensitive their result is on the diffusion exponent.

3.1.2. Interchange

Another difference of Jupiter and Saturn from Earth is that these gas giants are orbited by moons that release material that is ionized and fills the magnetosphere. The mass of this plasma cannot accumulate forever but needs to be shed from the system. This can be done through interchange.

The interchange process

Interchange is the plasma equivalent of the Rayleigh Taylor instability: a dense liquid on top of a lighter liquid is not a stable configuration, and both liquids will eventually interchange positions. In the case of a fast rotating magnetosphere, as that of the giant planets, the driving force is the sum of gravity and centrifugal force. Parcels of plasma interchange their location if

$$\frac{\partial \eta}{\partial L} < 0 \tag{3-4}$$

where η is the flux tube content (number of particles on a magnetic flux tube) per magnetic flux (Southwood and Kivelson 1987; Ma et al., 2019).

$$\eta = \int n \frac{ds}{B} = \frac{NL^2}{2\pi B_P R_P^2} \tag{3-5}$$

n is the particle number density, B the space-dependent magnetic field, and ds an infinitesimal length along the field line. The expression to the right is the flux shell content per magnetic flux within L to $L + \Delta L$ (Siscoe et al. 1981a, b), and the equality is true for a dipole field (Sittler et al., 2008). N is the number of particles on a flux shell with "unit" extent $\Delta L = 1$, B_P is the magnetic field on the equatorial planetary surface, and R_P is the planetary radius. Flux tube, flux shell content, and this content normalized by magnetic flux are not always carefully distinguished.

For a weak centrifugal force with large pressure gradients in the magnetosphere, interchange can also occur for

$$\frac{\partial (pV^\gamma)}{\partial L} > 0 \tag{3-6}$$

where p is the thermal plasma pressure, V the flux shell volume, and γ the specific heat ratio (Southwood and Kivelson 1987). Such interchange may be one of the drivers (Pontius and Wolf 1990; Sergeev et al. 1996) of bursty bulk flows at the Earth (Baumjohann et al. 1990).

Note that interchange only occurs in certain regions in L, and only up to certain energies. It is only observed outward of the moons Io and Enceladus (Dumont et al. 2014; Azari et al. 2018), which is expected based on $\partial\eta/\partial L$ (Sittler et al. 2008; Bagenal et al. 2016). It is only observed up to energies of hundreds of keV, which is expected because high-energy particles have fast magnetic drifts out of the corotating and inwardly moving flux tube (Paranicas et al. 2016).

The interchange process is radially asymmetric (Hill et al. 2005; Chen et al. 2010): Inward transport occurs relatively quickly through narrow channels or small bubbles. Outward transport is slow and occurs over wide longitude ranges. Most studies on interchange are on its inward component as it leaves obvious "injection" signatures in plasma, radiation, energetic neutrals, fields, and wave measurements (Mitchell et al. 2015). The net outflow, alternatively, is less studied (Waldrop et al. 2015) and is even below detection limit in the regions where Saturn's interchange injections are observed (Wilson et al. 2013).

It has been suggested to describe interchanges as a diffusive process. Indeed, the inward transport resulting from interchange is roughly consistent with phenomenological diffusion coefficients at Jupiter (Krupp et al. 2005, their equation 7). Below, we first summarize the justification of describing interchange through diffusion, and then discuss the issues of this approach.

Diffusion from interchange

According to equation (2-29), the diffusion coefficient scales with $[(\Delta L)^2]$ – the expected value of $(\Delta L)^2$ – and Δt – a characteristic time for the interchange process. We will not be able here to constrain $(\Delta L)^2$ from theory, but we will calculate the timescale Δt, which will then immediately scale a diffusion coefficient that is used to describe the net effect of interchange.

Let us assume that a plasma parcel of size ΔL interchanges with another parcel, and in the process moves by ΔL. Recent studies show that injections transport particles inward over $\Delta L/L \leq 0.2$ (Krupp et al. 2005; Paranicas et al. 2016), while the outward portion is difficult to observe (Chen et al. 2010). A small $\Delta L/L$ is required because the derivation of the diffusion formalism uses a Taylor expansion that is only a good approximation for $\Delta L/L \ll 1$ (see also equation (2-14)).

During the interchange process, the net centrifugal energy, *U,* is released over the time, Δt, of the interchange process. The energy released is dissipated in the ionosphere due to the currents that are set between the magnetosphere and the ionosphere during interchange. It can be calculated as (Summers and Siscoe 1985)

$$\frac{U}{\Delta t} = 2\int_0^{\rho} J_r\, E_r\, dA \qquad (3\text{-}7)$$

where $J_r = E_r \sum$ is the radial current density that scales with the height-integrated Pedersen conductivity $\sum$. $E_r = B_{pol} v$ is the radial electric field that scales with the polar magnetic field $B_{pol} \approx 2B_P$ and the interchange bulk flow speed $v = 2\pi r/\Delta t$. $dA = 2\pi r\, dr$ is an infinitesimal area that is integrated over the injection flux tube of radius ρ. The factor 2 equation (3-7) is included to take account of both hemispheres. Inserting everything in equation (3-7) yields (Summers and Siscoe 1985)

$$\frac{1}{\Delta t} = \frac{U}{(2B_P \pi \rho^2)^2\, 4\pi \sum} \tag{3-8}$$

We identify $2B_P \pi \rho^2$ in (3-8) as the magnetic flux, Φ, in the equatorial interchange cell that equal to flux, $2B_P R_P^2 \Delta\theta^2$, on the planetary surface. This can be related to the step size in L if we approximate equation (3-2) with $\Delta\theta \sim -\Delta L/(2L^{3/2})$ (Siscoe and Summers 1981).

Let us now determine U in order to provide an absolute value of the radial diffusion coefficient. The centrifugal energy of a shell with ΔL per enclosed magnetic flux in the initial configuration shall be $E_1 = \widetilde{M}_1 \Omega^2 R_1^2/2 + \widetilde{M}_2 \Omega^2 R_2^2/2$, and the equivalent quantity of the final configuration $E_2 = \widetilde{M}_1 \Omega^2 R_2^2/2 + \widetilde{M}_2 \Omega^2 R_1^2/2$, where $\widetilde{M} = m\eta$ is the mass of particles on a flux shell with extent $\Delta L = 1$ per magnetic flux, with m being the single particle mass. Ω is the angular rotation frequency of the planet. The released energy per magnetic flux $U_c^* = U/\Phi$ is (Siscoe et al. 1981b)

$$U_c^* = E_2 - E_1 = -\frac{\Omega^2 m}{2\pi B_P} \frac{d(NL^2)}{dL}\, \Delta L^2\, L \tag{3-9}$$

To calculate the second equality, we used $R_2^2 - R_1^2 = (R_1 + \Delta R)^2 - R_1^2 \sim 2R_1\, \Delta R$ to approximate the difference in distance and $R_1 \sim L R_p$. We also expressed the difference in masses through $\widetilde{M}_2 - \widetilde{M}_1 = \left(d\widetilde{M}/dL\right)\Delta L$.

Combining equations (2-29), (3-8), (3-9) yields (Summers and Siscoe 1985)

$$D_{LL,i} = \frac{-m\Omega^2 L^4}{8\pi^2 B_P^2 R_P^2 \sum} \frac{d(NL^2)}{dL} [(\Delta L)^2] = D_i \frac{d(NL^2)}{dL} \quad \text{for } \frac{d(NL^2)}{dL} < 0 \tag{3-10a}$$

$$D_{LL,i} = 0 \quad \text{for } \frac{d(NL^2)}{dL} \geq 0 \tag{3-10b}$$

The second equality in equation (3-10a) is a definition for the proportionality constant D_i. We distinguish between (3-10a) and (3-10b), because interchange only occurs for $d(NL^2)/dL < 0$.

Interchange acts on the bulk plasma. A diffusion equation for interchange therefore does not use the phase space density at fixed 1st and 2nd adiabatic invariants but uses instead η or NL^2. Like the phase space density, η is a conserved quantity during transport. This is because n does not

change (in the absence of sources or losses removing particles) and because interchange conserves magnetic flux.

In equation (2-30), the diffusion coefficient is independent of the particle distribution, meaning that the efficiency of the physical drivers of radial diffusion is independent of particle distribution. The drivers provide each single particle with the same chance of moving inward or outward. Yet if there are more particles at one J_3 than at another (i.e., if the distribution function radial gradient is nonzero), it will look as if the particles were behaving so as to smooth the radial gradient of the distribution function. Therefore, $\partial f/\partial t$ depends on f, even though D_{LL} does not usually depend on it. Interchange-driven diffusion is different. Its diffusion equation is nonlinear in the sense that the diffusion coefficient itself depends on the particle distribution (equation (3-10)), so that the efficiency of the physical drivers of radial diffusion is already a function of particle distribution.

$$\frac{\partial(NL^2)}{\partial t} = L^2 \frac{\partial}{\partial L}\left(\frac{D_i}{L^2}\left(\frac{d(NL^2)}{dL}\right)^2\right) \tag{3-11}$$

Equations (2-30) and (3-11) yield a different overall behavior: Equation (2-30) smoothes out any L-gradient in the distribution function F, and Equation (3-11) only smoothes out $d(NL^2)/dL < 0$ L-gradients.

For a steady state with $\partial(NL^2)/\partial t = 0$, no additional sources or losses, and assuming $D_i \propto L^m$, equation (3-11) is solved by a power law

$$NL^2 = \frac{A}{L^{\frac{m}{2}-2}} + B \tag{3-12}$$

which is, coincidentally, formally the same as the equivalent solution of the diffusion equation (2-30) given in equation (2-32). This similarity between the solutions disappears when sources or losses are added to equation (3-11).

Challenges

There has been a discussion if and to what extent the diffusion formalism is applicable to interchange (Hill 1983; Southwood and Kivelson 1989; Pontius and Hill 1989), for example because interchange may be better described through a systematic convection flow pattern instead of random motions.

NL^2 used in equation (3-11**)** is a quantity that describes the bulk plasma, summing over all energies and species. This is why equation (3-11**)** is used to model plasma distributions (Sittler et al. 2008; Jurac and Richardson 2005). Radiation belt studies are interested in the high energy population that does not contribute significantly to NL^2. In case of interchange, generalizing (3-11) to distinguish invariants is not that straightforward. Higher energy particles can be included

in the above formalism as a second population with flux shell content N^*L^2 (Siscoe et al. 1981b). This population contributes to the interchange energy, U, not through its mass and centrifugal energy U_c. Instead, the radiation component U_R to the interchange energy U contributes through the change in internal energy density u due to adiabatic heating and the change in flux tube volume V when interchanging parcels 1 and 2 between the initial state (index i) and final state (index f).

$$U_R = \left(u_{1f}V_{1f} + u_{2f}V_{2f}\right) - \left(u_{1i}V_{1i} + u_{2i}V_{2i}\right) \tag{3-13}$$

The L-dependence of this expression can be evaluated through $V \propto L^4$ for a dipole field, $u = 3p/2$ when treating the energetic particles as an ideal gas, and $pV^\gamma = cst.$ for adiabatic compression of that gas (Gold 1959). Repeating the same derivation for the diffusion coefficient as above but now combining $U=U_c+U_R$ leads to a diffusion coefficient of the form (Summers and Siscoe 1985)

$$D_{LL,i2} = D_i \frac{d(NL^2)}{dL} + D_{i2} \frac{d(N^*L^2)}{dL} \tag{3-14}$$

This new diffusion coefficient couples NL^2 and N^*L^2, each of which needs to described by two separate diffusion equations sharing the same $D_{LL,i2}$ that need to be solved self-consistently.

Even N^*L^2 is not sufficient for radiation belt studies that are interested in the phase space density at specific values of the 1st and 2nd adiabatic invariants or their equivalent quantities. There is no readily available diffusion coefficient for these cases. The diffusion coefficients in equations (3-10) and (3-14) do not account for the energy dependence of the interchange. The latter occurs because the actual transport does not involve the whole flux shell but occurs in narrow flux tubes. High-energy particles quickly leave the flux tube due to their magnetic drift (different to the low-energy, corotating plasma), meaning that increasingly energetic particles will have smaller $[(\Delta L)^2]$ and are not efficiently transported through interchange (Paranicas et al. 2016). Such particles with fast magnetic drifts will relatively frequently pass through interchange flow channels. The magnetic field in these channels is enhanced compared to the background magnetospheric field within the plasma sheet and depleted above it (Lai et al. 2016). As the magnetic gradients are steep, they may change L^* of the passing particles, depending on the bounce phase.

In summary: it is under debate whether interchange can be described with the diffusion formalism in the first place. In either case, there is no sufficient theoretical basis to describe energy or invariant resolved distribution functions, as it is needed for many practical applications. It remains an open question how to implement interchange injections into magnetosphere models that use radial diffusion.

3.1.3. Corotation cancellation

Another difference between Earth, Jupiter and Saturn is that the orientation of the magnetic field relative to the direction of the planetary rotation is opposite. While this at first appears to be an unimportant detail, it may, in fact, be a game changer for the transport of radiation belt electrons.

Theory

The total drift of a charged particle around a planet is the sum of a magnetic drift, due to the gradient and the curvature of the magnetic field, plus an electric drift, due mainly to the corotation electric field that arises when the planet is conducting and rotating (see, for instance, equation (2-3) in the equatorial case). The corotation electric drift only depends on the planetary rotation period and distance to the planet and is the same for all particle species. The direction and value of the magnetic drifts depend on the orientation of the planetary's magnetic field and the particle energy and charge. It is, therefore, possible that corotation and magnetic drifts cancel each other out so that particles become stationary in their azimuthal location if they have the right energy. This energy condition is sometimes referred to with the generic term "resonance." If the electrons are close to this resonance, where these drifts cancel out, they follow banana orbits that are not centered around the planet but orbit around a point away from the planet (Cooper et al. 1998).

In the case of Earth, corotation cancellation occurs for keV protons and therefore does not play a role at radiation belt energies (e.g. Korth et al. 1999). Jupiter and Saturn both have their magnetic dipole moments oriented opposite to how it is at Earth. This means that corotation cancellation occurs for electrons, not protons. The corotation cancellation energy is L-shell dependent and is < 10 MeV at Saturn and < 200 MeV at Jupiter (Roussos et al. 2018).

Local time stationary electrons are sensitive to any local time fixed electric field component beyond the steady, radial corotation field. Perturbations in the total electric field will change the L-shell of the electrons, depending on their initial azimuthal location (Selesnick et al. 2016; Roussos et al. 2018). The change in L-shell is significant for corotation-resonant electrons and vanishes away from the corotation cancellation energy (**Fig. 8**). When the electric field stops changing, the changes in L-shell also stop. This behavior is equivalent to the scenario described in **Fig. 6**, following a compression of the magnetosphere. It can therefore be described through radial diffusion using a generalized version of equation (2-50) that accounts for the corotation drift (Han et al. 2018), instead of only using the magnetic gradient drift that is sufficient at Earth.

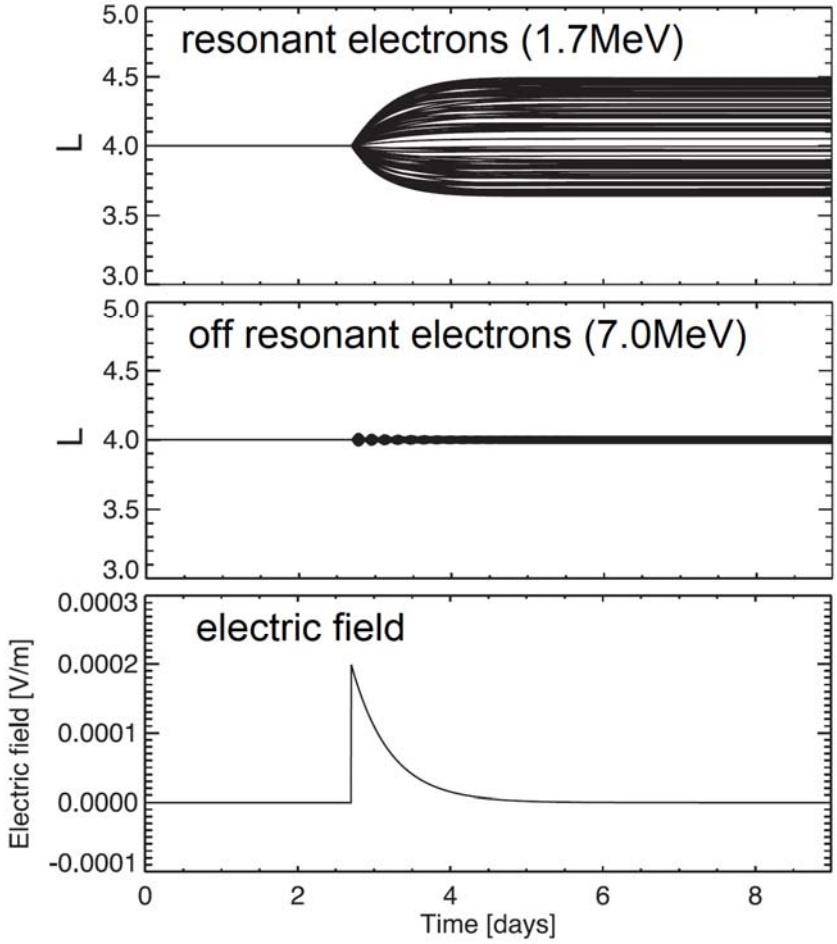

Fig. 8 Guiding center traces of electrons starting at different local times under the action of a time-dependent electric field (lower panel). It can be seen that resonant electrons with energies where corotation and magnetic drifts cancel out strongly change their *L*-shell (upper panel), while electrons of other energies (example shown in the middle panel) are less affected. The change in location as a response to field changes is similar to what was sketched in **Fig. 6**. Figure adapted from (Roussos et al. 2018).

Experimental evidence

Saturn's electron radiation belt is highly dynamic. It shows abrupt enhancements following corotating interaction regions, coronal mass ejections, and tail reconnection (Roussos et al. 2014, 2018). These enhancements decay over several weeks (Roussos et al. 2018). This behavior can be qualitatively reproduced by tracing particles under changes in the electric field (see **Fig. 8**) that are consistent with field changes that have been observed (Andriopoulou et al. 2014). So far there has been no attempt made to reproduce this through a diffusion coefficient calculated through equation (2-50).

Also, Jupiter's electron belt shows dynamics on the timescale of days (de Pater et al. 1995; Tsuchiya et al. 2011). There has been a case study discussing in-situ observations where the

enhancement was only near energies where corotation cancelled out (Roussos et al. 2018), supporting a highly energy-dependent radial transport resulting from corotation cancellation. Electron spectra at both Jupiter and Saturn show intensity cutoffs at energies in the MeV range that depend on magnetospheric location in a similar way as corotation cancellation does, supporting the theory (Kollmann et al. 2018; Sun et al. 2019).

3.2. Phenomenological radial diffusion coefficients

Methods

Radial diffusion coefficients at the giant planets can be determined phenomenologically from fitting measured moon absorption signatures under the assumption that the absorption occurs solely due to collisions with the insulating body of a moon, which is then refilled by radial diffusion (Van Allen et al. 1980b, **Section 2.2.3**). These assumptions are valid for Saturn's inner moons like Tethys and Mimas (Roussos et al. 2007), and some of Jupiter's moons like Amalthea (Fillius et al. 1974) or Callisto. It might still be approximately valid for moons with ionospheres like Enceladus or Europa (Mogro-Campero 1976). It obviously breaks down at Ganymede, which has an internal magnetic field, and Io, where absorption at the moon body is insufficient and additional losses like pitch angle diffusion are needed (Nénon et al. 2017). The signatures that these latter moons leave in the particle measurements may still be used to constrain radial diffusion, but this requires us to first properly describe the particle loss/deflection that occurs in their direct vicinity.

If theoretical radial diffusion profiles are fit to measured radial phase space density curves, the moon macrosignatures must be deep, as is the case for Saturn's proton belts (Kollmann et al. 2013; **Fig. 5 Section 2.2.3**), in order to robustly estimate the radial diffusion coefficient. There have been attempts to fit more subtle moon signatures (Hood 1983). However, fitting extended regions where supposedly only radial diffusion is acting is challenging. The solution to a radial diffusion equation (2-28) without further sources or losses requires two boundary conditions (**Section 2.3.2**; Thomsen et al. 1977). In the absence of a strong moon absorption, there is no physically preferred location from which to choose the boundary conditions. One may select them in a region where one expects radial diffusion to happen and then calculate the solution for a larger L range. Comparison between this solution and the measurements may reveal regions where non-diffusive processes, like moon losses, occur, that can then be further analyzed, for example to determine the diffusion coefficient. However, the diffusion solution is very sensitive to the boundary conditions: A small change in the phase space density at one location used as a boundary condition can cause strong changes at another location, as calculated from the radial diffusion equation. Robust solutions therefore require phase space density gradients that are steeper than the variability in the solutions due to the different boundary conditions.

Besides in-situ particle measurements, one can also use remote observations of synchrotron emission to determine diffusion coefficients. This technique is most feasible for the high electron intensities close to Jupiter (Hegedus et al. 2020). These measurements can be compared or fit to a physical model that includes radial diffusion (Nénon et al. 2017).

When fittingmeasured phase space density profiles or synchrotron emission with diffusion models, it is important that transport in the fit region is indeed occurring dominantly through radial diffusion, and that all other source and loss processes, like energy loss in dense plasma, rings, and neutral tori, are properly accounted for. Large parts of the magnetospheres of Jupiter and Saturn show signatures of radial transport through injection events (Clark et al. 2016; Azari et al. 2018) and it is still questionable to model injection transport with diffusion (**Section 3.1.2**).

Results

Diffusion coefficients are usually fit well with power laws $D_{LL} \propto L^n$. At Jupiter, there is evidence for $2 < n < 4$, and at Saturn for $6 < n < 10$ (**Section 3.1.1**).

Absolute values for diffusion coefficients can be found, for example, in Mogro-Campero (1976); Van Allen (1984); de Pater and Goertz (1994); Roussos et al. (2007); Tsuchiya et al. (2011); Kollmann et al. (2013); Nénon et al. (2017, 2018); Han et al. (2018). Values for ions and electrons do not seem to differ significantly. There is a scatter in the calculated values by an order of magnitude or more, even when comparing results using the same method. This suggests that diffusion is time-dependent. It has not been studied whether this apparent time dependence can be organized through another quantity, like the magnetic activity index Kp at Earth for instance (e.g., Lanzerotti and Morgan 1973; Lejosne et al. 2013; Ali et al. 2016).

4. EVOLUTION: Why and how did radial diffusion research evolve in the Earth's radiation belts?

4.1. Motivation

4.1.1. Improved spatial and temporal resolutions for radiation belt observations

In the 1990s, the spatial and temporal resolutions of radiation belt observations improved significantly. Complex structures and rapid dynamics were revealed thanks to a growing network of satellites and ground stations providing multipoint measurements (with data from the Polar spacecraft, the Global Positioning System GPS satellites, the Solar Anomalous and Magnetospheric Particle Explorer SAMPEX, the Combined Release and Radiation Effects Satellite CRRES, the Geostationary Operational Environmental Satellite System GOES, the Wind spacecraft close to the L1 Lagrange point, the Canadian array of ground instruments CANOPUS, etc.). These new sets of observations led to a reassessment of the traditional description of the Earth's radiation belts provided by the Fokker-Planck equation.

In particular, it was noticed that relativistic electron fluxes near geostationary orbit could increase significantly (by a couple orders of magnitude), much faster than expected (on a timescale ranging from a couple of hours to a couple of days). Given the strategic importance of

geostationary orbit, understanding the dynamics of these "killer" electrons became a priority (e.g., Baker 1994). A good correlation between ultra-low frequency (ULF) wave power and enhanced relativistic electron fluxes was found near geostationary orbit (Rostoker 1998, Mathie and Mann 2000). Thus, mechanisms involving ULF waves were proposed to explain large and rapid enhancements of outer belt relativistic electron fluxes during geomagnetic storms. While some of the proposed processes required pitch angle scattering (e.g., Liu et al. 1999; Summers and Ma 2000), the ULF wave drift resonance theory proposed an explanation consistent with the conservation of the first two adiabatic invariants.

4.1.2. Drift resonance to account for outer belt relativistic electron flux enhancements

The ULF wave drift resonance theory provides a mechanism by which electrons can be continuously accelerated and transported towards the Earth by the work of a time-varying electric field. The process was first proposed by Hudson et al. (1999). It was then developed by Elkington et al. (1999, 2003).

In this model, equatorial electrons are drifting in an asymmetric time-stationary magnetic field, similar to the magnetic field model introduced in **Section 2.3.3** (**Fig. 9, Left**). Because the magnetic field depends on local time, the time-stationary drift contour of an electron population is not circular, as it would be in a dipole. The electrons drift away from the Earth from midnight to noon, and they drift towards the Earth from noon to midnight. Thus, the radial electric field oscillation of a toroidal ULF wave (E_r **Fig. 9, Left**) works on the particles ($q\boldsymbol{E} \cdot \boldsymbol{V_D} \neq 0$). This leads to a variation of the particle kinetic energy. Indeed, the energy equation is:

$$\frac{dW}{dt} = M\frac{\partial B}{\partial t} + q\boldsymbol{E} \cdot \boldsymbol{V_D} \tag{4-1}$$

where W is the notation for the kinetic energy of the equatorial electron guiding center chosen by Elkington et al. (1999, 2003), M is the first invariant, $\boldsymbol{E}$ is the electric field, and $\boldsymbol{V_D}$ is the drift velocity.
In the studies, the effect of the associated magnetic field oscillations is neglected. Thus,

$$\frac{dW}{dt} = q\boldsymbol{E} \cdot \boldsymbol{V_D} \tag{4-2}$$

If the electric field variations are such that $q\boldsymbol{E} \cdot \boldsymbol{V_D}$ is always positive, the electrons interacting with the ULF wave will experience a net energy gain. The magnitude of this energy gain depends on the power delivered along the drift trajectory. Thus, it is a function of the angle between the radial electric field, $\boldsymbol{E}$, and the drift velocity, $\boldsymbol{V_D}$. In the presence of a radial electric field of constant amplitude, the angle between the electric fields $\boldsymbol{E}$ and the drift velocity $\boldsymbol{V_D}$ depends on the radial component of the magnetic drift velocity ($-M\boldsymbol{\nabla}B \times \boldsymbol{B}/\gamma q B^2$). Thus, it depends on the magnetic field distortion ($\partial B/\partial\varphi$). The more asymmetric the magnetic field is, the more distorted the drift shell is, and thus, the more power is delivered. Similarly, the

azimuthal electric field oscillation of a poloidal mode ULF wave also works on the particles. Thus, a resonant interaction between an electron and a poloidal mode wave can exist under certain special conditions (Elkington et al. 2003; Perry et al. 2005, 2006).

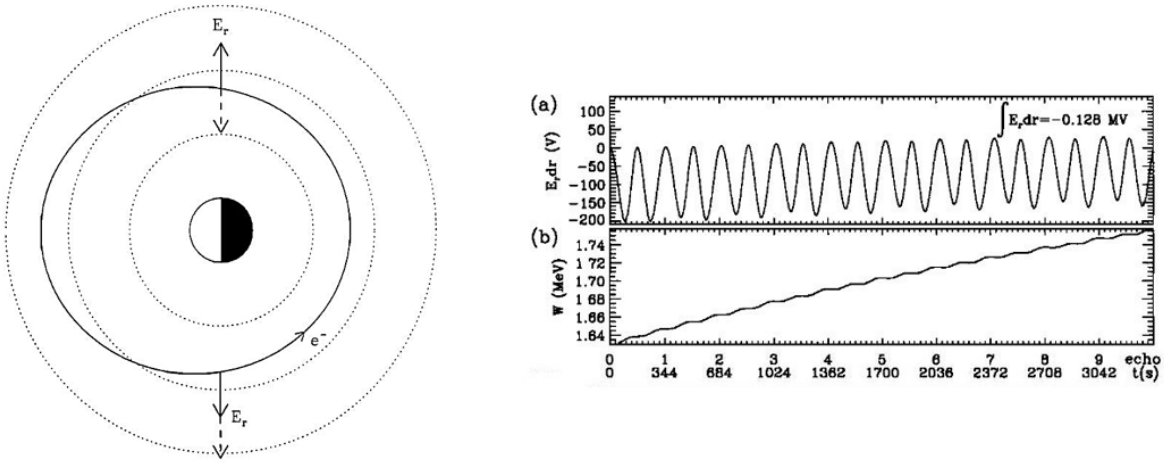

Fig. 9 (Left) Drift contour of an equatorial electron trapped in an asymmetric time-stationary magnetic field and orientation of the radial electric field oscillation of a toroidal ULF wave. The solid arrows show the orientation of the electric field at t = 0 for an electron starting at dusk, and the dashed arrows indicate the electric field direction half a drift period later. (Right) (a) Numerical evaluation of a quantity proportional to the work of the electric field $(\mathbf{E} \cdot \mathbf{V_D})$dt and (b) evolution of the particle kinetic energy (W) as a function of time. The electric field is always pointing outward when the electron is drifting radially inward, and it is inward when the electron is drifting outward. Thus, $q\mathbf{E} \cdot \mathbf{V_D}$ is always positive, and the electron is continuously gaining energy as it drifts around Earth. Left: (Hudson et al. 1999). Right: (Elkington et al 1999).

In all cases, the drift resonance mechanism characterizes the action of a monochromatic oscillation in one single global mode. It is important to remember that the drift resonance theory was proposed to suggest a process by which radiation belt particles would rapidly gain significant energy, while conserving their first two adiabatic invariants. Drift resonance requires a monochromatic oscillation in a single mode. This mechanism differs from the core mechanism for radial diffusion.

The connection between drift resonance and radial diffusion comes from the theoretical considerations that (re-)emerged at the time of the analysis of drift resonance: namely that the most asymmetric background field would lead to the most efficient energization mechanism. Indeed, from the analysis of drift resonance processes, Elkington et al. (2003) suggested that the asymmetric nature of the background magnetic field could lead to a form of enhanced radial diffusion in the presence of multiple ULF frequencies (i.e., in the presence of a broadband ULF wave). It is this suggestion that motivated the derivation of a new set of analytic expressions for radial diffusion: the analytic expressions by Fei et al (2006).

1771
1772 It is interesting to note that Schulz and Eviatar (1969) had already analyzed radial diffusion
1773 driven by magnetic disturbances in the case of a slightly asymmetric background magnetic field.
1774 They found that in the case of a slightly asymmetric background field, the value of the radial
1775 diffusion coefficient is proportional to the power spectrum of the field fluctuations at all
1776 harmonics of the drift frequency, although the first harmonic remains the main contributor. In a
1777 background dipole field, only the first harmonic of the power spectrum of the magnetic
1778 fluctuations contributes to radial diffusion. Thus, experimental works following Schulz and
1779 Eviatar's study assumed a background magnetic dipole field. As shown in the following, Fei et
1780 al.'s (2006) study had similar consequences: subsequent works relying on Fei et al.'s formulas
1781 also assumed a background magnetic field.
1782

1783 ## 4.2. New analytic expressions for radial diffusion
1784

1785 ### 4.2.1. Fei et al.'s analytic expressions for radial diffusion
1786
1787 New expressions for the radial diffusion coefficients were proposed by Elkington et al. (2003),
1788 and further developed by Fei et al. (2006) to include the effect of an asymmetric background
1789 magnetic field. Because of the popularity of these formulas, the assumptions underlying the
1790 various resulting expressions for radial diffusion are highlighted in the following paragraph.
1791 However, the magnetic and electric contributions to diffusion in Fei formalism are not self-
1792 consistent, leading to problems discussed in **Section 4.2.2**.
1793
1794 *Time-stationary asymmetric magnetic field model*
1795 The background magnetic field model considered is the superposition of a dipole field and a
1796 time-stationary asymmetric disturbance. In the equatorial plane, the magnitude of the magnetic
1797 field B_0 at a location (r, φ) is:
1798

$$B_0 = \frac{B_E R_E^3}{r^3} + (\Delta B)\cos\varphi \tag{4-3}$$

1799
1800 where ΔB is a small perturbation: $(\Delta B) r^3 / B_E R_E^3 \ll 1$.
1801 The unperturbed drift contour for equatorial radiation belt particles at Earth is characterized by
1802 $B_0 = \text{cst.}$ (see also **Section 5.1.1**). With the magnetic field model chosen for equation (4-3), the
1803 equation of the drift contour is:
1804

$$r(\varphi) = r_o\left(1 + \frac{\Delta B}{3B_E R_E^3} r_o^3 \cos\varphi\right) \tag{4-4}$$

1805
1806 where r_o is the average radius of the drift contour.
1807
1808 *L^* as the normalized average radius of the time-stationary drift contour*

Because the magnetic field is assumed to be time-stationary, the third adiabatic coordinate L^* is regarded as a spatial coordinate (see also **Section 5.1.1** for more info about L^*). For a radiation belt population of equatorial particles with an average radius of the drift contour equal to r_o, it is considered that L^* becomes the normalized average radius of the contour:

$$L^* = r_o/R_E \tag{4-5}$$

Differentiating the equation (4-4), the authors obtained that:

$$\frac{dL^*}{dr} = \frac{1}{R_E}\left(1 - \frac{4}{3}\frac{\Delta B}{B_E}L^{*3}\cos\varphi\right) \tag{4-6}$$

Thus, with Fei et al.'s model, a displacement of an equatorial particle away from the initial drift contour leads to a time variation of the L^* parameter:

$$\frac{dL^*}{dt} = \frac{dL^*}{dr}\frac{dr}{dt} \tag{4-7}$$

where dr/dt corresponds to the radial motion away from the drift contour driven by field fluctuations. In Fei et al.'s model, two different drivers for radial diffusion are discussed separately: (1) the magnetic field disturbances and (2) the electric field disturbances.

Magnetic disturbances

The magnetic field fluctuations are in the direction of the background magnetic field (compressional perturbations). They are described by a Fourier sum around r_o:

$$\delta B(r, \varphi, t) = \sum_{n=1} \delta B_n(t)\cos(n\varphi) \tag{4-8}$$

The radial drift motion driven by the magnetic field disturbances is equal to

$$\frac{dr}{dt} = -\frac{M}{q\gamma B_d r_o}\frac{\partial(\delta B)}{\partial\varphi} \tag{4-9}$$

where $B_d = B_E R_E^3/r_o^3$ is the amplitude of the magnetic dipole field at the equatorial radial distance r_o. Combining equations (4-6), (4-7), (4-8) and (4-9), it results that

$$\frac{dL^*}{dt}(r,\varphi,t) = \frac{ML^{*2}}{q\gamma B_E R_E^2}\sum_{n=1} n\delta B_n(t)\sin(n\varphi) - \frac{2}{3}\frac{ML^{*5}}{q\gamma B_E R_E^2}\frac{\Delta B}{B_E}\sum_{n=1} n\,\delta B_n(t)\sin\big((n+1)\varphi\big) - \frac{2}{3}\frac{ML^{*5}}{q\gamma B_E R_E^2}\frac{\Delta B}{B_E}\sum_{n=1} n\,\delta B_n(t)\sin((n-1)\varphi) \quad (4\text{-}10)$$

The resulting diffusion coefficient is obtained with an approach similar to the one proposed by Fälthammar (1965) (see also **Section 2.3.3**). The equation (4-10) is integrated between a time, $t = 0$, and a time, t, to obtain the variation of L^*. Then, the variation of L^* is squared.

$$\big(L^*(t) - L^*(0)\big)^2 = (a+b+c)^2 \quad (4\text{-}11)$$

where a, b and c are the integrals of the 3 terms on the right-hand side of the equation (4-10). It is then considered that the different integrals are uncorrelated, so that:

$$\langle\big(L^*(t) - L^*(0)\big)^2\rangle = \frac{d}{dt}\Big[\big(L^*(t) - L^*(0)\big)^2\Big] = \frac{d}{dt}[a^2] + \frac{d}{dt}[b^2] + \frac{d}{dt}[c^2] \quad (4\text{-}12)$$

where the symbol $\langle\ \ \rangle$ denotes the expected rate of change of the bracketed quantity, the symbol $[\ \ ]$ denotes the expectation value, and d/dt denotes the rate of change.
As a result, Fei et al. (2006) obtained a diffusion coefficient driven by compressional magnetic disturbances equal to:

$$D_{LL,b,eq} = \frac{M^2}{8q^2\gamma^2 B_E^2 R_E^4}L^{*4}\sum_{n=1} n^2 P_n^B(n\Omega) + \frac{2}{9}\frac{M^2}{q^2\gamma^2 B_E^2 R_E^4}\left(\frac{\Delta B}{B_E}\right)^2 L^{*10}\sum_{n=1} n^2 P_n^B((n+1)\Omega) + \frac{2}{9}\frac{M^2}{q^2\gamma^2 B_E^2 R_E^4}\left(\frac{\Delta B}{B_E}\right)^2 L^{*10}\sum_{n=1} n^2 P_n^B((n-1)\Omega) \quad (4\text{-}13)$$

where Ω is the angular drift velocity of the population considered, and P_n^B is the power spectrum of the nth harmonic of the magnetic field fluctuation δB:

$$P_n^B(\omega) = 4\int_0^\infty [\delta B_n(t)\delta B_n(t+\xi)]cos(\omega\xi)d\xi \quad (4\text{-}14)$$

The subscript b in $D_{LL,b,eq}$ indicates that the coefficient quantifies radial diffusion driven by magnetic disturbances according to Fei et al.'s model.
The first term on the right-hand side of equation (4-13) does not depend on the asymmetry of the *background* magnetic field ΔB. It characterizes radial diffusion in the case of a background dipole field, to which small, local, time-dependent, magnetic disturbances are superimposed (equation (4-8)). The second and third terms on the right-hand side of equation (4-13) characterize radial diffusion enabled by the asymmetry of the background field. Because they are proportional to $(\Delta \mathrm{B}/\mathrm{B_E})^2$, they are small in comparison to the first term (Fei et al. 2006).

Electric disturbances
The electric field disturbance is assumed to be in the azimuthal direction. It is described by a Fourier sum around $\mathrm{r_o}$:

$$\delta E_\varphi(r,\varphi,t) = \sum_{n=1} \delta E_{\varphi n}(t)\cos(n\varphi) \tag{4-15}$$

The motion driven by electric field fluctuations is:

$$\frac{dr}{dt} = \frac{\delta E_\varphi}{B_d} \tag{4-16}$$

And it results that

$$\begin{aligned}\frac{dL^*}{dt}(r,\varphi,t) = &\frac{1}{B_d}\sum_{n=1}\delta E_{\varphi n}(t)\cos(n\varphi)\\ &-\frac{2}{3}\frac{\Delta B}{B_d^2}\sum_{n=1}\delta E_{\varphi n}(t)\cos\big((n+1)\varphi\big)\\ &-\frac{2}{3}\frac{\Delta B}{B_d^2}\sum_{n=1}\delta E_{\varphi n}(t)\cos((n-1)\varphi)\end{aligned} \tag{4-17}$$

Following an approach similar to the one presented in the case of magnetic disturbances, the authors obtained that:

$$\begin{aligned}D_{LL,\epsilon.eq} = &\frac{L^{*6}}{8B_E^2R_E^2}\sum_{n=1}P_n^E(n\Omega)\\ &+\frac{2}{9B_E^2R_E^2}\left(\frac{\Delta B}{B_E}\right)^2 L^{*12}\sum_{n=1}n^2P_n^E\big((n+1)\Omega\big)\end{aligned} \tag{4-18}$$

$$+\frac{2}{9B_E^2R_E^2}\left(\frac{\Delta B}{B_E}\right)^2 L^{*12}\sum_{n=1} n^2 P_n^E((n-1)\Omega)$$

where P_n^E is the power spectrum of the n[th] harmonic of the electric field fluctuation δE_φ. The subscript ϵ in $D_{LL,\epsilon.eq}$ indicates that the coefficient quantifies radial diffusion driven by azimuthal electric disturbances according to Fei et al.'s model. The first term on the right-hand side of equation (4-18) does not depend on the asymmetry of the magnetic field ΔB. The second and third terms on the right-hand side of equation (4-18) characterize radial diffusion enabled by the asymmetry of the field. Because they are proportional to $(\Delta B/B_E)^2$, they are small in comparison with the first term.

Radial diffusion as an aggregate

When both electric and magnetic diffusion mechanisms are concurrent, it is assumed that their actions are uncorrelated. Therefore, Fei et al. (2006) assumed that the radial diffusion coefficient D_{LL} can be written as the sum of the two diffusion coefficients:

$$D_{LL,eq} = D_{LL,b,eq} + D_{LL,\epsilon,eq} \tag{4-19}$$

The subscript eq indicates that the coefficients have been computed in the case of equatorial particles. No theoretical description was proposed for non-equatorial particles.

4.2.2. A comparison between Fei et al.'s expressions and Fälthammar's formulas

Despite apparent similarities, none of the electric and magnetic diffusion coefficients derived by Fei et al. (2006) (**Section 4.2.1**) are identical to the electric and magnetic diffusion coefficients derived by Fälthammar (1965) (**Section 2.3.3**) (**Fig. 10**). By discussing the action of the magnetic field perturbations and the action of the induced electric fields separately, the underlying assumption of Fei et al.'s approach is that electric and magnetic perturbations are uncorrelated. The validity of this assumption is often wrongly attributed to Brizard and Chan (2001). Yet, it is inconsistent with Faraday's law ($\boldsymbol{\nabla} \times \boldsymbol{E} = -\partial \boldsymbol{B}/\partial t$).

Fei et al.'s formulas for radial diffusion are incorrect. They provide an underestimation of the total radial diffusion coefficient by a factor of 2 in the case of magnetic disturbances described by the simplified Mead model introduced **Section 2.3.3** (equation (2-33), in the absence of electrostatic potential fields – and forcing $S(t) = 0$ (Lejosne 2019). Given the uncertainties in measuring actual field fluctuations, this factor of 2 may not seem extremely important in its own right. Yet, it is enough to demonstrate the difference between the two coexisting formalisms.

Although Fei et al.'s formalism is inadequate from a theoretical standpoint, it is very convenient from a practical standpoint. It is indeed difficult to differentiate the induced and electrostatic components of an electric field measurement. This poses a serious problem when it comes to

applying Fälthammar's formalism to quantify radial diffusion. The same problem is circumvented when applying Fei et al.'s erroneous formalism.

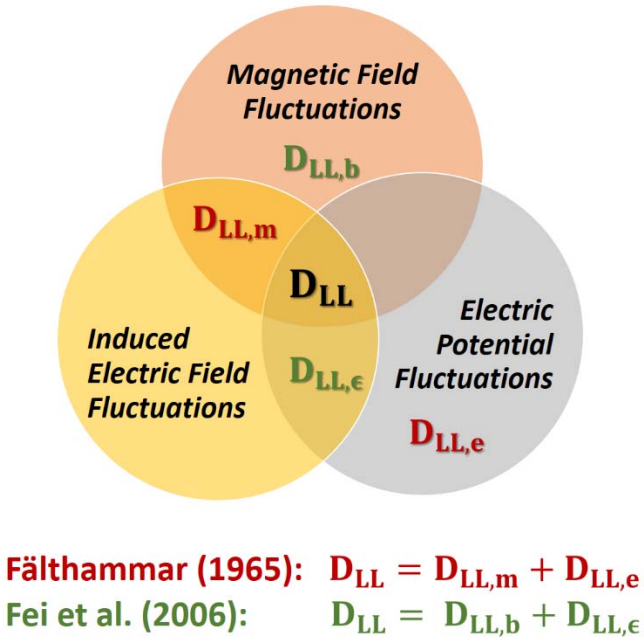

Fig. 10 Separating the field perturbations according to the nature of the source: different models of D_{LL} counted and combined different types of electromagnetic fluctuations (Lejosne 2019).

In all cases, the Fokker-Planck equation (equation (2-28) **Section 2.3.2**) calls for only one global radial diffusion coefficient to characterize the statistical properties of cross drift shell motion. It is represented in the center of **Fig. 9**. The cross drift shell motion is generated by all perturbations, regardless of their nature. Thus, the validity of the approach, which consists of dividing the radial diffusion coefficient into a sum of distinct contributions, is worth questioning. The artificial separation between electric potential disturbances and magnetic disturbances in Fälthammar's study was justified by the fact that these disturbances originate from different sources. In practice, the correlation between electric potential disturbances and magnetic disturbances is unknown. A potential correlation between these fluctuations would result in a global radial diffusion coefficient distinct from the sum of the different contributions.

4.3. Modern methods to quantify radial diffusion

Many modern studies rely on Fei et al.'s analytic expressions to quantify radial diffusion. Magnetohydrodynamics (MHD) simulations, ground-based data, and/or satellite measurements are analyzed to determine the power spectrum of the compressional component of the magnetic field, and the power spectrum of the azimuthal component of the electric field. These power spectra are then used to compute a magnetic diffusion coefficient and an electric diffusion coefficient, following equations (4-13) and (4-18), respectively. It is usually considered that the

background magnetic field is a dipole field ($\Delta B = 0$). Thus, only the first terms of the equations (4-13) and (4-18) are computed (e.g., Tu et al. 2012; Ozeke et al. 2012, 2014; Ali et al. 2015, 2016; Liu et al. 2016; Li et al. 2017; Jaynes et al. 2018b). The resulting electric diffusion coefficients $D_{LL,\epsilon,eq}$ are usually one or two orders of magnitude greater than the magnetic diffusion coefficients $D_{LL,b,eq}$, even though this result has been the object of discussion (e.g., Olifer et al. 2019).

Ozeke et al. (2014) analyzed many years of ground- and space-based measurements to derive new analytic expressions for the radial diffusion coefficients. The power spectrum of the azimuthal component of the electric field was derived from ground measurements of the D component (geomagnetic east-west) of the magnetic field, following a mapping method developed by Ozeke et al. (2009). The power spectrum of the magnetic field compressional component was derived from in situ measurements by the Active Magnetospheric Particle Tracer Explorers (AMPTE), GOES and the Time History of Events and Macroscale Interactions during Substorms (THEMIS) spacecraft. In-situ field measurements were used because, according to Ozeke et al. (2012), it is difficult to estimate compressional fields using ground data. Mapping approaches such as the one assumed by Lanzerotti and Morgan (1973) – discussed in **Section 2.4.2** – yield "results which are not a good representation of the in-situ data." Yet, the final radial diffusion parameterization obtained by Ozeke et al. (2014) is similar to Brautigam and Albert's formulation for radial diffusion driven by magnetic disturbances $D_{LL,m,eq}^{B\&A}$ (see also **Section 2.4.2**). In fact, the difference between radiation belt simulations with either of the two parameterizations for radial diffusion has been found to be negligible (Drozdov et al. 2017). The parameterization for radial diffusion according to Ozeke et al. (2014) is:

$$\begin{cases} D_{LL,b,eq}^{Oz}(L,Kp) = 6.62 \times 10^{-13} L^8 10^{-0.0327L^2+0.625L-0.0108Kp^2+0.499Kp} \\ D_{LL,\epsilon,eq}^{Oz}(L,Kp) = 2.16 \times 10^{-8} L^6 10^{0.217L+0.461Kp} \end{cases} \quad (4\text{-}20)$$

Where the unit is day^{-1} and "OZ" stands for Ozeke et al.'s empirical law for radial diffusion.

5. NAVIGATION: What are radial diffusion key concepts?

The objective of this section is to provide the essential toolkit to navigate radial diffusion research. It includes three principles:

(1) The appropriate coordinate to study radial diffusion is L^*;

(2) Radial diffusion requires violation of L^*;

(3) Radial diffusion is a formalism that trades accuracy for expediency.

In the following, we detail each of these different aspects, and we highlight the caveats and the challenges associated with each of them.

5.1. L^* is the appropriate coordinate to study radial diffusion

The terminology of "radial" diffusion is confusing, because it seems to imply that the variable of reference is the equatorial radial distance. However, this is inaccurate. The variable of reference is L^*. "Radial" is a misnomer that is used to date for historical reasons: there was a decade's worth of major works (e.g., Kellogg 1959b; Fälthammar 1965) before the adiabatic coordinate L^* was even introduced (Roederer 1970). L^* accounts for adjustments in particle drift motions that result from the difference between the real magnetic field and a magnetic dipole field under stationary conditions. In contrast, early works on radial diffusion were carried out assuming a background magnetic dipole field! The Fokker-Planck diffusion equation, whose inputs includes the radial diffusion coefficient, is set in adiabatic reference space. Thus, the appropriate coordinate to study radial diffusion is not radial distance, it is the third adiabatic invariant - or equivalently L^*.
In this section, we introduce the L^* coordinate, describe the characteristic features resulting from the distinction between L^* and normalized equatorial radial distance, and discuss the associated challenges.

5.1.1. Adiabatic theory of magnetically trapped particles and definition of the L^* coordinate

The analysis of radiation belt dynamics requires mapping measured particle fluxes into a three-dimensional adiabatic reference space (e.g. Roederer and Lejosne 2018, and references therein). The three adiabatic coordinates of this reference space (M, J, L^*) characterize the magnitudes of the three distinct pseudo-periodic motions of the trapped radiation belt population: (1) gyration perpendicular to the magnetic field direction (M), (2) bounce along equipotential magnetic field lines between mirror points (J) and (3) drift around the Earth (L^*). M and J are defined in **Section 2.1**.

Under stationary conditions, radiation belt particles are represented by guiding centers bouncing and drifting along closed surfaces called drift shells. The intersection of a drift shell with the minimum-B surface defines a closed curve called a drift contour (Γ). These notions are illustrated in **Fig. 11**.

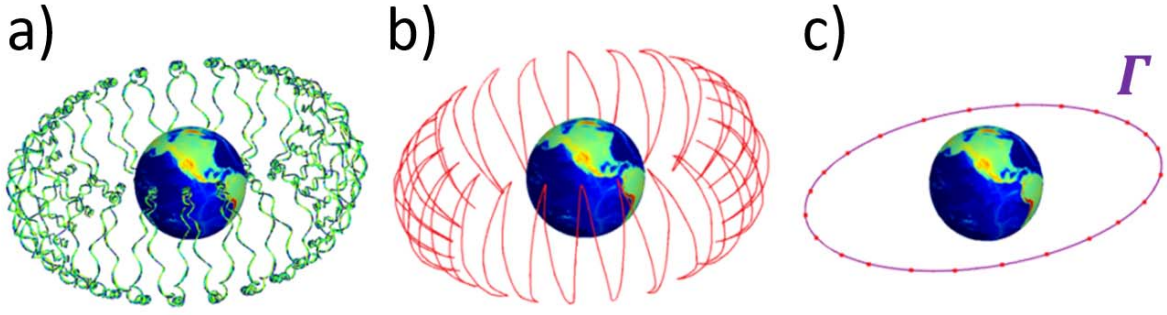

Fig. 11 An illustration of the path of a radiation belt particle trapped in the Earth's stationary magnetic field, with different levels of accuracy: a) Exact path of a radiation belt particle trapped in the Earth's magnetic field; b) Guiding center approximation: the guiding center bounces and drifts along its drift shell; c) Bounce-averaged description of the guiding center drift path: the intersection of the drift shell with the minimum-B surface is called the drift contour (Γ). The 3D diffusion-driven radiation belt models (equation (2-24) **Section 2.3.2**) are even more compact: they provide a description of the radiation belt dynamics that is averaged over the drift phase.

An adiabatic coordinate can vary if the forces acting on a particle vary on a timescale shorter than the corresponding period.

Definition of L^*:

The adiabatic invariants are calculated by an integral over the periodic motion. The third adiabatic invariant is

$$J_3 = \oint_{shell} (\boldsymbol{p} + q\boldsymbol{A}) \cdot \boldsymbol{dl} \tag{5-1}$$

where $\boldsymbol{p}$ is the particle's momentum, $\boldsymbol{A}$ is the local magnetic vector potential, and $\boldsymbol{dl}$ is the path length. The integral goes over the entire drift around the planet. If the particles do not surround the planet, J_3 cannot be computed, and L^* is not defined.

Because the contribution from the particle's momentum, $\boldsymbol{p}$, is negligible, the third adiabatic invariant is proportional to the magnetic flux, Φ, encompassed by the drift contour, Γ:

$$\Phi = \oint_{\Gamma} \boldsymbol{A} \cdot \boldsymbol{dl} \tag{5-2}$$

where $\boldsymbol{A}$ is the local magnetic vector potential and $\boldsymbol{dl}$ is the path length along the drift contour, Γ. Because the notion of magnetic flux is not very intuitive, Roederer (1970) introduced the adiabatic coordinate L^*, defined by the equation:

$$L^* = \frac{2\pi B_E R_E^2}{|\Phi|} \tag{5-3}$$

where $B_E = 30{,}000\ nT$ is the magnitude of the equatorial magnetic field at one Earth radius $R_E = 6{,}372\ km$. Note that other values have also been used throughout the years since the value of the Earth's dipole moment slowly varies with time.

Thus, L^* is a normalized quantity related to the magnetic flux encompassed by the drift contour of a given particle. Therefore, to determine L^*, it is necessary to determine the drift contour Γ.

Characterization of the drift contour Γ in the general case:

In a steady state, the total energy of the guiding center ε is constant along the drift contour Γ (e.g. Schulz and Lanzerotti 1974). In other words, for all bounce-averaged guiding center locations, $\boldsymbol{r}$, which are elements of Γ:

$$\varepsilon(\boldsymbol{r}) = T(\boldsymbol{r}) + qU(\boldsymbol{r}) = cst. \tag{5-4}$$

where U is the electrostatic potential (measured either at the mirror point or equivalently at the magnetic equator – U is constant along equipotential magnetic field lines), and T is the guiding center kinetic energy:

$$T = E_o \sqrt{1 + \frac{2MB_m}{E_o}} - E_o \tag{5-5}$$

where $E_o = m_o c^2$ is the rest mass energy (511 keV for an electron, 938 MeV for a proton), M is the relativistic magnetic moment, and B_m is the mirror point magnetic field intensity. Therefore, the definition of the drift contour depends on (1) the characteristics of the population considered (energy, charge, mass, pitch angle), and (2) the characteristics of the fields (magnetic and electric field geometry).

Characterization of the drift contour Γ for energetic particles:

For Earth's radiation belt populations, it is commonly assumed that the kinetic energy is so high that the effect of electrostatic potentials on trapped particle drift motion can be omitted ($T \geq 100\ keV \gg |qU|$, thus $\varepsilon \approx T$). As a result, the drift shell and the corresponding drift contour are characterized by the relation:

$$B_m(\boldsymbol{r}) = cst. \tag{5-6}$$

Therefore, the tracing of a drift contour related to a radiation belt population does not depend on the population charge, mass, or energy. It only depends on the magnetic field geometry and the population equatorial pitch angle.

It is important to keep in mind that this approximation can break down, even at Earth (e.g., Selesnick et al. 2016). At Saturn, the magnetic field close to the planet is very symmetric, and yet a non-radial electric field component forces energetic and plasma particles to deviate from $B_m(\boldsymbol{r}) = cst.$ contours (Andriopoulou et al. 2012; Thomsen et al. 2012).

Characterization of the drift contour, Γ, for energetic particles in a dipole field:

In the special case of radiation belt particles trapped in a magnetic dipole field, the drift contour Γ is a circle ($r = cst. = r_0$), and the magnetic flux encompassed by the drift contour, Γ, is equal to $|\Phi| = 2\pi B_E R_E^3 / r_0$. Thus, for radiation belt particles in a dipole field, L^* merges with the normalized equatorial radial distance ($L^* = r_0/R_E$). That is why the L^* coordinate is often associated with the equatorial radial distance of a particle's drift shell.

Physical meaning of L:*

The association between the L^* coordinate and the normalized equatorial radial distance of a particle's drift shell is not possible in magnetic topologies other than the magnetic dipole field. However, since L^* is an adiabatic invariant, L^* remains constant when all non-dipolar contributions to the magnetic field are turned off adiabatically (that is, with a characteristic time that is extremely slow compared to the population drift period).

The coordinate L^* corresponds to the normalized radius of the circular guiding contour on which particles are found after non-dipolar contributions to the magnetic field and all electric field components have been turned off adiabatically.

An illustration of this concept is provided in **Fig. 12**.

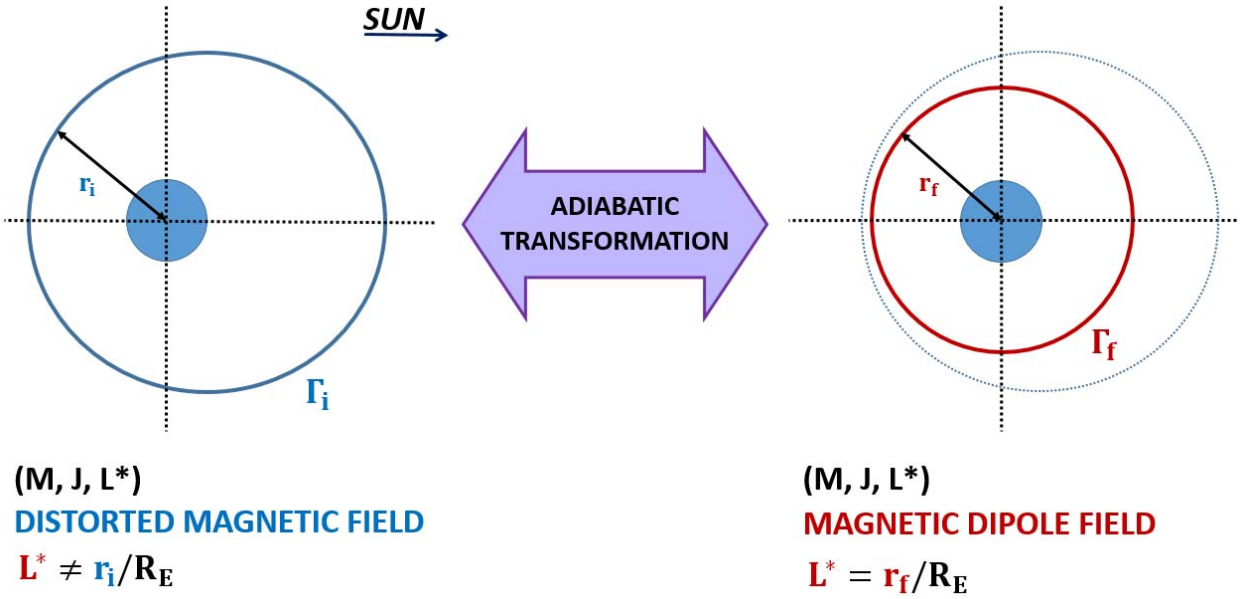

Fig. 12 Representation of the physical meaning of the L^* coordinate. (Left) A population with adiabatic invariants (M, J, L^*) is trapped in a distorted magnetic field. The initial drift contour Γ_i is represented in blue. When the magnetic field is adiabatically transformed into a dipole field, the population conserves all three invariants. (Right) In the resulting dipole field, the drift contour for the population with the same adiabatic invariants (M, J, L^*) is a circle of radius $R_E L^*$ The final drift contour Γ_f is represented in red.

5.1.2. Misconceptions about L^*

L is not a spatial coordinate, it is the electromagnetic coordinate of a geomagnetically trapped particle:*

Azimuthal asymmetries in the electric and/or magnetic fields lead to drift shell distortions that are pitch-angle-dependent. Particles with different pitch angles that are observed on a common field line at a given local time have different L^* coordinates, and they populate different drift

shells. This effect is called shell splitting (e.g., Stone 1963; Roederer and Schulz 1971; Roederer 1972; Schulz 1972; Roederer et al. 1973; Selesnick et al. 2016). Therefore, the point at which a field line crosses the equatorial plane does not uniquely define the drift contour.

"Energization by radial transport" is not equivalent to "violation of the third adiabatic invariant":

Too often, the L^* coordinate is hastily introduced as "roughly the normalized equatorial distance of particle drift shells." A side effect of the routine association between L^* and normalized equatorial radial distance is the incorrect belief that energization by radial transport requires violation of the third adiabatic invariant.

In fact, it is possible to vary particles' energy while conserving all three adiabatic invariants. In **Fig. 12**, for instance, the distorted magnetic field (left) is slowly transformed into a dipole field (right). The conservation of the third invariant means that the magnetic flux encompassed by the initial drift contour, Γ_i (left), is equal to magnetic flux encompassed by the final drift contour, Γ_f (right). Because the area within the initial drift contour, Γ_i, is larger than the area within the final drift contour, Γ_f, we deduce that the initial amplitude of the magnetic field at the mirror point along Γ_i is smaller than the final amplitude of the dipole magnetic field at the mirror point along Γ_f. Therefore, because of the conservation of the first adiabatic invariant (see equation (2-1)), the kinetic energy of the population considered is higher in the dipole configuration (right) than in the initially distorted configuration (left). In other words, there is an energy gain that accompanies the magnetic dipolarization represented in **Fig. 12**.

If the dipole field (right) slowly returns to its initially distorted configuration (left), the population considered will lose exactly the same amount of kinetic energy as it had gained during the dipolarization. The kinetic energy of the population considered will return to its initial value. Therefore, adiabatic energization is a reversible process. Even so, fully adiabatic changes in particle fluxes are known to play an important role in the storm time dynamics of the Earth's radiation belts (e.g., Dessler and Karplus 1961; Kim and Chan 1997).

It is worth emphasizing the key role played by induced electric fields during adiabatic energization. It is indeed the induced electric fields that make the connection between changing magnetic fields and particles' acceleration. During changes in the magnetic field configuration, the energy transfer results from two betatron effects acting simultaneously: a gyro-betatron, in which the curl of the induced electric field acts around the circle of gyration, and a drift betatron, in which the curl of the induced electric field acts around the drift circle. If the magnetic field changes slowly enough, the gyro-betatron acceleration ensures conservation of the first adiabatic invariant while the drift betatron acceleration ensures conservation of the third adiabatic invariant (e.g. Fillius and McIlwain 1967; Roederer 1970).

Finally, let us discuss another possible misconception related to the violation of the third adiabatic invariant: the idea that radial diffusion only results in energy gain (i.e., radiation belt acceleration). The violation of the third adiabatic invariant corresponds to an irreversible energy

variation whose sign depends on the trapped population drift phase (e.g., Figure 6, Section 2.3.3). Within the diffusive regime, multiple violations of the third adiabatic invariant correspond to random walks in L^*. In other words, at each time step, there is equal likelihood that L^* increases (irreversible energy loss) or L^* decreases (irreversible energy gain) for an individual particle of a given radiation belt population (q, M, J, L^*). That there is equal chance that L^* increases or decreases is directly related to the assumption of phase mixing, i.e., to the assumption that the phase space density is dependent of the drift phase φ_3 (e.g., equations (2-17) – (2-19)). On the other hand, the phase space density of a trapped population (q, M, J) usually varies with L^*. Because the L^*-gradient is typically positive in phase space, there are usually more particles moving inward than outward along L^*, i.e., radial diffusion usually results in a net irreversible energy gain. Yet, when the gradient in L^* is negative, radial diffusion results in a net irreversible energy loss because there are more particles moving outward than inward along L^*.

5.1.3. Challenges inherent to the L^* coordinate

The L^* coordinate depends on the topologies of the electric and magnetic fields, and on the characteristics of the population considered (charge, mass, energy, pitch angle) (equation (5-4)). This definition becomes somewhat simpler for Earth's radiation belt populations (equation (5-6)). Even so, L^* is a cumbersome parameter to handle:

- It requires knowledge of the global electromagnetic field geometry at a given instance – information that no measurement can provide. Thus, the quantification of L^* is always somewhat uncertain.
- The standard method for determining L^* requires a computationally expensive drift contour tracing (see, for instance, the numerical recipe provided by Roederer and Zhang (2014)). Therefore, some approximation of the L^* parameter is often preferred in practice.

Thus, any work on radial diffusion requires setting a magnetic field model, and setting a method to quantify the L^* coordinate. It is understood that both parameterizations should be as accurate as possible.

In addition, it is important to keep in mind that L^* is a parameter for stably trapped populations. This poses a limit to radial diffusion studies. Indeed, the drift contour needs to be a closed curve for L^* to be determined. Thus, populations located on open field lines and quasi-trapped populations cannot be parametrized with L^*. For instance, particles located in the nightside of the geostationary orbit can be in the drift loss cone during active times, drifting towards regions of open field lines in the dayside where they are lost ("magnetopause shadowing"). In addition, there exist regions of space close to the dayside magnetopause of the Earth where each field line has two minima. This particular geometry leads to drift orbit bifurcations (also known as Shabansky orbits), and it precludes the definition of L^* (e.g. Öztürk and Wolf 2007). Therefore, if the population considered is not stably trapped, it is, strictly speaking, impossible to attribute a L^* coordinate, never mind computing a radial diffusion coefficient!

5.2. Violation of the third adiabatic invariant

Radial diffusion is a statistical characterization of the violation of the third adiabatic invariant across a particle population. Thus, this concept involves variations of the magnetic flux encompassed by the drift contour of a trapped population. In the following, we discuss the ingredients required for the violation of the third adiabatic invariant, in the most general way.

5.2.1. Relation between magnetic field variations and violation of L^*

The violation of L^* requires field fluctuations that depend on local time

The broadening of an initially thin drift shell is indicative of the violation of the L^* coordinate for the population considered. In the following, we expand on the mechanism proposed by Parker (1960), introduced in **Section 2.3.1**. We show that the condition for an initially thin drift shell to broaden is the presence of asymmetric field fluctuations, i.e., field fluctuations that depend on local time, with a characteristic time comprised between the bounce and the drift periods of the population considered. The case of equatorial particles trapped in a time-varying magnetic field is discussed for the sake of simplicity. Generalization is straightforward (via an appropriate redefinition of the drift contour – equation (5-4)).

Let us track the drift motions of two radiation belt equatorial guiding centers with the same three adiabatic invariants ($M, J = 0, L^*$), located at $\boldsymbol{r_1}$ and $\boldsymbol{r_2}$ along the same drift contour Γ_i (**Fig. 13**). By definition of a drift contour, the equatorial magnetic field intensity is the same at $\boldsymbol{r_1}$ and $\boldsymbol{r_2}$ at time t: $B(\boldsymbol{r_1}, t) = B(\boldsymbol{r_2}, t) = B_i$.

As the magnetic field starts varying (with a characteristic time that is long enough so as to conserve the first two invariants, but short in comparison with the drift period of the trapped population), the drift velocity departs from its value under stationary conditions, and the guiding centers move away from their initial drift contour, Γ_i (the motions are represented by the red and blue arrows in **Fig. 13**, right panel).

At time, $t + dt$, the guiding center initially located at $\boldsymbol{r_1}$ is now at $\boldsymbol{r_1} + \boldsymbol{dr_1}$, and the guiding center initially located at $\boldsymbol{r_2}$ is now at $\boldsymbol{r_2} + \boldsymbol{dr_2}$. In order for the two guiding centers to share the same guiding contour at $t + dt$, and thus remain on the same drift shell at $t + dt$, the new locations should be such that $B(\boldsymbol{r_1} + \boldsymbol{dr_1}, t + dt) = B(\boldsymbol{r_2} + \boldsymbol{dr_2}, t + dt)$.

With a first order approximation in dt, one obtains that $B(\boldsymbol{r_1} + \boldsymbol{dr_1}, t + dt) = B(\boldsymbol{r_1}, t) + (dB(\boldsymbol{r_1}, t)/dt)dt$, and $B(\boldsymbol{r_2} + \boldsymbol{dr_2}, t + dt) = B(\boldsymbol{r_2}, t) + (dB(\boldsymbol{r_2}, t)/dt)dt$. Since $B(\boldsymbol{r_1}, t) = B(\boldsymbol{r_2}, t) = B_i$, it results that $B(\boldsymbol{r_1} + \boldsymbol{dr_1}, t + dt) = B(\boldsymbol{r_2} + \boldsymbol{dr_2}, t + dt) = cst. \Leftrightarrow dB(\boldsymbol{r_1}, t)/dt = dB(\boldsymbol{r_2}, t)/dt$. In other words, if the magnetic field varies in a similar way all along the initial drift shell ($dB(\boldsymbol{r}, t)/dt = cst.$ along Γ_i), the guiding centers will stay on a common shell. On the other hand, if the magnetic field variations depend on local time, the initially thin drift shell will broaden.

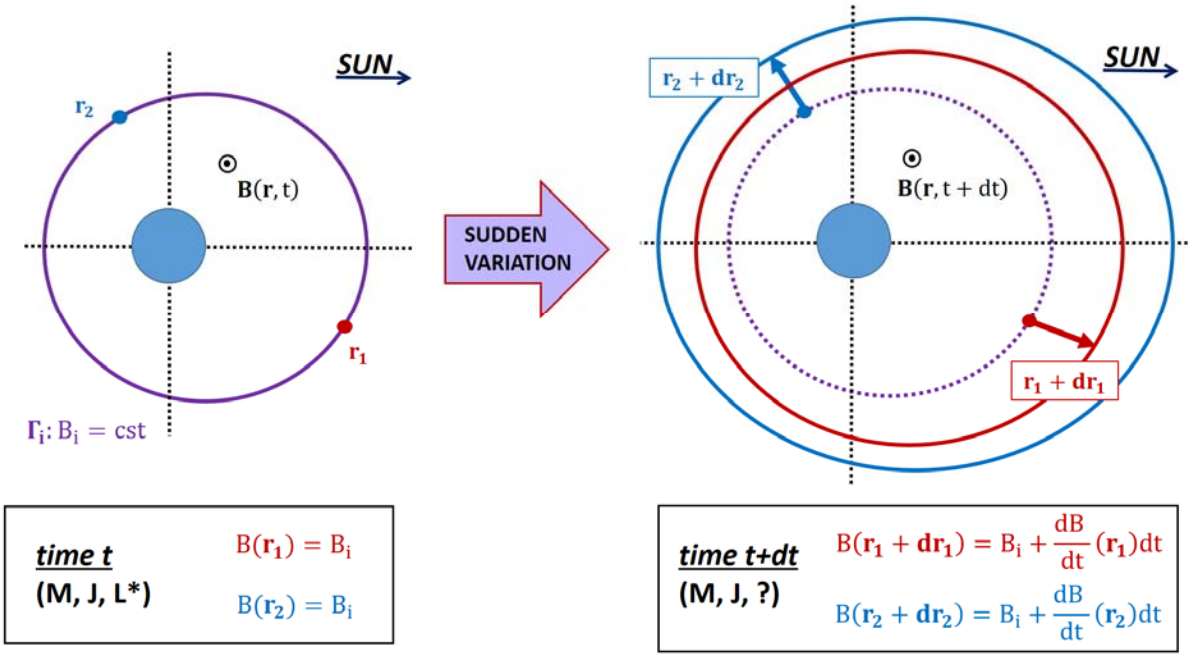

Fig. 13 Schematic drawing of the broadening of the drift shell. (Left) Initially, the guiding centers located at $\boldsymbol{r_1}$ and $\boldsymbol{r_2}$ have the same adiabatic invariants. They share the same drift contour, Γ_i. The magnetic field varies during dt, a time interval that is long enough so as to conserve the first two invariants, but small enough so that the third invariant can be violated. At $t + dt$, the guiding centers have new locations ($\boldsymbol{r_1 + dr_1}$ and $\boldsymbol{r_2 + dr_2}$, respectively). These new locations determine new drift contours ($B(\boldsymbol{r_1 + dr_1}) = cst.$, in red in the right panel, and $B(\boldsymbol{r_2 + dr_2}) = cst.$, in blue in the right panel). For the drift contours to merge, it is necessary that $\left(B(\boldsymbol{r_1 + dr_1}) = B(\boldsymbol{r_2 + dr_2})\right)$. That is, the variation of the magnetic field should be the same at $\boldsymbol{r_1}$ and $\boldsymbol{r_2}$.

In Parker's scenario (**Section 2.3.1**), the compression of the magnetic field is stronger on the dayside than on the nightside, which commonly happens as a result of enhanced solar wind pressure. Particles are transported closer to Earth on the dayside than on the nightside, and different portions of the initial ring of particles populate different shells as the particles drift around the Earth.

More generally, we find that the condition for a thin drift shell of equatorial radiation belt particles to broaden is that the time variations of the equatorial magnetic field depend on local time. This concept is at the heart of the formulation of the instantaneous rate of change of L^*.

Analytical expressions for the instantaneous rate of change of L^* (dL^*/dt):

The following results have been demonstrated in real space (**r**) by Lejosne et al. (2012) and Lejosne (2013). Equivalent formulas had already been demonstrated by Northrop (1963) in the $(\alpha, \beta, \varepsilon)$ coordinate system, where α and β are coordinates related to the magnetic field topology (Euler potentials), and ε identifies with the total energy of particles in the static case. The

underlying theoretical framework and formula derivations are gathered in the **Appendix**. In the following, the quantities considered are averages over the bounce period of the population considered – because it is assumed that the first two adiabatic invariants are conserved.
In the most general case, the instantaneous rate of change of L^* is:

$$\frac{dL^*}{dt}(\boldsymbol{r_o}, t) = \frac{L^{*2}}{2\pi B_E R_E^2} \oint_{\boldsymbol{r}\in\Gamma(r_o)} \frac{B_o(\boldsymbol{r}, t)}{|\nabla_o \varepsilon(\boldsymbol{r}, t)|} \left(\frac{d\varepsilon}{dt}(\boldsymbol{r}, t) - \frac{d\varepsilon}{dt}(\boldsymbol{r_o}, t) \right) dl \tag{5-7}$$

where $\boldsymbol{r_o}$ is the guiding center location along the drift contour $\Gamma(r_o)$ at time t, B_o is the equatorial magnetic field intensity, ε is the total (kinetic+potential) energy of the guiding center, and $\nabla_o \varepsilon$ is the gradient of ε determined with constant mirror point magnetic field intensity. The drift contour, Γ, is comprised of all equatorial radial distances around the planet that a particle with fixed adiabatic invariants can have. The integral goes over the full drift contour. dl is an infinitesimal displacement along Γ. Equation (5-7) is equivalent to (5-9), as shown in the **Appendix**.

Reformulations in terms of deviation from the drift-average:
Let us introduce the drift-average spatial operator $[\quad]_D$, such that

$$[f]_D(t) = \frac{1}{\tau_D} \oint_{\boldsymbol{r}\in\Gamma} \frac{f(\boldsymbol{r}, t)}{|\boldsymbol{V_D}(\boldsymbol{r}, t)|} dl = \frac{1}{\tau_D} \int_{\tau=0}^{\tau_D} f(\boldsymbol{r}(\tau), t) d\tau \tag{5-8}$$

where the integral is over the drift contour, $\boldsymbol{V_D}$ is the bounce-averaged drift velocity, τ_D indicates the drift period of the population considered, and Γ is the associated drift contour at time, t. $[f]_D(t)$ determines the spatial average of an arbitrary quantity, f, at time, t, along the drift contour Γ. Each drift contour element is weighted by the time spent drifting through that location if the electromagnetic conditions were time-stationary.

With that operator, the equation (5-7) is also:

$$\frac{dL^*}{dt}(\boldsymbol{r_o}, t) = \frac{L^{*2}}{q\Omega B_E R_E^2} \left(\left[\frac{d\varepsilon}{dt} \right]_D (t) - \frac{d\varepsilon}{dt}(\boldsymbol{r_o}, t) \right) \tag{5-9}$$

where $\Omega = 2\pi/\tau_D$ is the population angular drift velocity. This is the same formula as the one derived by Northrop (1963), reviewed by Cary and Brizard (2009), and derived here in the **Appendix** as equation (A-43).

5.2.2. Requirements for L^* violations

L can only be violated if the time variations of the field depend on local time:*

If the time variations of the fields are the same all along the drift contour *($d\varepsilon/dt\,(\boldsymbol{r_o}, t) = [d\varepsilon/dt]_D(t)$* for all guiding center locations $\boldsymbol{r_o}$ along the drift contour) then it follows, in a symmetric field:

$$\frac{dL^*}{dt}(\boldsymbol{r_o}, t) = 0 \tag{5-10}$$

This is consistent with the result obtained in section **5.2.1.**

dL^*/dt is zero on drift-average along the drift contour:

The instantaneous rate of change of L^* for a guiding center located at $(\boldsymbol{r_o}, t)$ along the drift contour is proportional to $\left([d\varepsilon/dt]_D(t) - d\varepsilon/dt\,(\boldsymbol{r_o}, t)\right)$. Thus, the drift average of the variations of L^* along $\Gamma(r_o)$ is zero:

$$\left[\frac{dL^*}{dt}\right]_D(t) = 0 \tag{5-11}$$

This result is consistent with the fact that there is no net transport of the third adiabatic invariant if all guiding centers are homogenously distributed along the drift contour (i.e., it is zero under the assumption of phase mixing).

There is a competition between the drift period and the characteristic time for the variation of the fields:

The general expression of dL^*/dt (equation (5-9)) highlights the competition between the characteristic time for the variation of the field, τ_C, and the drift period, τ_D, of the population considered. Since the instantaneous rate of change of L^* is proportional to τ_D/τ_C (equation (5-9)), L^* remains approximately constant if the characteristic time for the variation of the field is very long in comparison with the drift period : $(\tau_D/\tau_C \ll 1) \Rightarrow (dL^*/dt \ll 1)$. This is in agreement with the fact that L^* is an adiabatic invariant associated with drift motion.

5.2.3. Challenges

In the most general case, the quantification of dL^*/dt requires:

- to define the drift contour of the population considered at a given instance,
- to evaluate the electric and magnetic fields, together with their total time derivatives – i.e., to evaluate the total changes as seen by the particles ($d/dt = \partial/\partial t + \boldsymbol{V_D} \cdot \boldsymbol{\nabla}$), over the entire drift shell, at a given instance.

Since no measurement can provide such information, there is ineluctable uncertainty when quantifying dL^*/dt. Thus, it is important to approach any work on radial diffusion by determining the fields chosen, together with the approximation chosen to evaluate dL^*/dt.

In addition, it is important to keep in mind that the proposed framework relies on the frozen field condition (See also **Section 2.3.1; Appendix**). This requires no electric field component parallel to the magnetic field direction and a perfectly conducting Earth's surface. In practice, both assumptions should be examined in the region of interest.

5.3. Radial diffusion is a formalism

The radial diffusion formalism and the associated Fokker-Planck equation are commonly assumed to apply *de facto*. Yet, this is incorrect (see also **Section 2.3.2**). The concept of radial diffusion has been introduced to tackle the degree of randomness in cross drift shell motion. It provides a simple average description for the dynamics of a given population. In addition to the derivation of the diffusion equation introduced and discussed **Section 2.3.2**, we review in the following the computation of a radial diffusion coefficient. That way, we highlight the set of assumptions underlying the radial diffusion formalism.

5.3.1. Derivation of a radial diffusion coefficient

Let us derive a general formulation for the radial diffusion coefficient, starting from the expression of the instantaneous rate of change of L^*at a location, $\boldsymbol{r}$, and a time, t:

$$V_L(q, M, J;\ \boldsymbol{r}, t) = \frac{dL^*}{dt}(q, M, J; \boldsymbol{r}, t) \tag{5-12}$$

with dL^*/dt described in the general equation (5-9). V_L is called the the Lagrangian velocity in L^* of a radiation belt particle with characteristics (q, M, J).

Integration over a time interval t

After a time, t, the variation in the L^* of a particle (q, M, J) is equal to

$$\Delta L^* = L^*(\boldsymbol{r}(t), t) - L^*(\boldsymbol{r}(0), 0) = \int_0^t V_L(\boldsymbol{r}(u), u)\, du \tag{5-13}$$

Computation of the expectation value for the mean square displacement

The expectation value of the square of the displacement is equal to

$$[(\Delta L^*)^2] = \int_0^t \int_0^t [V_L(\boldsymbol{r}(u), u) V_L(\boldsymbol{r}(v), v)]\, du dv \tag{5-14}$$

where [ ] denotes the expectation value. Therefore, it is necessary to compute the autocorrelation function of the Lagrangian velocity, V_L, a function of both time and space, in order to derive the radial diffusion coefficient.

Separation of the spatial and temporal dependence for the velocity V_L

How does one describe the Lagrangian velocity $V_L(\boldsymbol{r}(t), t)$? The traditional assumption is that the spatial and temporal functions are independent ($V_L(\boldsymbol{r}, t) = \lambda(t)\gamma(\boldsymbol{r})$). In addition, because the particles are drifting in close shells around Earth, it is considered that the spatial function is a periodic function in local time, with a periodicity defined by the particle drift period. Because the radial diffusion formalism assumes small variations for the coordinate of interest, the radial dependence of the spatial function is often omitted $\big(\gamma(\boldsymbol{r}) = \gamma(\varphi) = \gamma(\Omega t - \varphi_0)\big)$. As a result, the velocity, V_L, is rewritten in terms of a product:

$$V_L(\boldsymbol{r}(t), t) = \lambda(t) cos(\Omega t - \varphi_0) \tag{5-15}$$

where λ describes the temporal variations of the Lagrangian velocity, and $cos(\Omega t - \varphi_0)$ represents the particle location at time, t (Ω and φ_0 are respectively the angular drift velocity and the initial drift phase of the particle considered). This formulation could be further elaborated by rewriting $V_L(\boldsymbol{r}(t), t)$ as a Fourier sum $\sum_n \lambda_n(u) cos\big(n\varphi + \varphi_{0,n}\big)$. For the sake of simplicity, we only consider the first harmonic *n=1* in the following. The generalization is straightforward.

Drift phase averaging

We compute the expectation value of $V_L(\boldsymbol{r}(u), u)V_L(\boldsymbol{r}(v), v)$ by averaging over multiple scenarios, and including all possible initial drift phases.

As a result:

$$[V_L(\boldsymbol{r}(u), u)V_L(\boldsymbol{r}(v), v)] = \frac{1}{2}[\lambda(u)\lambda(v)] cos(\Omega(u - v)) \tag{5-16}$$

Stationary signals

It is then assumed that the signal, λ, is stationary in the wide sense (e.g., Taylor 1922). The mean and the autocovariance of λ do not vary with time. Thus, the autocorrelation $[\lambda(u)\lambda(v)]$ only depends on the lag between u and v. The integral (5-14) becomes:

$$[(\Delta L^*)^2] = t \int_0^t [\lambda(T)\lambda(T + \tau)] cos(\Omega\tau)\, d\tau \tag{5-17}$$

where $[\lambda(T)\lambda(T + \tau)]$ does not depend on T. Once the time, τ, becomes longer than the autocorrelation time of the signal, λ, the expectation value of $[\lambda(T)\lambda(T + \tau)]$ becomes zero. Thus, the integral reaches a finite value once t is large enough.

In that context, the mean square of the displacement will grow linearly with time, and the rate of change of $[(\Delta L^*)^2]$ will be constant:

$$\frac{d}{dt}([(\Delta L^*)^2]) = \int_0^\infty [\lambda(T)\lambda(T+\tau)]cos(\Omega\tau)\, d\tau \tag{5-18}$$

It is the magnitude of the rate of change of $[(\Delta L^*)^2]$ that determines the radial diffusion coefficient (see also **section 2.3**):

$$D_{LL} = \frac{1}{2}\frac{d}{dt}([(\Delta L^*)^2]) \tag{5-19}$$

We identify part of equation (5-17) as being the power spectrum, P_λ, of the fluctuations, λ, at the angular drift velocity, Ω:

$$P_\lambda(\Omega) = 4\int_0^\infty [\lambda(t)\lambda(t+\tau)]cos(\Omega\tau)\, d\tau \tag{5-20}$$

Note that we assume $\lambda(t)$ to be in a way that P_λ is independent on time. With this, it results that:

$$D_{LL} = \frac{P_\lambda(\Omega)}{8} \tag{5-21}$$

For instance, if the autocorrelation of the signal, λ, is described by an exponential function:

$$[\lambda(T)\lambda(T+\tau)] = [\lambda_0^2]\, e^{-\tau/\tau_\lambda} \tag{5-22}$$

where $[\lambda_0^2]$ is the mean square velocity, and the exponential time constant, τ_λ, represents the characteristic time over which the signal, λ, is correlated with its previous values, it results that

$$D_{LL}(\Omega) = \frac{[\lambda_0^2]}{2}\frac{\tau_\lambda}{1+\Omega^2\tau_\lambda^2} \tag{5-23}$$

Thus, if $\tau_\lambda \ll 1/\Omega$, i.e., if the autocorrelation time is very small in comparison with the population drift period, $D_{LL}(\Omega) = [\lambda_0^2]\tau_\lambda/2$. The diffusion coefficient becomes independent of energy. It increases when the mean square velocity increases (i.e., when the field fluctuations increase), and when the autocorrelation time increases (i.e., when the particles are pushed in the same direction for a longer time). On the other hand, if $\tau_\lambda \gg 1/\Omega$, $D_{LL}(\Omega) = [\lambda_0^2]/(2\Omega^2\tau_\lambda)$, the diffusion coefficient decreases with increasing energy. Thus, the variations of the diffusion coefficient with particles' energy can provide information on the autocorrelation time of the signal λ, and vice versa.

5.3.2. Applicability of the concept of diffusion

Applicability of the concept of radial diffusion:

Radial diffusion can be used pragmatically in order to describe planetary environments. It is important to keep in mind that the concept of radial diffusion is a formalism that trades accuracy and complexity for expediency and simplicity. Expediency is of practical use when trying to forecast or "now-cast" space weather. The diffusion coefficient is free from the mathematical standpoint. It can, in principle, be tailored to fit observations, therefore allowing good control over the model solutions, which is not the case for more sophisticated methods like particle tracing. The simplicity of diffusion can be needed in data-starved scenarios, where no multi-point observations and/or observations of similar locations at different times are available that would be needed to constrain more sophisticated approaches. While the limitation on data has reduced at Earth in the recent decades, it is still true for the outer planets. Simplicity and expediency make diffusion a useful data analysis tool because it allows us to change the parameters of the model and quickly see the outcome of the numerical experiment.

To what extent the diffusion formalism is a realistic description of the actual physics is a separate question. Radial diffusion is germane to the Fokker-Planck equation, which provides an average description of the particle dynamics, based on average properties of the field. The modeled distribution function is a drift-averaged function, and information on the drift phase is lost. Several important assumptions were made in the derivation of the Fokker-Planck equation. For example, it was assumed that there were many very small fluctuations in L^*, and that the distribution function was always uniform in longitude. Radial diffusion is the result of many small uncorrelated perturbations of the particles' drift motion. Since none of these assumptions hold true during active times in a magnetosphere, the radial diffusion formalism cannot apply to major events. In particular, it cannot describe the massive injections characteristic of a substorm. Thus, in addition to the difficulty in proposing and calculating radial diffusion coefficients, solving the proposed Fokker-Planck equation does not prove that radial diffusion occurs.

Radial diffusion can be more or less adequate, depending on the region considered. For electrons in Earth's outer radiation belt, radial diffusion agrees poorly with the results obtained by tracking test particles when applied to event analysis (Riley and Wolf 1992; Ukhorskiy et al. 2008, 2009). This can be tested by describing radial motion of trapped equatorial particles in a time-dependent electric field model (1) by tracking test particles, and (2) by solving the radial diffusion equation, with the appropriate radial diffusion coefficient calculated from the assumed electric field characteristics. This shows that:

- The agreement between the simulation results and the diffusion theory predictions is mediocre when the comparison is performed for one event. Particle tracking results show much more structure in the particle distribution as a function of time and location. The results differ depending on the details of the wave (like its phase), even if the statistical wave parameters (like the average size of its structures) are the same.

- The diffusion formalism describes the average outcome of different wave fields that differ in their details but share the same statistical parameters. It is also able to bracket the extreme values covered by the particle tracking results (Ukhorskiy et al. 2009).
- The diffusion formalism does much better in the case of a series of sequential small storms (Riley and Wolf 1992).

This behavior is similar to a finite 1D random walk process, in which the distribution function approaches the Gaussian distribution only after a sufficiently large number of steps. Having said that, it is important to keep in mind that particle tracing techniques also rely on a lot of simplifying assumptions (in particular when it comes to modeling the spatial and temporal characteristics of the field variations). As a result, the practical limitations to the concept of radial diffusion remain unclear.

There are cases where radial diffusion appears to be a very adequate description of both the physics and the measurements. An example is the inner ion belts of magnetized planets such as Earth's inner proton belt and Saturn's proton belts between the main rings and the orbit of the moon Tethys. These belts vary only slowly on the timescale of years (Qin et al. 2015) and are smoothly distributed in space, both of which have been described very well with models that are based on radial diffusion (Selesnick et al. 2013; Kollmann et al. 2017). Particularly, Saturn's proton belts appear like a prototype for radial diffusion, because neither internal injections nor strong solar events (Roussos et al. 2008) appear to strongly affect their population.

A brief discussion on the general concept of diffusion in planetary radiation belts

Diffusion is not just limited to the radial mode, it can also occur in energy and pitch angle (or equivalent coordinates) when the first and second invariants are violated (Shprits et al. 2008b). It might be useful to highlight similarities and differences between models describing the statistical evolution of the distribution function when the first two adiabatic invariants are violated with that of radial diffusion. The commonly used formalism to describe statistically the temporal evolution of particle species experiencing violation of the first two adiabatic invariants in planetary radiation belts is quasi-linear theory (Sagdeev and Galeev 1969; Kennel and Engelman 1966). Just like radial diffusion, quasi-linear theory characterizes the evolution of the distribution function in its respective phase-space, in terms of a Fokker-Planck equation. Likewise, a number of crucial assumptions are also necessary. For instance, for such a formalism to hold, the distribution function must experience very little change on time scales associated with the motion of the first and/or second adiabatic invariant. In other words, similarly to radial diffusion, the change in the action-angle variables must be very small, i.e., $\Delta J/J \ll 1$, where J stands for one of the first two adiabatic invariants.

Moreover, requirement of time-stationarity of the turbulent fluctuations responsible for the violation of the adiabatic invariants and small autocorrelation times are required to reduce the coupled Vlasov-Maxwell system in terms of a Fokker-Planck diffusion equation. In the presence of long autocorrelation times, or put differently, if particles can sample the electric and magnetic field fluctuations, phase-space structures and other nonlinear structures could form in the distribution function and affect the transport (i.e., diffusion and advection coefficients).

In situ observations of large-amplitude fluctuations and nonlinear phase-space structures in the Earth's radiation belts (Cattell et al. 2008, Cully et al. 2008, Mozer et al. 2014) indicate that some caution might be required when applying quasi-linear formalisms to quantify the energization and losses of charged particles in the Earth's radiation belts. Confirmed by multiple independent experiments in the last ten years and across a wide range of geomagnetic conditions, the existence of nonlinear and/or large-amplitude fluctuations put into question the fundamental assumptions underlying quasi-linear formalisms.

6. CONCLUSION: 60 years of radial diffusion research, at Earth and beyond

6.1. Summary: Observations and theory

The concept of radial diffusion was introduced in the year following the discovery of the Earth's radiation belts to explain the existence of the belts. Experimental evidence was found indicating that magnetically trapped particles of external origin were transported in the outer zone of the Earth's radiation belts by processes consistent with the conservation of the first two adiabatic invariants. In the same years, high-altitude nuclear explosions evidenced the existence of a radial diffusion mechanism in the inner belt.

Early theoretical descriptions of cross drift shell motion in a background dipole field showed that electric and/or magnetic field fluctuations could drive radial diffusion, provided that the fluctuations depend on local time and occur on a timescale comprised between the bounce and the drift period of the population considered. Assuming that the field fluctuations are stationary, and that the spatial and temporal variations of the field are decoupled, the radial diffusion coefficient is proportional to the power spectrum of the field fluctuations at harmonics of the population drift frequency. Early estimates of the radial diffusion coefficients based on particle and/or field measurements showed consistency, suggesting the validity of the underlying theoretical picture.

There is a variety of physical drivers for the field fluctuations. Electric field fluctuations can be induced by magnetic field disturbances (due to variations in currents flowing inside or outside of the planetary magnetosphere). They can be driven from above (by variations in the coupling between the solar wind and the planetary magnetosphere), or from below (by variations in the coupling between the thermosphere and the ionosphere, which usually map directly into the magnetosphere). Ultimately, it is the sum of all these different field fluctuations that drives radiation belt particle cross drift shell motion.

As the temporal and spatial accuracy for radiation belt observations improved at Earth in the 90s, the data revealed complex structure and rapid dynamics which challenged the traditional picture of radiation belt dynamics provided by the Fokker-Planck equation. In particular, it was realized

that relativistic electron fluxes could increase significantly on time scales that were shorter than expected. It was proposed that the rapid outer belt relativistic electron flux enhancements could be due to a drift resonant interaction with a monochromatic ULF oscillation in a distorted magnetic field. From these considerations re-emerged the idea that the asymmetry of the background magnetic field could drive a form of enhanced radial diffusion in the presence of multiple ULF frequencies. As a result, new theoretical expressions were developed in order to characterize radial diffusion in an asymmetric background field. These new formulas diverge from the traditional ones, even in the absence of asymmetry. This discrepancy indicates that the new theoretical expressions are unlikely to be fully effective in forwarding our understanding of radial diffusion. In addition, even current radial diffusion coefficient estimates rely on the assumption of a background magnetic dipole field, which poses a limit to their accuracy.

6.2. Summary: Physics of radial diffusion

Given the importance of advancing radial diffusion research for further progress in our ability to understand and model radiation belt dynamics, it is necessary to clarify and to reassess the sets of assumptions underlying the theoretical picture of radial diffusion.

The first possible source of confusion associated with radial diffusion is the variable of interest. It is important to keep in mind that the appropriate coordinate to discuss radial diffusion is L^*. This adiabatic coordinate allows the separation between adiabatic and non-adiabatic energization effects in a realistic magnetic field. In the early days of radiation belt science, it was assumed that the background magnetic field was a dipole, thus, cross drift shell motion merged with radial motion in the magnetic equatorial plane. We now know that planetary magnetic fields depart from a dipole field, and that the discrepancy can sometimes be drastic, even at Earth. In the currently commonly accepted formulas for radial diffusion, the coordinate of reference is the normalized equatorial radial distance. This inescapably leads to flawed estimates.

Secondly, radial diffusion requires violation of the third adiabatic invariant. In other words, it requires a variation of the magnetic flux encompassed by the drift contour of a trapped population. The conditions for the third adiabatic invariant to vary (and for the first two adiabatic invariants to remain constant) are well known - even though they have been the object of little attention so far. Violation of the third adiabatic invariant requires field fluctuations that depend on local time, on timescales comprised between the bounce and the drift period of the population considered. Drift resonance is not required.

Thirdly, it is important to keep in mind that the concept of radial diffusion is a formalism that trades accuracy for expediency. It is germane to the Fokker-Planck equation, which provides an average description of the particle dynamics, based on average properties of the field. The modeled distribution function is a drift-averaged function, and information on the drift phase is lost. Radial diffusion is the result of many small uncorrelated perturbations of the particles' drift motion. Therefore, the radial diffusion formalism cannot describe injections. It agrees poorly with the results obtained by tracking test particles when applied to event analysis. It agrees well

with observations of slowly changing particle populations, like the inner ion belts of Earth and Jupiter. In summary, the use of the radial diffusion formalism and the associated Fokker-Planck equation requires caution.

6.3. Some challenges for the future, near and far

Particles transported through L^* shells via radial diffusion gain or lose kinetic energy from the fields. Thus radial diffusion is often contrasted to local acceleration processes (that is, processes that accelerate particles without necessarily transporting them), when it comes to assessing the most important acceleration mechanism for the Earth's radiation belts. However, radial diffusion is not the only way to accelerate particles on the macroscale. Slow variations of the magnetic field and the associated gyro-betatron and drift betatron effects lead to adiabatic and reversible acceleration. Injections, as they follow substorms or interchange, can, in parts, lead to transport consistent with the conservation of the first two adiabatic invariants, and energization similar to diffusion. Thus, a careful analysis requires differentiating between adiabatic and non-adiabatic effects, which always depends on the accuracy of the models chosen for the fields.

On the other hand, it may be worth keeping in mind that predictions provided by the radial diffusion formalism provide mediocre agreement with test particle simulations when doing event analysis. Thus, a temporary discrepancy between event observations and numerical simulations relying on the Fokker-Planck equation does not necessarily mean that additional processes are occurring. It may only highlight the limits of radial diffusion formalism.

It is interesting to note that the theoretical picture of violation of the third adiabatic invariant relies on the assumption that the plasma obeys the "frozen-field condition." Yet, there are times and regions where this is not necessarily true. What happens to the trapped population drift motion in that context is unknown.

It is common practice to break down the global radial diffusion coefficient into a sum of different components. This approach is based on the assumption that the different sources of cross drift shell motion are uncorrelated. In practice, the correlation is unknown. A potential correlation between the different field fluctuations would result in a global radial diffusion coefficient distinct from the sum of the different contributions.

In addition, the theoretical models for the radial diffusion coefficients rely on idealized field fluctuations in which the spatial and temporal variations of the fields are decoupled. The extent to which this assumption is valid is unknown.

In that context, multi-spacecraft data analysis and numerical modeling in the Earth's outer belt such the global hybrid-Vlasov simulation Vlasiator (e.g., Palmroth et al. 2018) could provide useful information because they can provide global information on the variations of the field, in particular: on the characteristic times for the variations of the field, on the spatial and temporal coupling, on the correlation between the field components, etc.

Let us conclude by mentioning that there is also a need to improve the spatial and temporal accuracy of the radiation belt simulations, by introducing local time as a 4^{th} dimension in the codes, and by developing event-specific models (e.g., Shprits et al. 2015). In that case, it is pivotal to realize the limitations of the Fokker-Planck equation, which originate by design. Finding a compromise between accuracy and expediency requires a statistical reformulation of the radiation belt dynamics able to model localized (non-diffusive) radial transport, drift phase bunching, and drift echoes. Such features are specific to trapped population drift motion. Yet, they cannot be reproduced by the current numerical simulations that consist of solving a 3D Fokker-Planck equation.

APPENDIX: Derivation for the instantaneous rate of change of the third adiabatic invariant

In this section, we present two different ways to derive the analytic formulation of dL^*/dt that was used in Section 5.2. Both proofs provide complementary physical insights on the process at play. The results are then reformulated in more compact ways.

A.1. Theoretical Framework and Working Hypotheses

In the following proofs, it is assumed that:

- the frozen-in condition applies;
- all three adiabatic invariants of the population are well-defined and meaningful (no open drift shells, and the Lamor radius is small compared to field gradients, etc.);
- the first two adiabatic invariants are conserved;
- the characteristic time for the variation of the field, τ_C, is very long in comparison with the bounce period of the population considered τ_B, and very short in comparison with the drift period τ_D:

$$\tau_G \ll \tau_B \ll \tau_C \ll \tau_D \tag{A-1}$$

where τ_G, τ_B, τ_D are respectively the gyration, bounce, and drift periods of the particle considered, and τ_C is the characteristic time for the variation of the field.

We use an infinitesimal time step, dt, adapted to this ordering:

$$\tau_G \ll \tau_B \ll dt \approx \tau_C \ll \tau_D \tag{A-2}$$

so that we can track the bounce-averaged drift motions of the particle guiding centers.

In a time-varying field, the guiding center drift velocity $\boldsymbol{V_D}$ is:

$$\boldsymbol{V_D} = \frac{\boldsymbol{B}}{qB^2} \times \left(-q\boldsymbol{E} + \frac{m}{2B}\left(v_\perp^2 + 2v_\parallel^2\right)\boldsymbol{\nabla}_\perp B + m\frac{d\boldsymbol{V_D}}{dt} \right) \tag{A-3}$$

where m is the mass of the particle, q is the electric charge, and $v_\perp$ and $v_\parallel$ correspond to the particle velocities perpendicular and parallel to the magnetic field direction (e.g., Roederer 1970).

The order of magnitude of the inertia term (last term in the brackets of the equation (A-3)) is very small:

$$\frac{\left|\frac{m\boldsymbol{B}}{qB^2} \times \frac{d\boldsymbol{V_D}}{dt}\right|}{|\boldsymbol{V_D}|} = \left|\frac{m}{qB}\right| \cdot \frac{\left|\frac{dV_D}{dt}\right|}{|V_D|} = \frac{\tau_G}{\tau_C} \ll 1 \tag{A-4}$$

Thus, the inertia term is omitted and the drift velocity is equal to its bounce-averaged expression at the magnetic equator for every time step:

$$\boldsymbol{V_D} = \frac{2p\boldsymbol{\nabla_o} I \times \boldsymbol{e_o}}{q\tau_B B_o} + \frac{\boldsymbol{E_o} \times \boldsymbol{e_o}}{B_o} \tag{A-5}$$

where p is the particle momentum, $\boldsymbol{e_o} = \boldsymbol{B_o}/B_o$, $\boldsymbol{B_o}$ is the magnetic field at the magnetic equator (minimum B surface), $\boldsymbol{E_o}$ is the equatorial electric field (with both induced and electrostatic components), $I = \int_{s_m}^{s'_m} \sqrt{1 - B(s)/B_m}\, ds$ is the integral function of B_m between the mirror points s_m and s'_m, and $\boldsymbol{\nabla_o} I$ is the equatorial gradient of the quantity, I, determined at constant magnetic field intensity, B_m, at the mirror points (e.g., Roederer 1970).

Finally, all variations will be expressed as first-order approximations in dt, and the total rate of change of the third invariant during *dt* will be merged with its instantaneous rate of change:

$$dL^* = \left(\frac{dL^*}{dt}\right) dt \tag{A-6}$$

The objective is to compute the rate of change of the magnetic flux encompassed by the drift contour of an equatorial particle in a time-varying magnetic field, in the absence of electrostatic fields.

A.2. Proof #1

Let us track the drift motion of an equatorial particle trapped in a magnetic field. At time, t, the three adiabatic invariants are $(M, J = 0, L^*)$, and the particle's guiding center is located at $\boldsymbol{r_o}$ along its drift contour $\Gamma(r_o)$. The magnetic field changes during an infinitesimal time step, dt. Due to the magnetic field variation and the resulting induced electric fields, the drift velocity is altered, and the guiding center moves away from its initial drift contour. At $t + dt$, the guiding center is located at $\boldsymbol{r_o} + \boldsymbol{dr_o}$. The equatorial magnetic field intensity along the new drift contour $\Gamma(r_o + dr_o)$ is a constant equal to $B(\boldsymbol{r_o} + \boldsymbol{dr_o}, t + dt)$.

The objective of this demonstration is to quantify the difference, $d\Phi(\boldsymbol{r_o}, t)$, between the magnetic flux, $\Phi(\boldsymbol{r_o} + \boldsymbol{dr_o}, t + dt)$, encompassed by the drift contour, $\Gamma(r_o + dr_o)$, at time, $t + dt$, and the magnetic flux, $\Phi(\boldsymbol{r_o}, t)$, encompassed by the drift contour, $\Gamma(r_o)$, at time, t.

$$\begin{aligned} d\Phi(\boldsymbol{r_o}, t) &= \Phi(\boldsymbol{r_o} + \boldsymbol{dr_o}, t + dt) - \Phi(\boldsymbol{r_o}, t) \\ &= \iint_{S(r_o + dr_o)} \boldsymbol{B}(\boldsymbol{r}, t + dt) \cdot \boldsymbol{dS} - \iint_{S(r_o)} \boldsymbol{B}(\boldsymbol{r}, t) \cdot \boldsymbol{dS} \end{aligned} \tag{A-7}$$

where $S(r_o + dr_o)$ indicates the area encompassed by $\Gamma(r_o + dr_o)$ at time, $t + dt$, and $S(r_o)$ indicates the area encompassed by $\Gamma(r_o)$ at time, t. They are represented in **Fig. 14**.

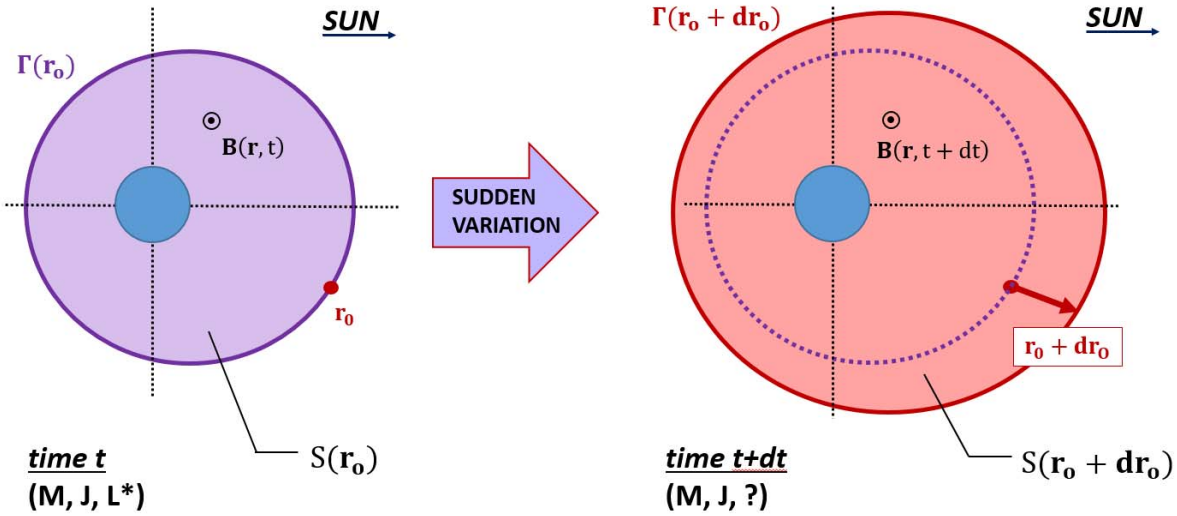

Fig. 14 Representation of the drift contours, $\Gamma(r_o)$, at time, t (dark purple line), and, $\Gamma(r_o + dr_o)$, at time, $t + dt$ (dark red line), and the associated integrating surface areas, $S(r_o)$, at time, t (purple area), and, $S(r_o + dr_o)$, at time, $t + dt$ (red area).

By adding and subtracting the quantity $\iint_{S(r_o)} \boldsymbol{B}(\boldsymbol{r}, t + dt) \cdot \boldsymbol{dS}$ to the equation (A-7), the variation of the magnetic flux associated with the guiding center initially located at $\mathbf{r_o}$ can be interpreted as the sum of a spatial contribution and a temporal contribution:

$$d\Phi(\boldsymbol{r_o}, t) = \left(\iint_{S(r_o + dr_o)} \boldsymbol{B}(\boldsymbol{r}, t + dt) \cdot \boldsymbol{dS} - \iint_{S(r_o)} \boldsymbol{B}(\boldsymbol{r}, t + dt) \cdot \boldsymbol{dS} \right) + \left(\iint_{S(r_o)} \boldsymbol{B}(\boldsymbol{r}, t + dt) \cdot \boldsymbol{dS} - \iint_{S(r_o)} \boldsymbol{B}(\boldsymbol{r}, t) \cdot \boldsymbol{dS} \right) \quad \text{(A-8)}$$

The spatial contribution is:

$$d\Phi_A(\boldsymbol{r_o}, t) = \iint_{S(r_o + dr_o)} \boldsymbol{B}(\boldsymbol{r}, t + dt) \cdot \boldsymbol{dS} - \iint_{S(r_o)} \boldsymbol{B}(\boldsymbol{r}, t + dt) \cdot \boldsymbol{dS} \quad \text{(A-9)}$$

It corresponds to the magnetic flux at time, $t + dt$, through the strip, $A(r_o)$, between $\Gamma(r_o)$ and $\Gamma(r_o + dr_o)$. The strip is represented in green in **Fig. 15**.

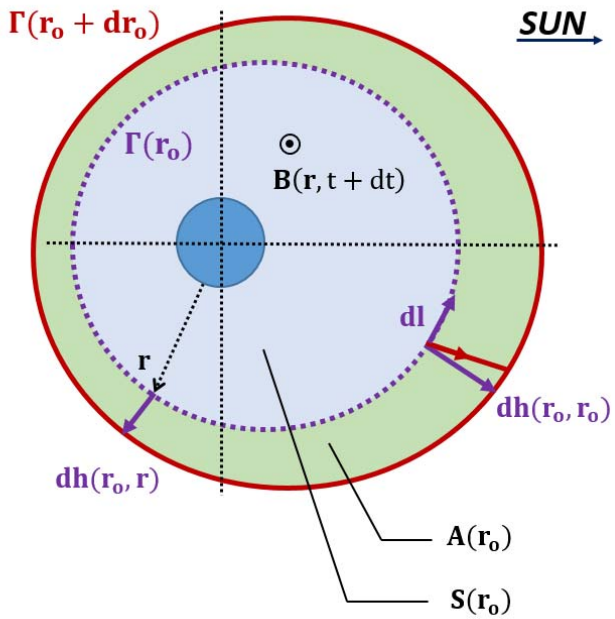

Fig. 15 Definition of the integrating surfaces: the strip $A(r_o)$ is in green, and the initial integrating surface area, $S(r_o)$, is in blue. The width of the strip, $A(r_o)$, starting from a location, **r**, along $\Gamma(r_o)$ is $dh(\boldsymbol{r_o}, \boldsymbol{r})$.

The temporal contribution is:

$$d\Phi_T(\boldsymbol{r_o}, t) = \iint_{S(r_o)} \boldsymbol{B}(\boldsymbol{r}, t + dt) \cdot \boldsymbol{dS} - \iint_{S(r_o)} \boldsymbol{B}(\boldsymbol{r}, t) \cdot \boldsymbol{dS} \qquad \text{(A-10)}$$

This contribution corresponds to the variation of the magnetic field through the initial integrating surface area $S(r_o)$. It results that:

$$d\Phi(\boldsymbol{r_o}, t) = d\Phi_A(\boldsymbol{r_o}, t) + d\Phi_T(\boldsymbol{r_o}, t) \qquad \text{(A-11)}$$

Let us quantify each component individually.

For the spatial component:

$$\begin{aligned} d\Phi_A(\boldsymbol{r_o}, t) &= \iint_{A(r_o)} \boldsymbol{B}(\boldsymbol{r}, t + dt) \cdot \boldsymbol{dS} \\ &= \oint_{\Gamma(r_o)} \boldsymbol{B}(\boldsymbol{r}, t + dt) \cdot (\boldsymbol{dh}(\boldsymbol{r_o}, \boldsymbol{r}) \times \boldsymbol{dl}) \end{aligned} \qquad \text{(A-12)}$$

For all points along $\Gamma(r_o)$, the width of the strip, $dh(\boldsymbol{r_o}, \boldsymbol{r})$, is such that

$$B(\boldsymbol{r}, t+dt) - |\nabla B(\boldsymbol{r}, t+dt)| dh(\boldsymbol{r_o}, \boldsymbol{r}) = B(\boldsymbol{r_o} + \boldsymbol{dr_o}, t+dt) \tag{A-13}$$

In addition, for all points along $\Gamma(r_o)$, $B(\boldsymbol{r}, t) = B(\boldsymbol{r_o}, t)$.
Thus, we have:

$$B(\boldsymbol{r}, t+dt) = B(\boldsymbol{r_o}, t) + \frac{\partial B}{\partial t}(\boldsymbol{r}, t) dt \tag{A-14}$$

As a result, for all points $\boldsymbol{r}$ along $\Gamma(r_o)$

$$dh(\boldsymbol{r_o}, \boldsymbol{r}) = \frac{dt}{|\nabla B(\boldsymbol{r}, t+dt)|}\left(\frac{\partial B}{\partial t}(\boldsymbol{r}, t) - \frac{dB}{dt}(\boldsymbol{r_o}, t)\right) \tag{A-15}$$

Consequently, the spatial component is, to the first order in dt:

$$d\Phi_A(\boldsymbol{r_o}, t) = dt \oint_{\Gamma(r_o)} \frac{B(\boldsymbol{r}, t)}{|\nabla B(\boldsymbol{r}, t)|} \cdot \left(\frac{\partial B}{\partial t}(\boldsymbol{r}, t) - \frac{dB}{dt}(\boldsymbol{r_o}, t)\right) dl \tag{A-16}$$

For the temporal contribution, one can write that:

$$\begin{aligned} d\Phi_T(\boldsymbol{r_o}, t) &= \iint_{S(r_o)} \boldsymbol{B}(\boldsymbol{r}, t+dt) \cdot \boldsymbol{dS} - \iint_{S(r_o)} \boldsymbol{B}(\boldsymbol{r}, t) \cdot \boldsymbol{dS} \\ &= dt \iint_{S(r_o)} \frac{\partial \boldsymbol{B}(\boldsymbol{r}, t)}{\partial t} \cdot \boldsymbol{dS} \end{aligned} \tag{A-17}$$

Thus, using the integral form of the Maxwell-Faraday equation:

$$d\Phi_T(\boldsymbol{r_o}, t) = -dt \oint_{\Gamma(r_o)} \boldsymbol{E_{ind}}(\boldsymbol{r}, t) \cdot d\boldsymbol{l} \tag{A-18}$$

In addition, the projection of the electric field vector, $\boldsymbol{E_{ind}}$, onto the local direction of the initial guiding drift contour is related to the drift velocity, $\boldsymbol{V_D} = -M\boldsymbol{\nabla} B \times \boldsymbol{B}/\gamma q B^2 + \boldsymbol{E_{ind}} \times \boldsymbol{B}/B^2$, by the relation:

$$\boldsymbol{E_{ind}}(\boldsymbol{r}, t) \cdot d\boldsymbol{l} = -\frac{B(\boldsymbol{r}, t)}{|\nabla B(\boldsymbol{r}, t)|} \boldsymbol{V_D}(\boldsymbol{r}, t) \cdot \boldsymbol{\nabla} B(\boldsymbol{r}, t) dl \tag{A-19}$$

2730
2731 Thus:

$$d\Phi_T(\boldsymbol{r_o}, t) = dt \oint_{\Gamma(r_o)} \frac{B(\boldsymbol{r}, t)}{|\nabla B(\boldsymbol{r}, t)|} \boldsymbol{V_D} \cdot \boldsymbol{\nabla} B(\boldsymbol{r}, t) dl \quad \text{(A-20)}$$

2732 Finally, let us note that for all points along $\Gamma(r_o)$

$$\frac{dB}{dt}(\boldsymbol{r}, t) = \frac{\partial B}{\partial t}(\boldsymbol{r}, t) + \boldsymbol{V_D}(\boldsymbol{r}, t) \cdot \boldsymbol{\nabla} B(\boldsymbol{r}, t) \quad \text{(A-21)}$$

2733 As a result, the sum of the spatial and temporal contributions to the variation of the magnetic flux
2734 is

$$\begin{aligned} d\Phi(\boldsymbol{r_o}, t) &= d\Phi_A(\boldsymbol{r_o}, t) + d\Phi_T(\boldsymbol{r_o}, t) \\ &= dt \oint_{\Gamma(r_o)} \frac{B(\boldsymbol{r}, t)}{|\nabla B(\boldsymbol{r}, t)|} \left(\frac{dB}{dt}(\boldsymbol{r}, t) - \frac{dB}{dt}(\boldsymbol{r_o}, t) \right) dl \end{aligned} \quad \text{(A-22)}$$

2735 Thus:

$$\frac{d\Phi}{dt}(\boldsymbol{r_o}, t) = \oint_{\Gamma(r_o)} \frac{B(\boldsymbol{r}, t)}{|\nabla B(\boldsymbol{r}, t)|} \left(\frac{dB}{dt}(\boldsymbol{r}, t) - \frac{dB}{dt}(\boldsymbol{r_o}, t) \right) dl \quad \text{(A-23)}$$

2736 with

$$\frac{dL^*}{L^{*2}} = \frac{d\Phi}{2\pi B_E R_E^2} \quad \text{(A-24)}$$

2737 we obtain

$$\frac{dL^*}{dt}(\boldsymbol{r_o}, t) = \frac{L^{*2}}{2\pi B_E R_E^2} \oint_{\Gamma(r_o)} \frac{B(\boldsymbol{r}, t)}{|\nabla B(\boldsymbol{r}, t)|} \left(\frac{dB}{dt}(\boldsymbol{r}, t) - \frac{dB}{dt}(\boldsymbol{r_o}, t) \right) dl \quad \text{(A-25)}$$

2738

2739 A.3. Proof #2
2740
2741 The second proof consists of tracking the drift motions over all guiding center locations along
2742 the same drift contour, $\Gamma(r_o)$. All guiding centers have initially the same three adiabatic
2743 invariants (*M, J=0, L**), but they have different drift phases at the time of the perturbation.
2744 This second proof relies on the fact that the magnetic flux, through a closed curve moving at
2745 $(\boldsymbol{E_{ind}} \times \boldsymbol{B})/B^2$ is conserved, which is what we will demonstrate as a first step.

2746

2747 A.3.1. Conservation of the magnetic flux through a closed curve moving at $(\boldsymbol{E_{ind}} \times \boldsymbol{B})/B^2$

2748

2749 Let us consider at time, $t + dt$, the closed curve, $\tilde{\Gamma}$, formed by all the new guiding center
2750 locations (see also **Fig. 16**).

2751

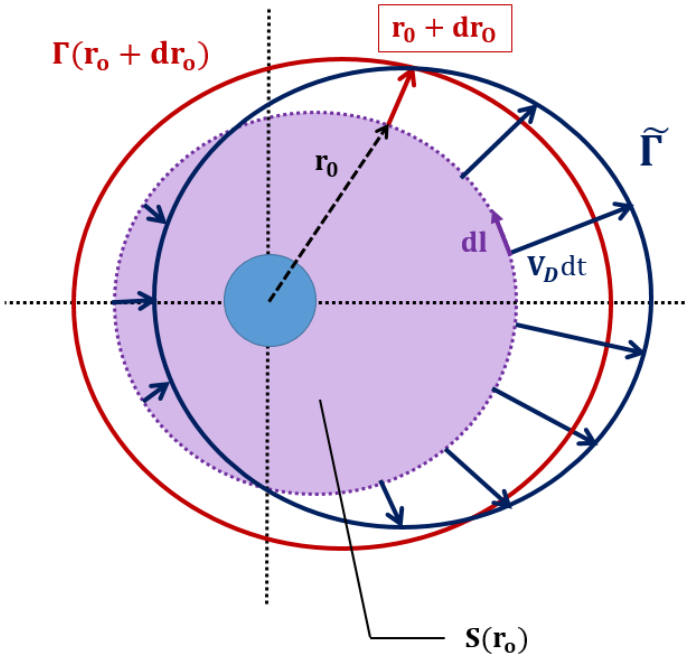

2752 **Fig. 16** Definition of the closed curve, $\tilde{\Gamma}$, formed by all the new guiding center locations.
2753 Because the equatorial magnetic field intensity along $\tilde{\Gamma}$ is not necessarily constant, $\tilde{\Gamma}$ is not
2754 necessarily a drift contour. Yet, because $(\boldsymbol{E_{ind}} \times \boldsymbol{B})/B^2$ is flux-preserving, the flux encompassed
2755 by $\tilde{\Gamma}$ is equal to the initial magnetic flux of the population considered.

2756

2757 Because the equatorial magnetic field intensity along $\tilde{\Gamma}$ is not necessarily constant, $\tilde{\Gamma}$ is not
2758 necessarily a drift contour. Yet, it is interesting to note that the magnetic flux, $\tilde{\Phi}$, encompassed
2759 by $\tilde{\Gamma}$ is equal to the initial magnetic flux through $\Gamma(r_o)$. Indeed:

$$\tilde{\Phi}(t+dt) = \iint_{S(r_o)} \boldsymbol{B}(\boldsymbol{r}, t+dt) \cdot d\boldsymbol{S} + \oint_{\Gamma(r_o)} \boldsymbol{B}(\boldsymbol{r}, t+dt) \cdot (\boldsymbol{V_D}(\boldsymbol{r}, t)dt \times d\boldsymbol{l}) \qquad \text{(A-26)}$$

2760 Because

$$\mathbf{B}(\boldsymbol{r}, t+dt) \cdot (\boldsymbol{V_D}(\boldsymbol{r}, t) \times d\boldsymbol{l}) = \big(\boldsymbol{B}(\boldsymbol{r}, t+dt) \times \boldsymbol{V_D}(\boldsymbol{r}, t)\big) \cdot d\boldsymbol{l} = \boldsymbol{E_{ind}}(\boldsymbol{r}, t) \cdot d\boldsymbol{l} \qquad \text{(A-27)}$$

2761 it results that

$$\oint_{\Gamma(r_o)} \boldsymbol{B}(\boldsymbol{r}, t+dt) \cdot (\boldsymbol{V_D}(\boldsymbol{r}, t)dt \times d\boldsymbol{l}) = dt \oint_{\Gamma(r_o)} \boldsymbol{E_{ind}}(\boldsymbol{r}, t) \cdot d\boldsymbol{l} \tag{A-28}$$

Using the integral form of the Maxwell-Faraday equation:

$$\begin{aligned} dt \oint_{\Gamma(r_o)} \boldsymbol{E_{ind}}(\boldsymbol{r}, t) \cdot d\boldsymbol{l} &= -dt \iint_{S(r_o)} \frac{\partial \boldsymbol{B}(\boldsymbol{r}, t)}{\partial t} \cdot \boldsymbol{dS} \\ &= \iint_{S(r_o)} \boldsymbol{B}(\boldsymbol{r}, t) \cdot \boldsymbol{dS} - \iint_{S(r_o)} \boldsymbol{B}(\boldsymbol{r}, t+dt) \cdot \boldsymbol{dS} \end{aligned} \tag{A-29}$$

Thus,

$$\begin{aligned} \widetilde{\Phi}(t+dt) = &\iint_{S(r_o)} \boldsymbol{B}(\boldsymbol{r}, t+dt) \cdot \boldsymbol{dS} \\ &+ \left(\iint_{S(r_o)} \boldsymbol{B}(\boldsymbol{r}, t) \cdot \boldsymbol{dS} - \iint_{S(r_o)} \boldsymbol{B}(\boldsymbol{r}, t+dt) \cdot \boldsymbol{dS} \right) \end{aligned} \tag{A-30}$$

We conclude that for all guiding center locations, $\boldsymbol{r_o}$, initially along $\Gamma(r_o)$:

$$\Phi(\boldsymbol{r_o}, t) = \widetilde{\Phi}(t+dt) \tag{A-31}$$

In other words, the drift contour distorts to conserve the magnetic flux. This is due to the fact that $(\boldsymbol{E_{ind}} \times \boldsymbol{B})/B^2$ is flux-preserving (Newcomb 1958).

A.3.2. Reformulation for the variation of the magnetic flux

We reformulate the variation of the magnetic flux (equation (A-7)), using the fact that the magnetic flux encompassed by the closed curve $\tilde{\Gamma}$ at $t+dt$ is equal to the initial flux (equation (A-31)) (see also **Fig. 17**)

$$\begin{aligned} d\Phi(\boldsymbol{r_o}, t) &= \Phi(\boldsymbol{r_o} + \boldsymbol{dr_o}, t+dt) - \Phi(\boldsymbol{r_o}, t) \\ &= \Phi(\boldsymbol{r_o} + \boldsymbol{dr_o}, t+dt) - \widetilde{\Phi}(t+dt) \end{aligned} \tag{A-32}$$

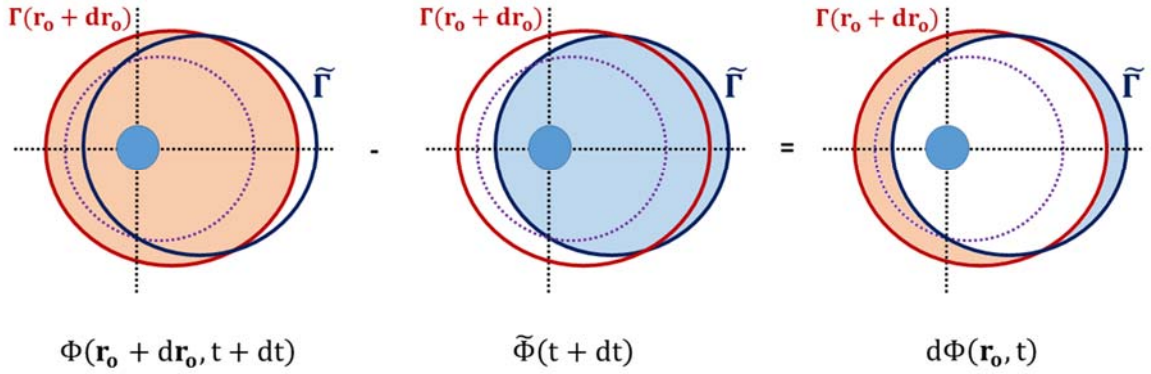

Fig. 17 Representation of the variation of the magnetic flux as the difference between the magnetic flux encompassed by the drift contour, $\Gamma(r_o + dr_o)$, at $t+dt$ and the magnetic flux encompassed by the distorted contour $\tilde{\Gamma}$

Combining the equations (A-9) and (A-26), we have

$$d\Phi(\boldsymbol{r_o}, t) = d\Phi_A(\boldsymbol{r_o}, t) - \oint_{\Gamma(r_o)} \boldsymbol{B}(\boldsymbol{r}, t + dt) \cdot (\boldsymbol{V_D}(\boldsymbol{r}, t)dt \times d\boldsymbol{l}) \tag{A-33}$$

From equation (A-12), we obtain that the variation of the magnetic flux is, to the first order in dt

$$d\Phi(\boldsymbol{r_o}, t) = \oint_{\Gamma(r_o)} \boldsymbol{B}(\boldsymbol{r}, t) \cdot \left((\boldsymbol{dh}(\boldsymbol{r_o}, \boldsymbol{r}) - \boldsymbol{V_D}(\boldsymbol{r}, t)dt) \times \boldsymbol{dl}\right) \tag{A-34}$$

This expression is also:

$$d\Phi(\boldsymbol{r_o}, t) = \oint_{\Gamma(r_o)} \boldsymbol{B}(\boldsymbol{r}, t) \cdot \left((\boldsymbol{dh}(\boldsymbol{r_o}, \boldsymbol{r}) - \boldsymbol{dh}(\boldsymbol{r}, \boldsymbol{r})) \times \boldsymbol{dl}\right) \tag{A-35}$$

Using equation (A-15), this result is equivalent to equation (A-25). A geometric definition for the variation of the magnetic flux according to equation (A-35) is represented in **Fig. 18**.

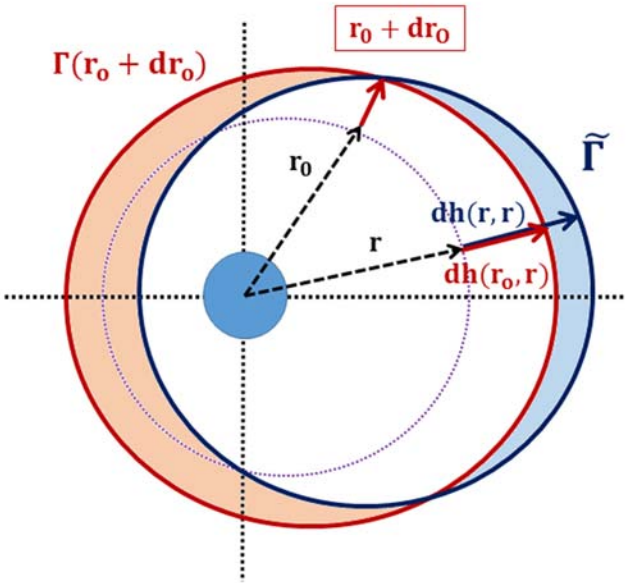

Fig. 18 Geometric interpretation of the variation of the magnetic flux

A.4. Reformulation in terms of deviation from the average

Noticing that the drift velocity of a guiding center trapped in a magnetic field in stationary conditions in the absence of electric fields is:

$$\boldsymbol{V_{D,s}}(\boldsymbol{r},t) = -\frac{M}{\gamma q}\frac{\nabla B(\boldsymbol{r},t)\times \boldsymbol{e_o}}{B(\boldsymbol{r},t)} \tag{A-36}$$

and introducing the infinitesimal time step spent along the drift contour, $d\tau$, such that

$$|d\tau| = \frac{dl}{\left|\boldsymbol{V_{D,s}}(\boldsymbol{r},t)\right|} \tag{A-37}$$

The equation (A-25) becomes:

$$\frac{d\Phi}{dt}(\boldsymbol{r_o},t) = \int_0^{\tau_D}\frac{M}{\gamma q}\left(\frac{dB}{dt}(\boldsymbol{r},t) - \frac{dB}{dt}(\boldsymbol{r_o},t)\right)d\tau \tag{A-38}$$

Let us introduce the linear operator $[\quad]_D$ to denote the spatial drift average along the guiding drift contour, Γ. It is defined by

$$[f]_D(t) = \frac{1}{\tau_D}\int_0^{\tau_D} f(\boldsymbol{r}(\tau),t)d\tau \tag{A-39}$$

2798 This operation determines the spatial average of the quantity, f, along the drift contour, Γ,
2799 weighted by the time spent drifting through each location under stationary conditions.
2800 Thus

$$\frac{d\Phi}{dt}(\boldsymbol{r_o}, t) = \frac{\tau_D}{q}\left(\left[\frac{M}{\gamma}\frac{dB}{dt}\right]_D(t) - \frac{M}{\gamma}\frac{dB}{dt}(\boldsymbol{r_o}, t)\right) \tag{A-40}$$

2801
2802 In the case of an equatorial guiding center trapped in a magnetic field in the absence of
2803 electrostatic fields

$$\frac{M}{\gamma}\frac{dB}{dt} = \frac{d\varepsilon}{dt} \tag{A-41}$$

2804 where ε is the total energy of the guiding center. Thus, we obtain that

$$\frac{d\Phi}{dt}(\boldsymbol{r_o}, t) = \frac{\tau_D}{q}\left(\left[\frac{d\varepsilon}{dt}\right]_D(t) - \frac{d\varepsilon}{dt}(\boldsymbol{r_o}, t)\right) \tag{A-42}$$

2805 This expression is identical to the one derived by Northrop (1963). It is valid in the most general
2806 case (e.g., Cary and Brizard 2009; Lejosne et al. 2012; Lejosne 2013). As a result,

$$\frac{dL^*}{dt}(\boldsymbol{r_o}, t) = \frac{L^{*2}}{q\Omega B_E R_E^2}\left(\left[\frac{d\varepsilon}{dt}\right]_D(t) - \frac{d\varepsilon}{dt}(\boldsymbol{r_o}, t)\right) \tag{A-43}$$

2807 where $\Omega = 2\pi/\tau_D$ is the population drift frequency.
2808

REFERENCES

A.F. Ali, S.R. Elkington, W. Tu, L.G. Ozeke, A.A. Chan, R.H.W. Friedel, Magnetic field power spectra and magnetic radial diffusion coefficients using CRRES magnetometer data. J. Geophys. Res. Space Physics, 120: 973–995 (2015). https://doi.org/10.1002/2014JA020419

A.F. Ali, D.M. Malaspina, S.R. Elkington, A.N. Jaynes, A.A. Chan, J. Wygant, C.A. Kletzing, Electric and magnetic radial diffusion coefficients using the Van Allen probes data. J. Geophys. Res. Space Physics, 121, 9586–9607 (2016). https://doi.org/10.1002/2016JA023002

M. Andriopoulou, et al., A noon-to-midnight electric field and nightside dynamics in Saturn's inner magnetosphere, using microsignature observations. Icarus, 220, 503–513 (2012). https://doi.org/10.1016/j.icarus.2012.05.010

M. Andriopoulou, et al., Spatial and temporal dependence of the convective electric field in Saturn's inner magnetosphere. Icarus, 229, 57–70 (2014). https://doi.org/10.1016/j.icarus.2013.10.028

A.R. Azari, M.W. Liemohn, X. Jia, M.F. Thomsen, D.G. Mitchell, N. Sergis, et al., Interchange injections at Saturn: Statistical survey of energetic H^+ sudden flux intensifications. J. Geophys. Res. Space Physics, 123, 4692–4711 (2018). https://doi.org/10.1029/2018JA025391

D.N. Baker, S. Kanekal, J.B. Blake, B. Klecker, G. Rostoker, Satellite anomalies linked to electron increase in the magnetosphere, Eos Trans., AGU, 75, 404 (1994). https://doi.org/10.1029/94EO01038

F. Bagenal, R.J. Wilson, S. Siler, W.R. Paterson, W.S. Kurth, Survey of Galileo plasma observations in Jupiter's plasma sheet. J. Geophys. Res. Planets, 121 (2016). https://doi.org/10.1002/2016JE005009

W. Baumjohann, G. Paschmann, H. Lühr, Characteristics of High-Speed Ion Flows in the Plasma Sheet, J. Geophys. Res., 95, A4, 3801-3809 (1990). https://doi.org/10.1029/JA095iA04p03801

T. Beutier, D. Boscher, A three-dimensional analysis of the electron radiation belt by the Salammbô code. J. Geophys. Res., 100 (A8), 14853–14861 (1995). https://doi.org/10.1029/94JA03066

T.J. Birmingham, F.C. Jones, Identification of moving magnetic field lines. J. Geophys. Res., 73, 5505–5510 (1968). https://doi.org/10.1029/JA073i017p05505

T.J. Birmingham, Convection electric fields and the diffusion of trapped magnetospheric radiation. J. Geophys. Res., 74(9), 2169–2181 (1969). https://doi.org/10.1029/JA074i009p02169

T. Birmingham, et al., The electron diffusion coefficient in Jupiter's magnetosphere. J. Geophys. Res, 79, 1, 87-97 (1974). https://doi.org/10.1029/JA079i001p00087

D.H. Brautigam, J.M. Albert, Radial diffusion analysis of outer radiation belt electrons during the October 9, 1990, magnetic storm. J. Geophys. Res., 105(A1), 291–309 (2000). https://doi.org/10.1029/1999JA900344

D.H. Brautigam, G.P. Ginet, J.M. Albert, J.R. Wygant, D.E. Rowland, A. Ling, J. Bass, CRRES electric field power spectra and radial diffusion coefficients. J. Geophys. Res., 110, A02214 (2005). https://doi.org/10.1029/2004JA010612

N. Brice, T.R. McDonough, Jupiter's radiation belts, Icarus, 18, 206–219 (1973). https://doi.org/10.1016/0019-1035(73)90204-2

A.J. Brizard, A.A. Chan, Relativistic bounce-averaged quasilinear diffusion equation for low-frequency electromagnetic fluctuations. Phys. Plasmas, 8(11), 4762–4771 (2001). https://doi.org/10.1063/1.1408623

W.L. Brown, Observations of the Transient Behavior of Electrons in the Artificial Radiation Belts. In: McCormac B.M. (eds) *Radiation Trapped in the Earth's Magnetic Field. Astrophysics and Space Science Library,* vol 5. Springer, Dordrecht (1966). https://doi.org/10.1007/978-94-010-3553-8_44

J.R. Cary, A.J. Brizard, Hamiltonian theory of guiding-center motion. Rev. Mod. Phys., 81, 2, 693-738 (2009). https://link.aps.org/doi/10.1103/RevModPhys.81.693

C. Cattell, et al. Discovery of very large amplitude whistler-mode waves in Earth's radiation belts. Geophys. Res. Lett., 35, L01105 (2008). https://doi.org/10.1029/2007GL032009

S. Chandrasekhar, Stochastic Problems in Physics and Astronomy. Reviews of Modern Physics, 15, 1 (1943). https://doi.org/10.1103/RevModPhys.15.1

Y. Chen, T. W. Hill, A. M. Rymer, R. J. Wilson, Rate of radial transport of plasma in Saturn's inner magnetosphere. J. Geophys. Res., 115, A10211 (2010). https://doi.org/10.1029/2010JA015412

A.F. Cheng, et al., Energetic ion and electron phase space densities in the magnetosphere of Uranus. J. Geophys. Res., 92, A13, 15315-15328 (1987). https://doi.org/10.1029/JA092iA13p15315

A.F. Cheng, et al., Energetic ion phase space densities in Neptune's magnetosphere. Icarus, 99, 420-429 (1992). https://doi.org/10.1016/0019-1035(92)90157-3

G. Clark, C. Paranicas, D. Santos-Costa, S. Livi, N. Krupp, D.G. Mitchell, E. Roussos, W.-L. Tseng, Evolution of electron pitch angle distributions across Saturn's middle magnetospheric region from MIMI/LEMMS. Planet. Space Sci., 104, 18–28 (2014). https://doi.org/10.1016/j.pss.2014.07.004

G. Clark, B.H. Mauk, C. Paranicas, P. Kollmann, H.T. Smith, Charge states of energetic oxygen and sulfur ions in Jupiter's magnetosphere. J. Geophys. Res. Space Physics, 121, 2264–2273 (2016). https://doi.org/10.1002/2015JA022257

J.F. Cooper, Nuclear cascades in Saturn's rings - Cosmic ray albedo neutron decay and origins of trapped protons in the inner magnetosphere. J. Geophys. Res., 88, 3945–3954 (1983). https://doi.org/10.1029/JA088iA05p03945

J.F. Cooper et al., Local time asymmetry of drift shells for energetic electrons in the middle magnetosphere of Saturn. Adv. Space Res., 21, 11 1479-1482 (1998). https://doi.org/10.1016/S0273-1177(98)00022-2

J.F. Cooper, S.J. Sturner, Energetic radiation from galactic cosmic ray interactions with Saturn's main rings. J. Geophys. Res. Space Physics, 123 (2018). https://doi.org/10.1029/2018JA025583

J.M. Cornwall, Diffusion Processes Influenced by Conjugate-Point Wave Phenomena. Radio Science, 3 (1968). https://doi.org/10.1002/rds196837740

F.V. Coroniti, Energetic Electrons in Jupiter's Magnetosphere. The Astronomical Journal Supplement Series, 244, 27, 261-281(1974). https://doi.org/10.1086/190296

S. W. H. Cowley, The Causes of Convection in the Earth's Magnetosphere: A Review of Developments During the IMS, Reviews of Geophysics and Space Physics, 20, 3, 531-565 (1982). https://doi.org/10.1029/RG020i003p00531

S. W. H. Cowley et al., Jupiter's polar ionospheric flows: Theoretical interpretation, Geophys. Res. Lett., 30(5), 1220 (2003). https://doi.org/10.1029/2002GL016030

S. W. H. Cowley, et al., Saturn's polar ionospheric flows and their relation to the main auroral oval, Annales Geophysicae, 22: 1379–1394 (2004). https://doi.org/10.5194/angeo-22-1379-2004

C.M. Cully, J.W. Bonnell, R.E. Ergun, THEMIS observations of long-lived regions of large-amplitude whistler waves in the inner magnetosphere. Geophys. Res. Lett., 35, L17S16 (2008). https://doi.org/10.1029/2008GL033643

G.S. Cunningham, V. Loridan, J.-F. Ripoll, M. Schulz, Neoclassical diffusion of radiation-belt electrons across very low L-shells. J. Geophys. Res. Space Physics, 123, 2884– 2901 (2018). https://doi.org/10.1002/2017JA024931

L. Davis Jr., D.B. Chang, On the effect of geomagnetic fluctuations on trapped particles. J. Geophys. Res., 67(6), 2169–2179 (1962). https://doi.org/10.1029/JZ067i006p02169

I. De Pater, C.K. Goertz, Radial diffusion models of energetic electrons and Jupiter's synchrotron radiation 2: Time Variability, J. Geophys. Res., 99, A1, 2271-2287 (1994). https://doi.org/10.1029/93JA02097

I. De Pater, et al., Outburst of Jupiter's synchrotron radiation after the impact of comet Shoemaker-Levy 9, Science, 268, 5219, 1879-1883 (1995). https://doi.org/10.1126/science.11536723

A.J. Dessler, R. Karplus, Some effects of diamagnetic ring currents on Van Allen radiation, J. Geophys. Res., 66(8), 2289–2295 (1961). https://doi.org/10.1029/JZ066i008p02289

A.Y. Drozdov, Y.Y. Shprits, N.A. Aseev, A.C. Kellerman, G.D. Reeves, Dependence of radiation belt simulations to assumed radial diffusion rates tested for two empirical models of radial transport. Space Weather, 15, 150–162 (2017). https://doi.org/10.1002/2016SW001426

M. Dumont et al., Jupiter's equatorward auroral features: Possible signatures of magnetospheric injections, J. Geophys. Res. Space Physics, 119, 10,068–10,077 (2014). https://doi.org/10.1002/2014JA020527

J.W. Dungey, Effects of Electromagnetic Perturbations on Particles Trapped in the Radiation Belts, Space Sci. Rev., 4, 199 (1965). https://doi.org/10.1007/BF00173882

S.R. Elkington, M.K. Hudson, A.A. Chan, Acceleration of relativistic electrons via drift-resonant interaction with toroidal-mode Pc-5 ULF oscillations. Geophys. Res. Lett. (1999). https://doi.org/10.1029/1999GL003659

S.R. Elkington, M.K. Hudson, A.A. Chan, Resonant acceleration and diffusion of outer zone electrons in an asymmetric geomagnetic field. J. Geophys. Res., 108, 1116, A3 (2003). https://doi.org/10.1029/2001JA009202

C.-G. Fälthammar, Effects of time-dependent electric fields on geomagnetically trapped radiation. J. Geophys. Res., 70(11), 2503–2516 (1965). https://doi.org/10.1029/JZ070i011p02503

C.-G. Fälthammar, On the transport of trapped particles in the outer magnetosphere. J. Geophys. Res., 71(5), 1487–1491 (1966). https://doi.org/10.1029/JZ071i005p01487

C.-G. Fälthammar, Radial diffusion by violation of the third adiabatic invariant, in *Earth's Particles and Fields*, edited by B. M. McCormac, pp. 157–169, Reinhold, New York (1968).

C.-G. Fälthammar, F. S. Mozer, On the concept of moving magnetic field lines. Eos Trans. AGU, 88 (2007). https://doi.org/10.1029/2007EO150002

T.A. Farley, Radial diffusion of electrons at low L values. J. Geophys. Res., 74(1), 377–380 (1969a). https://doi.org/10.1029/JA074i001p00377

T.A. Farley, Radial diffusion of starfish electrons. J. Geophys. Res., 74(14), 3591–3600 (1969b). https://doi.org/10.1029/JA074i014p03591

Y. Fei, A.A. Chan, S.R. Elkington, M.J. Wiltberger, Radial diffusion and MHD particle simulations of relativistic electron transport by ULF waves in the September 1998 storm. J. Geophys. Res., 111, A12209 (2006). https://doi.org/10.1029/2005JA011211

R.W. Fillius, C.E. McIlwain, Adiabatic betatron acceleration by a geomagnetic storm. J. Geophys. Res., 72(15), 4011–4015 (1967). https://doi.org/10.1029/JZ072i015p04011

R.W. Fillius, et al., Radiation belts of Jupiter: A second look. Science, 188, 4187, 465-467 (1974). https://doi.org/10.1126/science.188.4187.465

L.A. Frank, J.A. Van Allen, H. K. Hills, A study of charged particles in the Earth's outer radiation zone with explorer 14. J. Geophys. Res., 69(11), 2171–2191 (1964). https://doi.org/10.1029/JZ069i011p02171

L.A. Frank, Inward radial diffusion of electrons of greater than 1.6 million electron volts in the outer radiation zone. J. Geophys. Res., 70(15), 3533–3540 (1965). https://doi.org/10.1029/JZ070i015p03533

S.A. Glauert, R.B. Horne, N.P. Meredith, Three-dimensional electron radiation belt simulations using the BAS Radiation Belt Model with new diffusion models for chorus, plasmaspheric hiss, and lightning-generated whistlers. J. Geophys. Res. Space Physics, 119, 268–289 (2014). https://doi.org/10.1002/2013JA019281

S.A. Glauert, R.B. Horne, N.P. Meredith, A 30-year simulation of the outer electron radiation belt. Space Weather, 16, 1498–1522 (2018). https://doi.org/10.1029/2018SW001981

T.I. Gombosi, D.N. Baker, A. Balogh, et al., Anthropogenic Space Weather. Space Sci Rev 212: 985 (2017). https://doi.org/10.1007/s11214-017-0357-5

T. Gold, Motions in the magnetosphere of the Earth. J. Geophys. Res., 64, 9 (1959). https://doi.org/10.1029/JZ064i009p01219

J.C. Green, M.G. Kivelson, Relativistic electrons in the outer radiation belt: Differentiating between acceleration mechanisms. J. Geophys. Res., 109, A03213 (2004). https://doi.org/10.1029/2003JA010153

J.C. Green, J. Likar, Y. Shprits, Impact of space weather on the satellite industry. Space Weather, 15, 804–818 (2017). https://doi.org/10.1002/2017SW001646

S. Han et al., Investigating solar wind-driven electric field influence on long-term dynamics of Jovian synchrotron radiation. Journal of Geophysical Research: Space Physics, 123, 9508–9516 (2018). https://doi.org/ 10.1029/2018JA025849

A. Hegedus, et al., Measuring the Earth's Synchrotron Emission from Radiation Belts with a Lunar Near Side Radio Array. Radio Science (2020). https://doi.org/10.1029/2019RS006891

N. Herlofson, Diffusion of Particles in the Earth's Radiation Belts. Phys. Rev. Lett. 5, 414 (1960). https://doi.org/10.1103/PhysRevLett.5.414

T.W. Hill, Inertial Limit on Corotation. J. Geophys. Res., 84, A11 (1979). https://doi.org/10.1029/JA084iA11p06554

T.W. Hill, Longitudinal asymmetry of the Io plasma torus. Geophys. Res. Lett., 10: 969-972 (1983). https://doi.org/10.1029/GL010i010p00969

T.W. Hill, et al., Evidence for rotationally driven plasma transport in Saturn's magnetosphere. Geophys. Res. Lett.,, 32, L14S10 (2005). https://doi.org/10.1029/2005GL022620

R.H. Holzworth, F. S. Mozer, Direct evaluation of the radial diffusion coefficient near L=6 due to electric field fluctuations. J. Geophys. Res., 84(A6), 2559–2566 (1979). https://doi.org/10.1029/JA084iA06p02559

L.L. Hood, Radial diffusion in Saturn's radiation belts - A modeling analysis assuming satellite and ring E absorption. J. Geophys. Res., 88, 808–818 (1983). https://doi.org/10.1029/JA088iA02p00808

R.B. Horne, S.A. Glauert, N.P. Meredith, D. Boscher, V. Maget, D. Heynderickx, D. Pitchford, Space weather impacts on satellites and forecasting the Earth's electron radiation belts with SPACECAST. Space Weather, 11, 169– 186 (2013). https://doi.org/10.1002/swe.20023

R.B. Horne, D. Pitchford, Space Weather Concerns for All-Electric Propulsion Satellites. Space Weather, 13, 430– 433 (2015). https://doi.org/10.1002/2015SW001198

R.B. Horne, M.W. Phillips, S.A. Glauert, N.P. Meredith, A.D.P. Hands, K. Ryden, W. Li, Realistic worst case for a severe space weather event driven by a fast solar wind stream. Space Weather, 16, 1202–1215 (2018). https://doi.org/10.1029/2018SW001948

C.-L. Huang, H.E. Spence, M.K. Hudson, S.R. Elkington, Modeling radiation belt radial diffusion in ULF wave fields: 2. Estimating rates of radial diffusion using combined MHD and particle codes. J. Geophys. Res., 115, A06216 (2010). https://doi.org/10.1029/2009JA014918

M.K. Hudson, S.R. Elkington, J.G. Lyon, C.C. Goodrich, T.J. Rosenberg, Simulation of Radiation Belt Dynamics Driven by Solar Wind Variations. In Sun-Earth Plasma Connections (eds J.L. Burch, R.L. Carovillano and S.K. Antiochos) (1999). https://doi.org/10.1029/GM109p0171

S.A. Jacques, L. Davis Jr., Diffusion Models for Jupiter's Radiation Belt. NASA/Caltech technical report N75-15574, Report Number: NASA-CR-141967, Document ID: 19750007502, (1972). http://hdl.handle.net/2060/19750007502

A.N. Jaynes, D. Malaspina, A.A. Chan, S.R. Elkington, A.F. Ali, M. Bruff, H. Zhao, D.N. Baker, X. Li, S. Kanekal, Battle Royale: VLF-driven local acceleration vs ULF driven radial transport. AGU Fall Meeting Abstracts (2018a). https://agu.confex.com/agu/fm18/meetingapp.cgi/Paper/369848

A.N. Jaynes, A.F. Ali, S.R. Elkington, D.M. Malaspina, D.N. Baker, X. Li, et al., Fast diffusion of ultrarelativistic electrons in the outer radiation belt: 17 March 2015 storm event. Geophys. Res. Lett., 45, 10,874–10,882 (2018b). https://doi.org/10.1029/2018GL079786

S. Jurac, J.D. Richardson, A self-consistent model of plasma and neutrals at Saturn: Neutral cloud morphology. J. Geophys. Res., 110, A09220 (2005). https://doi.org/10.1029/2004JA010635.

P.J. Kellogg, Possible explanation of the radiation observed by Van Allen at high altitudes in satellites. Nuovo cimiento, [10] 11, 48 (1959a). https://doi.org/10.1007/BF02724906

P.J. Kellogg, Van Allen Radiation of Solar Origin. Nature, Lond. 183, 1295-7 (1959b). https://doi.org/10.1038/1831295a0.

C. F. Kennel, F. Engelmann, Velocity space diffusion from weak plasma turbulence in a magnetic field. The Physics of Fluids, 9(12), 2377-2388 (1966). https://doi.org/10.1063/1.1761629

H.-J. Kim, A.A. Chan, Fully adiabatic changes in storm time relativistic electron fluxes. J. Geophys. Res., 102(A10), 22107–22116 (1997). https://doi.org/10.1029/97JA01814

K.C. Kim, Y. Shprits, D. Subbotin, B. Ni, Understanding the dynamic evolution of the relativistic electron slot region including radial and pitch angle diffusion. J. Geophys. Res., 116, A10214 (2011). https://doi.org/10.1029/2011JA016684

P. Kollmann et al., Energetic particle phase space densities at Saturn: Cassini observations and interpretations. J.Geophys. Res., 116, A05222 (2011). https://doi.org/10.1029/2010JA016221

P. Kollmann, E. Roussos, C. Paranicas, N. Krupp, D. K. Haggerty, Processes forming and sustaining Saturn's proton radiation belts. Icarus, 222, 323–341 (2013). https://doi.org/10.1016/j.icarus.2012.10.033

P. Kollmann, E. Roussos, A. Kotova, C. Paranicas, N. Krupp, The evolution of Saturn's radiation belts modulated by changes in radial diffusion. Nature Astronomy 1, 872–877 (2017). https://doi.org/10.1038/s41550-017-0287-x

P. Kollmann, E. Roussos, C.P. Paranicas, E.E. Woodfield, B.H. Mauk, G. Clark, D.C. Smith, J. Vandegriff, Electron acceleration to MeV energies at Jupiter and Saturn. J. Geophys. Res. Space Phys, 123, 9110– 9129 (2018). https://doi.org/10.1029/2018JA025665

H. Korth, M.F. Thomsen, J.E. Borovsky, D.J. McComas, Plasma sheet access to geosynchronous orbit. J. Geophys. Res., 104(A11), 25047– 25061 (1999). https://doi.org/10.1029/1999JA900292

N. Krupp et al., Dynamics of the Jovian Magnetosphere. In: *Jupiter. The Planet, Satellites and Magnetosphere* (2005). Cambridge University Press. ISBN: 0-521-81808-7

H.R. Lai et al., Transport of magnetic flux and mass in Saturn's inner magnetosphere, J. Geophys. Res. Space Physics, 121, 3050–3057 (2016). https://doi.org/10.1002/2016JA022436

L.J. Lanzerotti, C.G. Maclennan, M. Schulz, Radial diffusion of outer-zone electrons: An empirical approach to third-invariant violation. J. Geophys. Res., 75(28), 5351–5371 (1970). https://doi.org/10.1029/JA075i028p05351

L.J. Lanzerotti, C.G. Maclennan, M. Schulz, Reply [to "Comments on 'Radial diffusion of outer-zone electrons'"]. J. Geophys. Res., 76(22), 5371–5373 (1971). https://doi.org/10.1029/JA076i022p05371

L.J. Lanzerotti, C.G. Morgan, ULF geomagnetic power near L = 4: 2. Temporal variation of the radial diffusion coefficient for relativistic electrons. J. Geophys. Res., 78(22), 4600–4610 (1973). https://doi.org/10.1029/JA078i022p04600

L.J. Lanzerotti, D.C. Webb, C.W. Arthur, Geomagnetic field fluctuations at synchronous orbit 2. Radial diffusion. J. Geophys. Res., 83(A8), 3866–3870 (1978). https://doi.org/10.1029/JA083iA08p03866

S. Lejosne, Modélisation du phénomène de diffusion radiale au sein des ceintures de radiation terrestres par technique de changement d'échelle. PhD thesis, Université de Toulouse, France (2013). https://hal.archives-ouvertes.fr/tel-01132913/document

S. Lejosne, Analytic expressions for radial diffusion. Journal of Geophysical Research: Space Physics, 124 (2019). https://doi.org/10.1029/2019JA026786

S. Lejosne, D. Boscher, V. Maget, G. Rolland, Bounce-averaged approach to radial diffusion modeling: From a new derivation of the instantaneous rate of change of the third adiabatic invariant to the characterization of the radial diffusion process. J. Geophys. Res., 117, A08231 (2012). https://doi.org/10.1029/2012JA018011

S. Lejosne, D. Boscher, V. Maget, G. Rolland, Deriving electromagnetic radial diffusion coefficients of radiation belt equatorial particles for different levels of magnetic activity based on magnetic field measurements at geostationary orbit. J. Geophys. Res. Space Physics, 118, 3147–3156 (2013). https://doi.org/10.1002/jgra.50361

X. Li, et al., Quantitative prediction of radiation belt electrons at geostationary orbit based on solar wind measurements. Geophys. Res. Let. 28, 9, 1887-1890 (2001). https://doi.org/10.1029/2000GL012681

Z. Li, M. Hudson, M. Patel, M. Wiltberger, A. Boyd, D.Turner, ULF wave analysis and radial diffusion calculation using a global MHD model for the 17 March 2013 and 2015 storms, J. Geophys. Res. Space Physics, 122, 7353– 7363 (2017). https://doi.org/10.1002/2016JA023846

A.J. Lichtenberg, M.A. Lieberman, *Regular and Chaotic Dynamics*, Second edition, Applied Mathematical Sciences, Springer-Verlag, New York (1992). https://doi.org/10.1007/978-1-4757-2184-3

W.W. Liu, G. Rostoker, D. N. Baker, Internal acceleration of relativistic electrons by large-amplitude ULF pulsations. J. Geophys. Res., 104(A8), 17391–17407 (1999). https://doi.org/10.1029/1999JA900168

W. Liu, W. Tu, X. Li, T. Sarris, Y. Khotyaintsev, H. Fu, H. Zhang, Q. Shi, On the calculation of electric diffusion coefficient of radiation belt electrons with in situ electric field measurements by THEMIS. Geophys. Res. Lett., 43, 1023–1030 (2016). https://doi.org/10.1002/2015GL067398

L. Lorenzato, A. Sicard, S. Bourdarie, A physical model for electron radiation belts of Saturn. J. Geophys. Res. Space Physics 117, A08214 (2012). https://doi.org/10.1029/2012JA017560

X. Ma et al., Flux tube entropy and specific entropy in Saturn's magnetosphere. Journal of Geophysical Research: Space Physics, 124, 1593–1611 (2019). https://doi.org/10.1029/2018JA026150

V. Maget, S. Bourdarie, D. Boscher, R.H.W. Friedel, Data assimilation of LANL satellite data into the Salammbô electron code over a complete solar cycle by direct insertion. Space Weather, vol. 5, no. S10003 (2007). https://doi.org/10.1029/2007SW000322

V. Maget, S. Bourdarie, D. Boscher, Direct data assimilation over solar cycle time-scales to improve proton radiation belt models. IEEE Trans. Nucl. Sci., vol. 55, no. 4, pp. 2188–2196 (2008). https://doi.org/10.1109/TNS.2008.921928

I.R. Mann, et al., Explaining the dynamics of the ultra-relativistic third Van Allen radiation belt. Nature Phys 12:978–983 (2016). https://doi.org/10.1038/nphys3799

I.R. Mann, et al. Reply to 'The dynamics of Van Allen belts revisited'. Nature Physics, 14(2), 103–104 (2018). https://doi.org/10.1038/nphys4351

R.A. Mathie, I.R. Mann, A correlation between extended intervals of Ulf wave power and storm-time geosynchronous relativistic electron flux enhancements. Geophys. Res. Lett.,27, 3261 (2000). https://doi.org/10.1029/2000GL003822

B.H. Mauk, et al., Fundamental Plasma Processes in Saturn's Magnetosphere, In: Saturn from Cassini-Huygens, Springer Science+Business Media B.V. (2009). https://doi.org/10.1007/978-1-4020-9217-6_11

B.H. Mauk, Comparative investigation of the energetic ion spectra comprising the magnetospheric ring currents of the solar system, J. Geophys. Res. Space Physics, 119 (2014). https://doi.org/10.1002/2014JA020392

G.D. Mead, Deformation of the geomagnetic field by the solar wind. J. Geophys. Res., 69(7), 1181– 1195 (1964). https://doi.org/10.1029/JZ069i007p01181

G.D. Mead, W.N. Hess, Jupiter's radiation belts and the sweeping effect of its satellites, J. Geophys. Res., 78(16), 2793– 2811 (1973). https://doi.org/10.1029/JA078i016p02793

D.G. Mitchell, et al., Injection, Interchange, and Reconnection: Energetic particle observations in Saturn's magnetosphere, In: *Magnetotails in the Solar System*, John Wiley & Sons Inc. (2015). ISBN 9781118842324. https://doi.org/10.1002/9781118842324.ch19

A. Mogro-Campero, Absorption of radiation belt particles by the inner satellites of Jupiter, In: *Jupiter: Studies of the interior, atmosphere, magnetosphere, and satellites*. The University of Arizona Press, ISBN 0-8165-530-6 (1976). http://adsabs.harvard.edu/abs/1976jsia.coll.1190M

F.S. Mozer, Power spectra of the magnetospheric electric field. J. Geophys. Res., 76(16), 3651–3667 (1971). https://doi.org/10.1029/JA076i016p03651

F.S. Mozer, et al., Direct observation of radiation-belt electron acceleration from electron-volt energies to megavolts by nonlinear whistlers. Physical review letters, 113(3), 035001 (2014). https://doi.org/10.1103/PhysRevLett.113.035001

M.P. Nakada, G. D. Mead, Diffusion of protons in the outer radiation belt. J. Geophys. Res., 70(19), 4777–4791 (1965). https://doi.org/10.1029/JZ070i019p04777

M.P. Nakada, J.W. Dungey, W.N. Hess, On the origin of outer-belt protons: 1..J. Geophys. Res., 70(15), 3529–3532 (1965). https://doi.org/10.1029/JZ070i015p03529

Q. Nénon, A. Sicard, S. Bourdarie, A new physical model of the electron radiation belts of Jupiter inside Europa's orbit. J. Geophys. Res Space Physics, 122, 5148– 5167 (2017). https://doi.org/10.1002/2017JA023893

Q. Nénon, A. Sicard, P. Kollmann, H.B. Garrett, S.P.A. Sauer, C. Paranicas, A physical model of the proton radiation belts of Jupiter inside Europa's orbit. J. Geophys. Res. Space Physics, 123, 3512–3532 (2018). https://doi.org/10.1029/2018JA025216

W.A. Newcomb, Motion of magnetic lines of Force. Annals of Physics, 3, 347-385 (1958). https://doi.org/10.1016/0003-4916(58)90024-1

L.L. Newkirk, M. Walt, Radial diffusion coefficient for electrons at $1.76 < L < 5$. J. Geophys. Res., 73(23), 7231–7236 (1968a). https://doi.org/10.1029/JA073i023p07231

L.L. Newkirk, M. Walt, Radial diffusion coefficient for electrons at low L values. J. Geophys. Res., 73(3), 1013–1017 (1968b). https://doi.org/10.1029/JA073i003p01013

T.G. Northrop, *The Adiabatic Motion of Charged Particles*. Wiley-Interscience, Hoboken, N. J. ISBN-13: 978-0470651391 (1963).

T.G. Northrop, E. Teller, Stability of the adiabatic motion of charged particles in the Earth's field. Phys. Rev., 117, 215–225 (1960). https://doi.org/10.1103/PhysRev.117.215

T.P. O'Brien, J.E. Mazur, T.B. Guild. What the Satellite Design Community Needs From the Radiation Belt Science Community. In *Dynamics of the Earth's Radiation Belts and Inner Magnetosphere* (eds D. Summers, I. R. Mann, D.N. Baker and M. Schulz) (2013). https://doi.org/10.1029/2012GM001316

T.P. O'Brien, Breaking all the invariants: Anomalous electron radiation belt diffusion by pitch angle scattering in the presence of split magnetic drift shells. Geophys. Res. Lett., 41, 216– 222 (2014). https://doi.org/10.1002/2013GL058712

T.P. O'Brien et al., Changes in AE9/AP9-IRENE Version 1.5, in *IEEE Transactions on Nuclear Science*, vol. 65, no. 1, pp. 462-466 (2018). https://doi.org/10.1109/TNS.2017.2771324

L. Olifer, I.R. Mann, L.G. Ozeke, I.J. Rae, S.K. Morley, On the relative strength of electric and magnetic ULF wave radial diffusion during the March 2015 geomagnetic storm. J. Geophys. Res. Space Physics, 124, 2569– 2587 (2019). https://doi.org/10.1029/2018JA026348

L.G. Ozeke, I.R. Mann, I.J. Rae, Mapping guided Alfvén wave magnetic field amplitudes observed on the ground to equatorial electric field amplitudes in space. J. Geophys. Res., 114, A01214 (2009). https://doi.org/10.1029/2008JA013041

L.G. Ozeke, et al., ULF wave derived radiation belt radial diffusion coefficients. J. Geophys. Res., 117, A04222 (2012). https://doi.org/10.1029/2011JA017463

L.G. Ozeke, I.R. Mann, K.R. Murphy, I.J. Rae, D.K. Milling, Analytic expressions for ULF wave radiation belt radial diffusion coefficients. J. Geophys. Res. Space Physics, 119, 1587–1605 (2014). https://doi.org/10.1002/2013JA019204

M.K. Öztürk, R.A. Wolf, Bifurcation of drift shells near the dayside magnetopause. J. Geophys. Res., 112, A07207 (2007). https://doi.org/10.1029/2006JA012102

M. Palmroth et al., Vlasov methods in space physics and astrophysics. Living Reviews in Computational Astrophysics, 4, 2365-0524 (2018). https://doi.org/10.1007/s41115-018-0003-2

M. Paonessa, Voyager observations of ion phase space densities in the Jovian magnetosphere. J. Geophys. Res., 90, A1, 521-525 (1985). https://doi.org/10.1029/JA090iA01p00521

C. Paranicas, et al., Effects of radial motion on interchange injections at Saturn. Icarus 264, 342–351 (2016). https://doi.org/10.1016/j.icarus.2015.10.002

E.N. Parker, Geomagnetic fluctuations and the form of the outer zone of the Van Allen radiation belt. J. Geophys. Res., 65(10), 3117–3130 (1960). https://doi.org/10.1029/JZ065i010p03117

K.L. Perry, M.K. Hudson, S.R. Elkington, Incorporating spectral characteristics of Pc5 waves into three-dimensional radiation belt modeling and the diffusion of relativistic electrons. J. Geophys. Res., 110, A03215 (2005). https://doi.org/10.1029/2004JA010760

K.L. Perry, M.K. Hudson, S.R. Elkington, Correction to "Incorporating spectral characteristics of Pc5 waves into three-dimensional radiation belt modeling and the diffusion of relativistic electrons". J. Geophys. Res., 111, A11228 (2006). https://doi.org/:10.1029/2006JA012040

D.H. Pontius Jr., T.W. Hill, Rotation driven plasma transport: The coupling of macroscopic motion and microdiffusion. J. Geophys. Res, 94, A11, 15041-15053 (1989). https://doi.org/10.1029/JA094iA11p15041

D.H. Pontius Jr., R.A. Wolf, Transient Flux Tubes in the terrestrial magnetosphere, Geophys. Res. Lett., 17, 1, 49-52 (1990). https://doi.org/10.1029/GL017i001p00049

M. Qin, X. Zhang, B. Ni, H. Song, H. Zou, Y. Sun, Solar cycle variations of trapped proton flux in the inner radiation belt. J. Geophys. Res. Space Physics, 119, 9658–9669 (2014). https://doi.org/10.1002/2014JA020300

J.D. Richardson, A Quantitative Model of Plasma in Neptune's Magnetosphere. Geophys. Res. Lett., 20, 14, 1467-1470 (1993). https://doi.org/10.1029/93GL01353

P. Riley, R.A. Wolf, Comparison of diffusion and particle drift descriptions of radial transport in the Earth's inner magnetosphere. J. Geophys. Res., 97(A11), 16865–16876 (1992). https://doi.org/10.1029/92JA01538

J.G. Roederer, On the adiabatic motion of energetic particles in a model magnetosphere. J. Geophys. Res., 72(3), 981– 992 (1967). https://doi.org/10.1029/JZ072i003p00981

J.G. Roederer, *Dynamics of Geomagnetically Trapped Radiation*. New York: Springer (1970). https://doi.org/10.1007/978-3-642-49300-3

J.G. Roederer, Geomagnetic field distortions and their effects on radiation belt particles. Rev. Geophys., 10(2), 599–630 (1972). https://doi.org/10.1029/RG010i002p00599

J.G. Roederer, M. Schulz, Effect of shell splitting on radial diffusion in the magnetosphere. J. Geophys. Res., 74(16), 4117– 4122 (1969). https://doi.org/10.1029/JA074i016p04117

J.G. Roederer, M. Schulz, Splitting of drift shells by the magnetospheric electric field. J. Geophys. Res., 76, 4, 1055-1059 (1971). https://doi.org/10.1029/JA076i004p01055

J.G. Roederer, H.H. Hilton, M. Schulz, Drift shell splitting by internal geomagnetic multipoles. J. Geophys. Res., 78, 133-144 (1973). https://doi.org/10.1029/JA078i001p00133

J.G. Roederer, H. Zhang, *Dynamics of Magnetically Trapped Particles, Foundations of the Physics of Radiation Belts and Space Plasmas*, Astrophysics and Space Science Library, vol. 403, Springer-Verlag, Berlin, Heidelberg (2014). https://doi.org/10.1007/978-3-642-41530-2

J.G. Roederer, S. Lejosne, Coordinates for representing radiation belt particle flux. J. Geophys. Res. Space Physics, 123, 1381–1387 (2018). https://doi.org/10.1002/2017JA025053

G. Rostoker, S. Skone, D.N. Baker, On the origins of relativistic electrons in the magnetosphere associated with some geomagnetic storms. Geophys. Res. Lett., 25, 3701 (1998). https://doi.org/10.1029/98GL02801

E. Roussos, et al., Electron microdiffusion in the Saturnian radiation belts: Cassini MIMI/LEMMS observations of energetic electron absorption by the icy moons. J. Geophys. Res. (Space Physics), 112, 6214 (2007). https://doi.org/862 10.1029/2006JA012027

E. Roussos, et al., Discovery of a transient radiation belt at Saturn. J. Geophys. Res., 35, L22106 (2008). https://doi.org/10.1029/2008GL035767

E. Roussos, et al., Energetic electron microsignatures as tracers of radial flows and dynamics in Saturn's innermost magnetosphere. J. Geophys. Res., 115, A03202 (2010). https://doi.org/10.1029/2009JA014808

E. Roussos, et al., The variable extension of Saturn's electron radiation belts. Planetary and Space Science, 104 ,3-17 (2014). https://doi.org/10.1016/j.pss.2014.03.021

E. Roussos, et al., Evidence for dust-driven, radial plasma transport in Saturn's inner radiation belts, Icarus, 274, 272–283 (2016). http://doi.org/10.1016/j.icarus.2016.02.054

E. Roussos, et al., A radiation belt of energetic protons located between Saturn and its rings. Science, 362(6410) (2018). https://doi.org/10.1126/science.aat1962

E. Roussos, et al., Drift-resonant, relativistic electron acceleration at the outer planets: Insights from the response of Saturn's radiation belts to magnetospheric storms. Icarus, 305, 160 – 173 (2018b). https://doi.org/10.1016/j.icarus.2018.01.016

R.Z. Sagdeev, A.A, Galeev, *Nonlinear Plasma Theory* (edited by T. M. O'Neil and D. L. Book), W. A. Benjamin, New York (1969).

D. Santos-Costa, S.A. Bourdarie, Modeling the inner Jovian electron radiation belt including non-equatorial particles. Planetary and Space Science, Volume 49, Issues 3–4, 2001, Pages 303-312, ISSN 0032-0633 (2001). https://doi.org/10.1016/S0032-0633(00)00151-3

D. Santos-Costa, M. Blanc, S. Maurice, S.J. Bolton, Modeling the electron and proton radiation belts of Saturn. Geophys. Res. Lett., 30, 2059 (2003). https://doi.org/10.1029/2003GL017972

D. Sawyer, J. Vette, AP-8 trapped proton environment for solar maximum and solar minimum. National Space Science Data Center, Report 76-06, Greenbelt, Maryland (1976).

M. Schulz, Drift-shell splitting at arbitrary pitch angle. J. Geophys. Res., 77(4), 624–634 (1972). https://doi.org/10.1029/JA077i004p00624

M. Schulz, The Magnetosphere, in *Geomagnetism*. Academic Press, J.A. Jacobs, Pages 87-293, ISBN 9780123786746 (1991). https://doi.org/10.1016/B978-0-12-378674-6.50008-X.

M. Schulz, Particle drift and loss rates under strong pitch angle diffusion in Dungey's model magnetosphere. J. Geophys. Res., 103, A1, 61-67 (1998). https://doi.org/10.1029/97JA02042

M. Schulz, A. Eviatar, Diffusion of equatorial particles in the outer radiation zone. J. Geophys. Res., 74(9), 2182–2192 (1969). https://doi.org/10.1029/JA074i009p02182

M. Schulz, and L.J. Lanzerotti, *Particle Diffusion in the Radiation Belts*. Springer-Verlag Berlin Heidelberg (1974). https://doi.org/10.1007/978-3-642-65675-0

R.S. Selesnick, E.C. Stone, Energetic electrons at Uranus: Bimodal diffusion in a satellite limited radiation belt. J. Geophys. Res., 96, A4, 5651-5665(1991). https://doi.org/10.1029/90JA02696

R.S. Selesnick, E.C. Stone, Radial diffusion of relativistic electrons in Neptune's magnetosphere. Geophys. Res. Lett., 21, 15, 1579-1582 (1994). https://doi.org/10.1029/94GL01357

R.S. Selesnick, M.D. Looper, R.A. Mewaldt, A theoretical model of the inner proton radiation belt. Space Weather, 5, S04003 (2007). https://doi.org/10.1029/2006SW000275

R.S. Selesnick, M.K. Hudson, B.T. Kress, Direct observation of the CRAND proton radiation belt source. J. Geophys. Res. Space Physics, 118, 7532–7537 (2013). https://doi.org/10.1002/2013JA019338

R.S. Selesnick, Y.-J. Su, J.B. Blake, Control of the innermost electron radiation belt by large-scale electric fields. J. Geophys. Res. Space Physics, 121 (2016). https://doi.org/10.1002/2016JA022973

V.A. Sergeev, V. Angelopoulos, J.T Gosling, C.A. Cattell, C. A., C.T. Russell, Detection of localized, plasma-depleted flux tubes or bubbles in the midtail plasma sheet. J. Geophys. Res., 101, A5, 10817-10825 (1996). https://doi.org/10.1029/96JA00460

Y.Y. Shprits et al., Radial diffusion modeling with empirical lifetimes: Comparison with CRRES observations. Ann. Geophys., 23(4), 1467–1471 (2005). https://doi.org/10.5194/angeo-23-1467-2005

Y.Y. Shprits et al., Review of modeling of losses and sources of relativistic electrons in the outer radiation belt I: Radial transport. J. Atmos. Sol. Terr. Phys., 70, 1679-1693 (2008). https://doi.org/10.1016/j.jastp.2008.06.008

Y.Y. Shprits et al., Review of modeling of losses and sources of relativistic electrons in the outer radiation belt II: Local acceleration and loss. J. Atmos. Sol. Terr. Phys., 70, 1694-1713 (2008b). https://doi.org/10.1016/j.jastp.2008.06.014

Y.Y. Shprits et al., Unusual Stable Trapping of the Ultra-Relativistic Electrons in the Van Allen Radiation Belts. Nature Phys., 9, 699–703 (2013). https://doi.org/10.1038/NPHYS2760

Y.Y. Shprits et al., Combined convective and diffusive simulations: VERB-4D comparison with 17 March 2013 Van Allen Probes observations, Geophys. Res. Lett., 42, 9600–9608 (2015). https://doi.org/10.1002/2015GL065230

Y.Y. Shprits et al., The dynamics of Van Allen belts revisited. Nature Physics, 14, 102–103 (2018). https://doi.org/10.1038/nphys4350

S.F. Singer, Trapped albedo theory of the radiation belt. *Phys. Rev. Lett., 1*, 181 (1958). https://doi.org/10.1103/PhysRevLett.1.300

G.L. Siscoe, D. Summers, Centrifugally driven diffusion of iogenic plasma. J. Geophys. Res., 86, A10, 8471-8479 (1981a). https://doi.org/10.1029/JA086iA10p08471

G.L. Siscoe, et al., Ring current impoundment of the Io plasma torus. J. Geophys. Res., 86, A10, 8480-8484 (1981b). https://doi.org/10.1029/JA086iA10p08480

E.C. Sittler, et al., Ion and neutral sources and sinks within Saturn's inner magnetosphere: Cassini results. Planetary and Space Science, 56, 3–18 (2008). https://doi.org/10.1016/j.pss.2007.06.006

D.J. Southwood, M.G. Kivelson, Magnetospheric interchange instability. J. Geophys. Res., 92(A1), 109– 116 (1987). https://doi.org/10.1029/JA092iA01p00109

D.J. Southwood, M.G. Kivelson, Magnetospheric interchange motions. J. Geophys. Res., 94 (A1), 299– 308 (1989). https://doi.org/10.1029/JA094iA01p00299

E.C. Stone, The physical significance and application of L, Bo, and Ro to geomagnetically trapped particles. J. Geophys. Res., 68(14), 4157–4166 (1963). https://doi.org/10.1029/JZ068i014p04157

Z. Su, F. Xiao, H. Zheng, S. Wang, STEERB: A three-dimensional code for storm-time evolution of electron radiation belt. J. Geophys. Res., 115, A09208 (2010). https://doi.org/10.1029/2009JA015210

Z. Su, et al., Ultra-low-frequency wave-driven diffusion of radiation belt relativistic electrons. Nature Communications, 6, 10096 (2015). https://doi.org/10.1038/ncomms10096

D.A. Subbotin, Y.Y. Shprits, Three-dimensional modeling of the radiation belts using the Versatile Electron Radiation Belt (VERB) code. Space Weather, 7 :10001 (2009). https://doi.org/10.1029/2008SW000452

D.A. Subbotin, Y.Y. Shprits, B. Ni, Long-term radiation belt simulation with the VERB 3-D code: Comparison with CRRES observations. J. Geophys. Res., 116, A12210 (2011). https://doi.org/10.1029/2011JA017019

D. A. Subbotin, Y.Y. Shprits. Three-dimensional radiation belt simulations in terms of adiabatic invariants using a single numerical grid. J. Geophys. Res., 117, A05205 (2012). https://doi.org/10.1029/2011JA017467

D. Summers, C. Ma, Rapid acceleration of electrons in the magnetosphere by fast-mode MHD waves. J. Geophys. Res., 105(A7), 15887–15895 (2000). https://doi.org/10.1029/1999JA000408

D. Summers, G.L. Siscoe, Coupled low-energy - ring current plasma diffusion in the Jovian magnetosphere. J. Geophys. Res. 90, A, 2665-2671 (1985). https://doi.org/10.1029/JA090iA03p02665

Y. X. Sun, et al., Spectral signatures of adiabatic electron acceleration at Saturn through corotation drift cancelation. Geophys. Res. Lett., 46, 10240-10249 (2019). https://doi.org/10.1029/2019GL084113

G.I. Taylor. Diffusion by continuous movements. Proc. London Math. Soc., 2, 196-211 (1922). https://doi.org/10.1112/plms/s2-20.1.196

M.F. Thomsen, C.K. Goertz, J.A. Van Allen, On Determining Magnetospheric Diffusion Coefficients From the Observed Effects of Jupiter's Satellite Io. J. Geophys. Res., 82, 35 (1977). https://doi.org/10.1029/JA082i035p05541

M.F. Thomsen, J.A. Van Allen, Motion of trapped electrons and protons in Saturn's inner magnetosphere. J. Geophys. Res., 85, 5831–5834 (1980). https://doi.org/10.1029/JA085iA11p05831

M.F. Thomsen, et al., Saturn's inner magnetospheric convection pattern: Further evidence. J. Geophys. Res., 117, A09208 (2012). https://doi.org/10.1029/2011JA017482

R.M. Thorne, Radiation belt dynamics: The importance of wave-particle interactions. Geophys. Res. Lett., 37, L22107 (2010). https://doi.org/10.1029/2010GL044990

A.D. Tomassian, T.A. Farley, A.L. Vampola, Inner-zone energetic-electron repopulation by radial diffusion. J. Geophys. Res., 77(19), 3441–3454 (1972). https://doi.org/10.1029/JA077i019p03441

F. Tsuchiya et al., Short-term changes in Jupiter's synchrotron radiation at 325 MHz: Enhanced radial diffusion in Jupiter's radiation belt driven by solar UV/EUV heating. J. Geophys. Res., 116, A09202 (2011). https://doi.org/10.1029/2010JA016303

W. Tu, et al., Quantifying radial diffusion coefficients of radiation belt electrons based on global MHD simulation and spacecraft measurements. J. of Geophys. Res., 117, A10210 (2012). https://doi.org/10.1029/2012JA017901

W. Tu, et al., Modeling radiation belt electron dynamics during GEM challenge intervals with the DREAM3D diffusion model. J. Geophys. Res. Space Physics, 118, 6197–6211 (2013). https://doi.org/10.1002/jgra.50560

B.A. Tverskoy, Space Research V, Proc. 5th Int. Space Science Symp, Amsterdam: North-Holland, p. 367 (1964).

A.Y. Ukhorskiy, M.I. Sitnov, Radial transport in the outer radiation belt due to global magnetospheric compressions. J. Atmos. Sol.-Terr. Phys. 70, 1714 (2008). https://doi.org/10.1016/j.jastp.2008.07.018

A.Y. Ukhorskiy, M.I. Sitnov, K. Takahashi, B.J. Anderson, Radial transport of radiation belt electrons due to stormtime pc5 waves. Ann. Geophys. 27, 2173 (2009). https://doi.org/10.5194/angeo-27-2173-2009

J.A. Van Allen, L.A. Frank, Radiation Around the Earth to a Radial Distance of 107,400 km. Nature, volume 183, pages 430–434 (1959). https://doi.org/10.1038/183430a0

J.A. Van Allen, et al., Sources and Sinks of Energetic Electrons and Protons in Saturn's Magnetosphere, J. Geophys. Res., 85, A11, 5679-5694 (1980a). https://doi.org/10.1029/JA085iA11p05679

J.A. Van Allen, et al., The Energetic Charged Particle Absorption Signature of Mimas. J. Geophys. Res., 85, A11, 5709-5718 (1980b). https://doi.org/10.1029/JA085iA11p05709

J.A. Van Allen, Energetic particles in the inner magnetosphere of Saturn. In: *Saturn*, The University of Arizona Press, ISBN 0-8165-0829-1 (1984).

A. Varotsou, et al., Three dimensional test simulations of the outer radiation belt electron dynamics including electron-chorus resonant interactions, J. Geophys. Res., 113, A12212 (2008). https://doi.org/10.1029/2007JA012862.

S.N. Vernov, et al., Possible mechanism of production of terrestrial corpuscular radiation under the action of cosmic rays. Soviet Phys., Doklady,4,154 (1959).

J. Vette, The AE-8 trapped electron model environment. National Space Science Data Center, Report 91-24, Greenbelt, Maryland (1991).

L.S. Waldrop et al., Three-dimensional convective flows of energetic ions in Jupiter's equatorial magnetosphere. J. Geophys. Res. Space Physics, 120, 10,506– 10,527 (2015). https://doi.org/10.1002/2015JA021103

M. Walt, Radial diffusion of trapped particles and some of its consequences. Rev. Geophys., 9(1), 11–25 (1971a). https://doi.org/10.1029/RG009i001p00011

M. Walt, The radial diffusion of trapped particles induced by fluctuating magnetospheric fields. Space Sci. Rev., 12: 446 (1971b). https://doi.org/10.1007/BF00171975

M. Walt, L.L. Newkirk, Comments [on "Radial diffusion of outer-zone electrons"]. J. Geophys. Res., 76(22), 5368–5370 (1971). https://doi.org/10.1029/JA076i022p05368

M. Walt, *Introduction to geomagnetically trapped radiation*. Cambridge University Press (1994). https://doi.org/10.1017/CBO9780511524981

M. Walt, Source and loss processes for radiation belt particles. in *Radiation Belts: Models and Standards*, vol. 97, edited by J.F. Lemaire, D. Heynderickx, and D.N. Baker, p.1, AGU, Washington D.C. (1996). https://doi.org/10.1029/GM097p0001

H. I. West Jr., R.M. Buck, G.T. Davidson, The dynamics of energetic electrons in the Earth's outer radiation belt during 1968 as observed by the Lawrence Livermore National Laboratory's Spectrometer on Ogo 5. J. Geophys. Res., 86(A4), 2111–2142 (1981). https://doi.org/10.1029/JA086iA04p02111

R.J. Wilson et al., Evidence from radial velocity measurements of a global electric field in Saturn's inner magnetosphere, J. Geophys. Res. Space Physics, 118, 2122–2132 (2013). https://doi.org/10.1002/jgra.50251

E.E. Woodfield, et al., The origin of Jupiter's outer radiation belt. J. Geophys. Res. Space Physics, 119, 3490–3502 (2014). https://doi.org/10.1002/2014JA019891

E.E. Woodfield, et al., Formation of electron radiation belts at Saturn by Z-mode wave acceleration. Nature Communications,5062, 9, 1, 2041-1723 (2018). https://doi.org/10.1038/s41467-018-07549-4

M. A. Xapsos, P. M. O'Neill and T. P. O'Brien, Near-Earth Space Radiation Models. in *IEEE Transactions on Nuclear Science*, vol. 60, no. 3, pp. 1691-1705 (2013). https://doi.org/10.1109/TNS.2012.2225846